AN ABSTRACT OF THE THESIS OF

Sean T. Moran for the degree of Master of Science in Mechanical Engineering presented on February 11, 2004.
Title: Elastic, Plastic and Total Strains in Human and Porcine Pedicle Trabecular Bone and PU-foam After Pedicle Screw Insertion by Utilizing Functional Micro-CT Imaging.

Abstract approved:
Redacted for Privacy

Brian K. Bay

Pedicle screw breakage and loosening remain as clinical complications of short segment instrumentation procedures for spinal stabilization. This study has directly visualized and measured elastic, plastic and total vertebral pedicle trabecular bone full-field strains in the regions immediately surrounding the pedicle screw during pedicle screw insertion by utilizing functional microCT imaging and digital volume correlation. Human, porcine and polyurethane foam samples were analyzed and compared. Analysis showed that when osteoporotic human, normal human and porcine pedicle trabecular bone samples were compared, osteoporotic samples showed higher peak plastic strains and greater variability of these strains from their means. This suggests that osteoporotic human samples are non-uniformly elastic and plastic, while normal human and porcine samples are more uniformly elastic and plastic throughout the trabecular structure. PU-foams are not appropriate as models for pedicle trabecular bone in the in vivo environment since strain results showed dissimilar plastic and elastic strain magnitudes than human and porcine pedicle trabecular bone. This study may aid in the development of performance criteria for new PU-foams and improved pedicle screw designs.

Elastic, Plastic and Total Strains in Human and Porcine Pedicle Trabecular Bone and PU-foam After Pedicle Screw Insertion by Utilizing Functional Micro-CT Imaging

by
Sean T. Moran

A THESIS

Submitted to

Oregon State University

In partial fulfillment of
the requirements for the
degree of

Master of Science

Presented February 11, 2004
Commencement June 2004

Master of Science thesis of Sean T. Moran
Presented on February 11, 2004.

APPROVED:

Redacted for Privacy

Major Professor, representing Mechanical Engineering

Redacted for Privacy

Head of the Department of Mechanical Engineering

Redacted for Privacy

Dean of the Graduate School

I understand that my thesis will become part of the permanent collection of Oregon State University libraries. My signature below authorizes release of my thesis to any reader upon request.

Redacted for Privacy

Sean T. Moran, Author

ACKNOWLEDGEMENTS

I would like to express my appreciation to all those who have offered support during my education, be it financial, emotion or material. My wife, Jenny, who's endlessly loving and supporting nature has given me inspiration to live life to its fullest. My parents who have shown me that the only limits on life are the ones we set for ourselves. My family, I thank for seeing the best in me always. The faculty of Oregon State University who have presented to me the fundamentals of my education without hopes of compensation. My fellow graduate students Scott Rutschman, Henri Saucy, Matt Sutton and especially Dan Berry for their willingness to help and offer council and training. Without their help this research would have been lost in 30GB of endless, encrypted numbers. Lastly, but definitely not least I would like to thank Dr. Brian Bay. His easy style of managing includes guidance, humor, intelligence and the desire to do something extraordinary. I have learned and improved beyond my hopes as a graduate student. May his good will come full-circle.

TABLE OF CONTENTS

LIST OF FIGURES

LIST OF FIGURES (Continued)

LIST OF TABLES

LIST OF APPENDIX FIGURES & TABLES

LIST OF APPENDIX FIGURES & TABLES (Continued)

LIST OF APPENDIX FIGURES & TABLES (Continued)

LIST OF APPENDIX FIGURES & TABLES (Continued)

LIST OF APPENDIX FIGURES & TABLES (Continued)

LIST OF APPENDIX FIGURES & TABLES (Continued)

Elastic, Plastic and Total Strains in Human & Porcine Pedicle Trabecular Bone After Pedicle Screw Insertion by Utilizing Functional Micro-CT Imaging

Introduction

Spinal Fixation & Stabilization

Patients with spinal injuries or disease which result in the instability or dysfunction of a vertebral motion segment may require surgical intervention. These injuries may include damage to intervertebral bodies or the disks that separate them (**Figure 1**). Intervention techniques usually require arthrodesis. Arthrodesis is the surgical immobilization of a joint. This procedure is commonly performed on the human spine in order to bring spinal stability, which helps to eliminate pain and restore normal function.

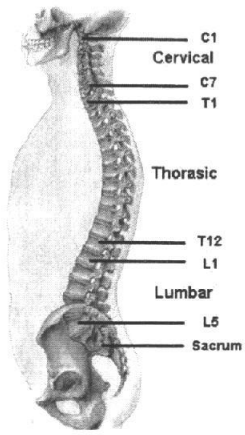

Figure 1. Human Spine. backpage.com

Arthrodesis of the human spine creates a union, or fusion, between two vertebral bodies after the removal of the intervertebral disk. Fusion may be accomplished by utilizing bone grafts, internal fixation devices or by intervertebral fusion cages. Many surgeons choose to use all three simultaneously.

The most common problems to occur in procedures for arthrodesis of the spine is the lack of fusion due to instability of the fusion construct or low quality bone. Low bone quality result from disease or age induced osteoporosis. Osteoporosis is a condition that results in the deossification of bone. Relative motion between vertebral bodies during healing may cause fibrous tissue growth near the healing zone instead of solid trabecular bone. Pedicle screw fixation has become a popular method for creating a rigid construct around the fusion site.

Pedicle Screws

Pedicle screws are used as a means to encourage fusion between vertebral bodies by creating a rigid construct around the site of injury or disease with the purpose of

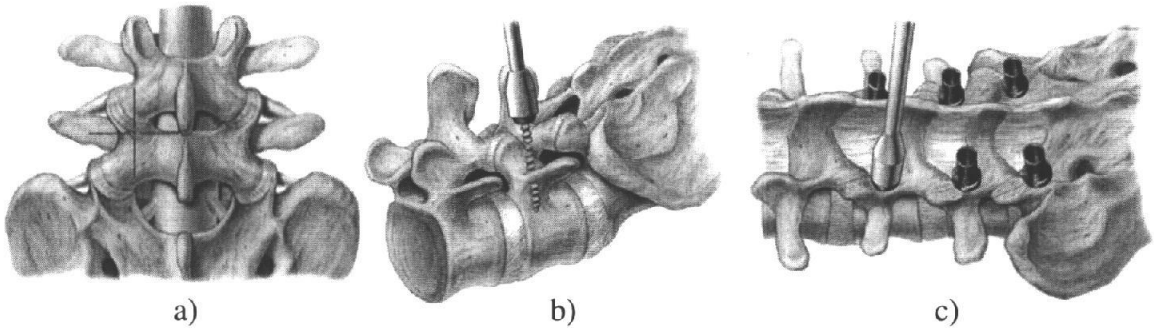

a) b) c)

Figure 2. Pedicle screw insertion in a typical posterior surgery. a) Pedicle screw insertion location, b) Pedicle screw insertion, and c) Multiple-level pedicle screws. (www.spine-surgery.com).

increased stability during healing (**Figure 2**). Preformed rods are often used to bridge the gap between pedicle screw heads. Multiple levels may be treated. **Figure 3** illustrates a multilevel pedicle screw fixation system by SofamorDanek. The connection rods are custom formed for each patient during the procedure. Ligaments, intervertebral disks and other material may be removed after the connection rods are tensioned. At this time, bone graft and/or intervertebral cages may be installed in the newly empty space between the vertebral bodies.

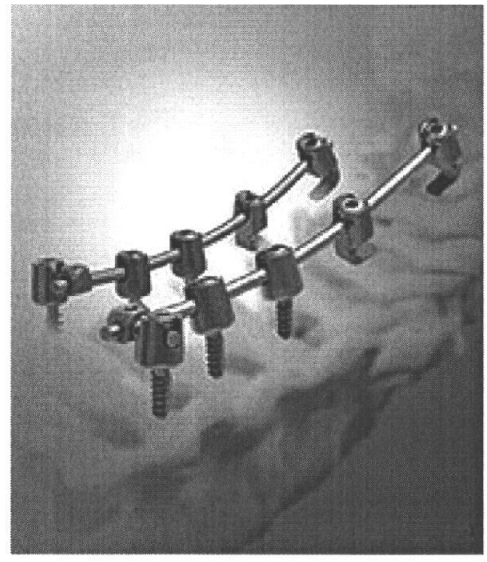

Figure 3. Pedicle screw system with precurved connection rods. (www.sofamordanek.com).

Previous Studies

The success of pedicle screws in spinal stabilization procedures, screw purchase in trabecular bone and human pedicle morphology have been well documented. Specific pedicle screw insertion techniques (Kowalsky et al., 2000) have been compared and have shown little difference in pullout performance. Many studies have been done by various groups with the purpose of finding correlations between bone density, insertion techniques, pedicle screw types and other variables to pullout strength. Isador et al. (1998) found that when a pullout resistant nut was added to the Universal Spine System anterior pedicle screw, that the pullout strength increased twofold. The nut also changed the mode of failure to rely on the strength of the vertebral body rather than the characteristics of the screw. Oktenoglu et al. (2001) used synthetic bone blocks to test the pullout resistance for cancellous lateral mass screws, cortical lateral mass screws, and pedicle screws. The group found that the optimum pilot hole preparation technique was to drill a short pilot hole will a drill bit diameter less than the core diameter of the screw. Chapman et al. (1996) tested 12 types of commercially available cannulated and noncannulated cancellous bone screws in synthetic bone analogs. The group found that tapping reduced the pullout strength by an average of 8% and that increasing the thread shape factor increased screw purchase. Kowalsky et al. (2000) compared the pullout resistance in human cervical pedicles after using the standard method and the Abumi insertion method of cervical pedicle screw insertion. The group found no difference between the two methods. Halvorson et al. (1994) found a correlation between bone mineral density and axial pullout strength when using one of four lumbar pedicle screw insertion techniques in frozen cadaveric lumbar spine segments. Pedicle screw pullout

strength was highly correlated with bone mineral density. Another group found that the effectiveness of spinal implants in fixation is dependent upon the bone-implant interface, and thus on vertebral bone density (Tan, 2003). The group found that pedicle screws did not behave in a similar manner during axial compression and bending while inserted into synthetic surrogates and lumbar vertebrae. Deformation magnitudes and toggle points for the screws varied between the sample types. Kwok et al. (1996) studied insertion torque and pullout strengths of conical and cylindrical pedicle screws that were inserted into cadaveric spine segments. The group found that although conical profile pedicle screws increased the required insertion torque, this did not allow the prediction of axial pullout strengths. Meyers et al. (1996) found that by using density determined by quantitative computed tomography used with insertion torque and in situ stiffness provides a strong predictive ability of screw pullout as compared with other variables in the system such as geometry and density as discovered by x-ray absorptiometry. Zdeblick et al. (1993) found that insertion torque is a good indicator of bone-metal interface failure during a cyclic failure mode. The group also found that smaller pedicle width correlated with increased insertion torque and cycles to failure. The group discussed how this might explain why patients with osteoporosis diagnosed through radiography may still obtain stable fixation with pedicle screw systems.

The internal morphology of human pedicles has been studied (Manohar et al., 2000) and correlated with the affects upon pedicle screw loading. McKinley et al. (1997) investigated how pedicle morphology affected pedicle screw bending moments in synthetic bone analogs by utilizing pedicle screws instrumented with internal strain gages. The group discovered that in situ loads increased significantly as the pedicle

length increases and as pedicle height decreased. Weinstein et al. (1992) studied the anatomical and technical consideration associated with pedicle screw instrumentation. Moran et al. (1989) studied pedicle morphology, insertion techniques and other concerns involved in transpedicular screw fixation. The group found that the use of a ganglion knife resulted in higher pullout forces in 8 of 10 trials and gave greater control to screw location and depth as compared to the use of a drilled hole.

The influence of body loading on implant loading has been studied by various groups. Smith et al. (1996) used internally instrumented 7mm Cotrel-Dubousset pedicle screws to measure flexion and extension moment at specific locations along the screw axis. The method was validated and the technique may be used to measure in situ forces within human pedicles for varying experiments. Rohlmann et al. (2000) studied the affects of load carrying on the loads in internal spinal fixators by using instrumented telemeterized internal fixators. The group found that for reasonable load carrying, the loads within the implants increased little. Yerby et al. (1997) substantiated previous analytical models of pedicle screw bending moments in situ by utilizing instrumented pedicle screws on cadaveric motion segments. McKinley et al. (1999) studied how variations in surgical technique directly affect pedicle screw bending moments by using instrumented pedicle screws.

Survivorship studies have been done in an attempt to quantify the efficacy of pedicle screw systems and fixation procedures. Dickman et al. (1992) studied 104 patients that underwent transpedicular spinal instrumentation procedures. Various conditions existed in patients yet severe back pain was consistent throughout the group. At a 20 month follow-up period there was a 96% fusion rate. There were no operative

deaths, but major complications included a spinal epidural hematoma, three isolated nerve root deficits, and three would infections. Instrumentation failure eventually developed in 18 patients; nine were asymptomatic with a solid fusion. The other 9 were symptomatic or had pseudarthrosis and required operative revision. Pseudarthrosis, or false joint, is characterized by deossification of a bone followed by a bending fracture, which affects the ability of the bone to form a normal callus. The author stated that transpedicular instrumentation procedures using pedicle screws is an excellent method in all respects.

McAfee et al. (1991) performed a case study of pedicle instrumentation cases from 1985 to 1989. The total number of cases was 120 using two different types of instrumentation. Out of 526 pedicle screws there were 22 problem screws. Those problem pedicle screws involved 12 patients, seven of which had complete fusions and the condition was only found incidentally during radiographic imaging. The remaining patients had screw breakage in association with a pseudarthrosis. The survivorship was predicted using life table calculation to be 80% at 10 years. The actual survivorship was 90% at 10 years, which is more closely related to other types of existing surgical implants such as total hip arthroplasty.

Glaser et al. (2003) studied the long-term results of lumbar spine fusion supplemented with pedicle screw fixation. Patients treated at the University of Iowa Department of Orthopedic Surgery with lumbar pedicle screw fixation were reviewed. Questionnaires were given before surgery and at follow-up evaluation time. Radiographs were reviewed for evidence of hardware complications, fusion status, deformity, and extent of degeneration around the fusion. Out of 234 patients, only 94 had complete

information. Radiographically, at the 10-year follow-up assessment, 242 of 244 instrumented segments showed no motion, with approximately 1/3 of these also showing evidence of definite fusion.

Synthetic bone analogs have been shown to be excellent materials to simulate trabecular bone for pullout strength testing. Chapman et al. (1996) showed that the mechanical properties of porous polyurethane (PU) foams might be matched to the mechanical properties of various trabecular bone qualities. The group showed similar shear properties and suggested that PU foams are an excellent choice to simulate the pullout strength of pedicle screws. Gibson and Ashby et al. (1997) studied cellular PU foams and found that they may be used as models for cellular solid (Gibson, 1985) and when formulated properly, correspond well to those of cancellous bone. Szivek et al. (1995) studied three different formulations of porous PU foams prepared from Daro foam components with a range of mechanical properties to simulate trabecular bone. Fenech et al. (1999) studied cellular solid criterion for the prediction of axial, shear and failure properties of bovine trabecular bone. The purpose was to use cellular solid criterion in application to multiaxial loading in order to understand the failure behavior of trabecular bone.

Thompson et al. (2003) studied four different commercially available PU foams, by Sawbones, Inc., two of which were investigated during this present study. The group found that Young's moduli for the PU foams were at the lower end for trabecular bone (Currey, 1998), while the three lowest density foams has shear moduli comparable with trabecular bone (Knauss, 1981). The foam samples had unexpected behavior in shear

failure suggesting that these foams should not be used to model failure or yield properties of trabecular bone.

Motivation for Present Study

Pedicle screw breakage and loosening remain as clinical complications of short segment instrumentation procedures for spinal stabilization. The mechanical behavior of various screw designs has largely been investigated through pullout testing, often in synthetic bone analogs (**Figure 4**) (see previous section). Although a useful approach, these tests do not provide information on the bone/screw micromechanical interaction, which is an important factor in both short and long-term stability of the construct. In addition, pedicle screw pullout failure rarely occurs alone in vivo. Typical pedicle screw failure is often complex and involves multiple failure modes simultaneously.

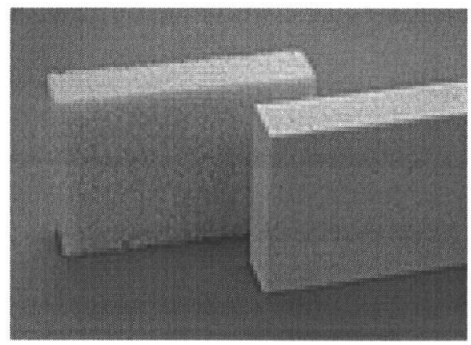

Figure 4. Cellular rigid polyurethane foams. (www.sawbones.com).

Animal models are often used to design and validate new spinal instrumentation technology. Although there are physical similarities between human and animal bone they are not the same and loading is not the same in vivo. PU-foams are often used to model screw pullout strength in trabecular bone. **Figure 5** illustrates typical cross-sectioned examples of human, porcine and PU-foam samples. It is clearly seen that these samples are different in trabecular density, geometry and uniformity. Comparison of human, porcine and PU-foam samples is necessary to gain insight into whether porcine

and foam samples are adequate to model human trabecular bone during pedicle screw insertion.

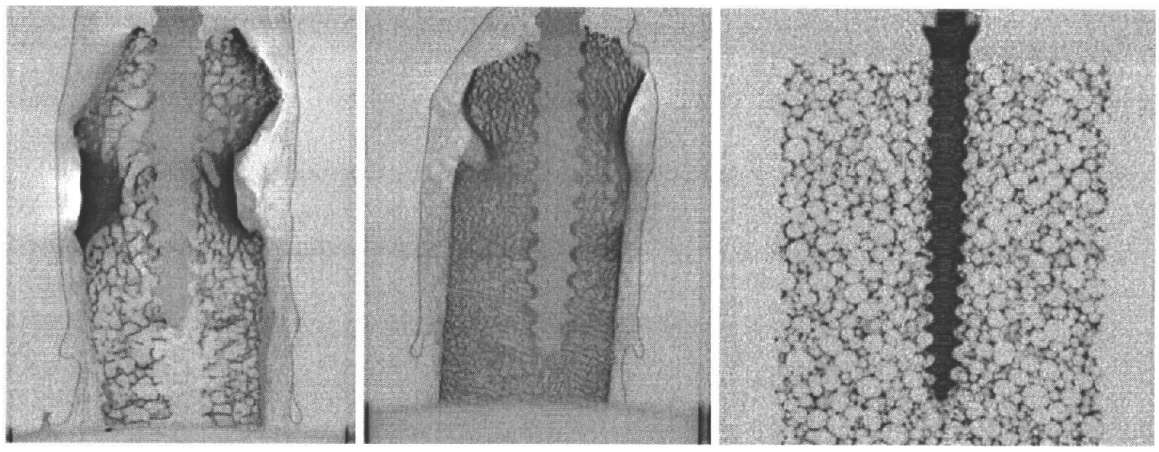

Figure 5. Cross-section of typical human, porcine and PU-foam samples (left to right).

Present Study

It is hypothesized that plastic and elastic strains within the vertebral pedicle trabecular bone contribute to pedicle screw purchase in different ways. Plastic strain or crushing of trabecular bone around the screw provides mechanical interlocking as the screw is fully inserted. Elastic strain in the trabecular bone surrounding the pedicle screw provides forces normal to screw geometry. These elastic forces not only help to hold the screw in place, but also help absorb energy during in vivo loading. By characterization of elastic and plastic strains it may be better understood how mechanical interlocking of crushed trabecular bone around the screw and elastic deformation of the surrounding trabecular bone are responsible for screw purchase.

Bone volume fraction (BVF), or apparent density (AD) may be used as a measurement of trabecular bone quality. Thompson et al. (2003) suggested that when

AD is compared to material properties for PU foams with different densities, similar relationships to theoretical cellular solid criterion and mechanical properties (Gibson and Ashby, 1997) exist. If cellular solid criteria are established for trabecular bone, and foam properties may be matched based upon AD, then validation for foam as models for trabecular bone may result. This may also lead to validation for the use of animal models for pedicle screw instrumentation research. Cellular solid criteria for trabecular bone may be the focus of future research, however this study will discuss whether PU foams are appropriate models for the simulation of pedicle screw insertion into pedicle trabecular bone. This will be investigated by comparing the elastic and plastic strains that develop within human and porcine pedicle trabecular bone and PU-foam samples.

Critical sectional areas give threaded fasteners their strength and fracture characteristics (Blake, 1986). **Figure 6** illustrates the geometry of screw threads.

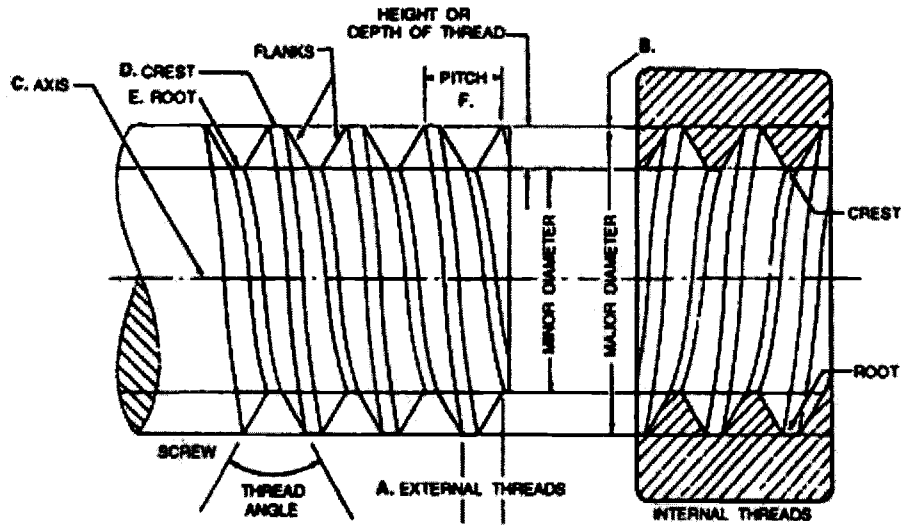

Figure 6. Definition of screw thread geometry.

These areas are important to the failure of the threaded fastener or the material that it is fastening. The cross-sectional area of the fastener, through the thread, is important to

resist tensile and shear failure. The shear area of the external thread resists shearing of the screw thread, resulting in pullout. These types of failures of instrumentation do occur in vivo and are directly associated with the material quality and the in vivo environment discussion. The shear area of the internal thread resists the pullout of the threaded fastener by shearing of the fastened material. This area is very important to pedicle screw instrumentation failure in vivo. The lines along the minor diameter in **Figure 6** define the shear area for the external threads, while the lines along the major diameter define the shear area for the internal threads. During a pullout failure of a pedicle screw, the trabecular bone surrounding the screw shears on a macroscopic level. Yet on a scale of similar magnitude to trabecular struts, local crushing of those struts begins and the trabecular structure fails as the screw shears the bulk material. Bulk material shear properties of trabecular bone govern this mode of failure. Trabecular bone is not a continuous material. It is made up of interconnected strut-type element that maintain an open-cell cellular solid (Gibson and Ashby, 1997). Although direct pullout of pedicle screws in vivo is rare, pullout is often a consequence of screw loosening due to cyclic in vivo loading.

This study has utilized a microCT based technique to directly measure bony deformation within the samples during pedicle screw insertion. This technique allows the direct calculation of strains from displacement data without any underlying assumptions for the internal material properties of the samples. This is valuable for this study due to the highly nonlinear nature of trabecular bone. Elastic, plastic and total strains within the vertebral pedicle trabecular bone directly surrounding the screw were calculated.

The assessment of plastic strains is based on the notion that the insertion process will produce both plastic and elastic strains, and that the elastic strains will disappear after screw removal. Comparison of digital volumes in the before insertion images with fully inserted images would give the total strain field, whereas comparison of before insertion with after extraction will isolate the plastic strain field. Finally, comparing fully inserted images with images after extraction would measure the elastic strain fields.

Quantification and spatial distribution of plastic and elastic pedicle trabecular bone strains may provide insight into the micro-interaction between pedicle trabecular bone and pedicle screws. Further investigation may prove useful in the design of pedicle screws for patients with varying levels of bone density or disease, such as osteoporosis.

Digital Volume Correlation and Present Study

Digital Volume Correlation (Bay et al., 1999; Smith et al., 2001, 2002) is the three-dimensional extension of two-dimensional digital image correlation (Bruck et al., 1989; Sutton et al., 1983). Two-dimensional image correlation uses distinct patterns that are inherent or added to the surface of the material to measure sample displacements during experimental procedures. Speckling the sample surface with an airbrush or spray paint often creates adequate surface patterns. A region of interest (ROI) is defined within the sample as a means to view the region of direct interest with respect to the experiment. The region of interest is created and meshed using the meshing tool of an FEA package. The mesh defines discrete points, which are used for direct experimental measure of displacements. Digital images are then taken of the sample before and after loading. A computer algorithm defines a subregion of speckle around each point for the unloaded

image. The algorithm then directly measures sample displacements by identifying the location of the subregion for each point in the unloaded and loaded images. Using this displacement data, strains may be directly calculated for the region of interest.

Digital Volume Correlation was utilized in this study to evaluate the plastic, elastic and total strains within the vertebral pedicle trabecular bone during pedicle screw insertion. High-resolution computed tomography was used to create digital image volumes of the samples. Varying grayscale value regions in the digital image volume represent the natural bone density variation within the trabecular bone in the samples. These grayscale regions allow the Digital Volume Correlation technique to track the bony deformations within the sample during pedicle screw insertion by matching patterns between the unloaded and loaded image volumes.

A pattern-matching algorithm is applied to each point in the region of interest that is defined within the original, unloaded digital image volume. This region of interest is meshed, which defines points that represent the location of distinct voxels, or three-dimensional pixels. **Figure 7** illustrates a meshed region of interest for a typical sample. A starting

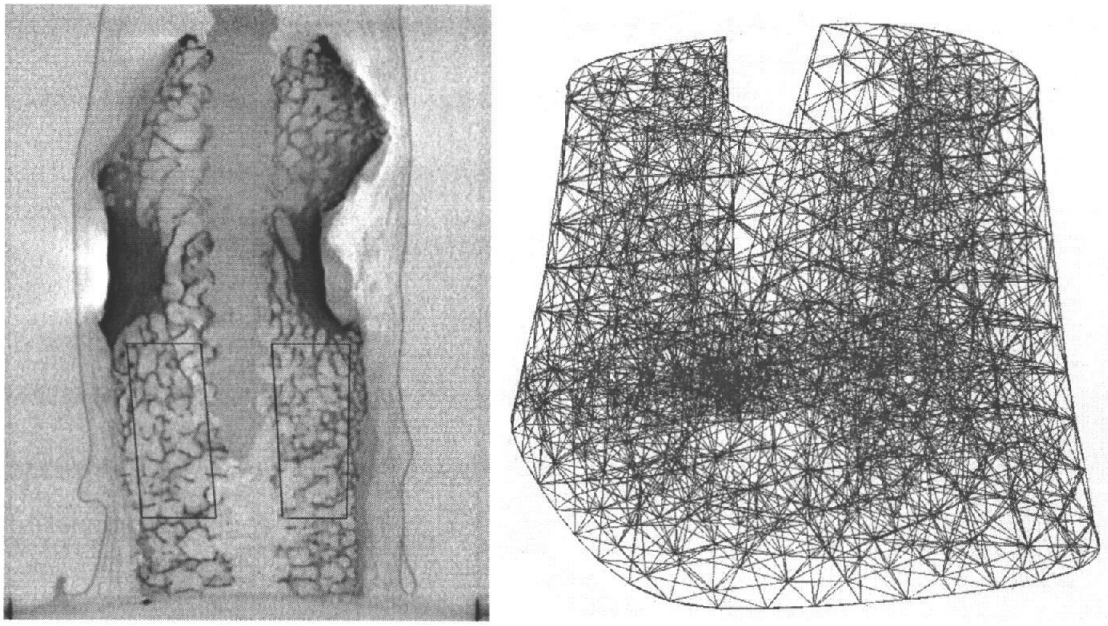

Figure 7. Example of a typical meshed region of interest shown for sample: 41270-11-right. An outline of the region of interest for a vertically resliced cross-section of the sample (left) and modeled three-dimensional region of interest (right) are shown.

point is selected and a subvolume around that point is used to match patterns between the unloaded and loaded image volumes by the minimization of a sum-of-squares objective function. This objective function minimization finds the location within the loaded image volume that is a best match for each point in the unloaded image volume. The objective function is defined as,

$$\min_{\mathbf{g}\in\Re^3} C(\mathbf{g}) = \frac{1}{2}\sum_{i=1}^{w}\{B(\mathbf{p}+\mathbf{g}+\mathbf{m}_i) - A(\mathbf{p}+\mathbf{m}_i)\}^2$$

where the parameters are as listed below:

p is the displacement measurement location,

g is a trial displacement vector,

$\mathbf{m_i}$ is an offset to a location within a subvolume,

w is the number of points within a subvolme,

A are the values from the unloaded image data,

B are the values from the loaded image data.

Determination of a starting point that is relatively close to the global minimum, and avoids local minima, is fundamental in the nonlinear minimization. To ensure this occurs a search range of voxel coordinates from **p** is defined and a coarse estimate for the minimum is calculated. This procedure directly minimizes the first location to within one voxel and sets the stage for the above outlined subvoxel minimization routine.

The minimization routine uses the Levenberg-Marquardt variation of the Gauss-Newton technique for subvoxel precision (Gill et al, 1981). This technique efficiently minimizes sum-of-square-differences objective functions. This method requires interpolation since voxel locations are integer valued and objective function and Jacobian values used in the procedure are real valued. Tricubic interpolation (Lancaster and Saldauskas, 1986) is used to determine the real intermediate values between voxels.

The result upon minimization for each point in the region of interest is a displacement vector for that point. This procedure is repeated for every point in the region of interest (**Figure 7**), which defines the displacement vector field. Displacement data is smoothed by fitting a second-order approximation of the strain tensor to a cloud of displacement values local to each point (Geers et al., 1996). This operation acts to reduce the noise associated with the measurement for each point in the region of interest. **Figure 8** illustrates the flowchart for Digital Volume Correlation.

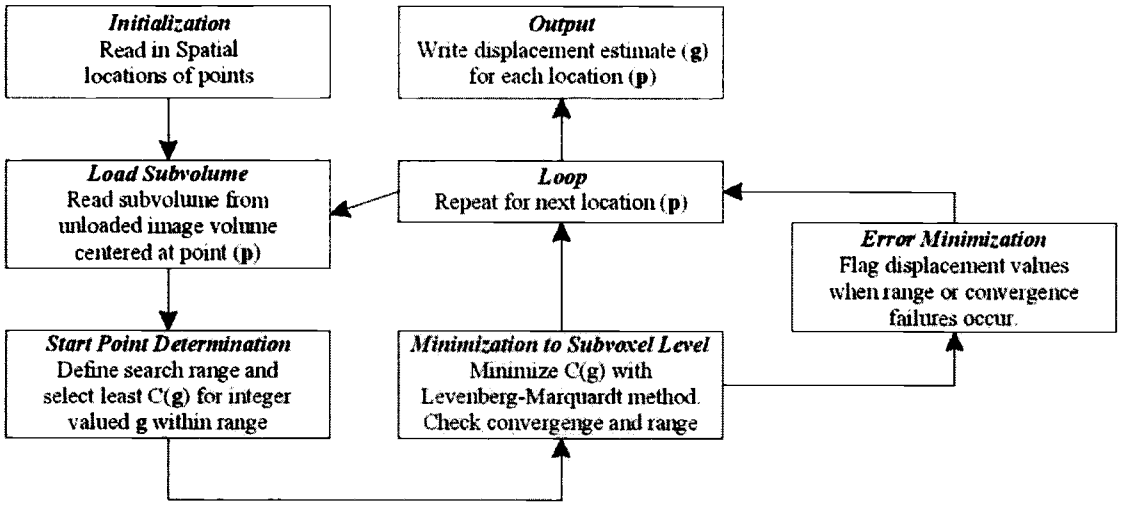

Figure 8. Flow-chart for Digital Volume Correlation.

The error minimization for the DVC procedure ensures that data for particular points with local minima and poorly defined objective functions are excluded during the minimization of the objective function. Many local minima may exist which minimize the objective function. The global minimum is the desired result of the minimization routine. The objective function may also be poorly defined for a particular point, which will never converge to a minimum. This convergence failure criterion ensures that objective functions that are poorly defined for particular points are neglected during data collection.

Materials and Methods

Samples' Sources and Preparation

This study included seven (7) human cadaveric and three (3) porcine pedicle samples as well as two (2) polyurethane (PU) foam samples. **Table 1** summarizes the label designation and source type for each sample. Tissue samples were prepared at the Department of Orthopaedic Surgery at the Cleveland Clinic Foundation in Cleveland, Ohio. Each tissue sample was removed from the patient or animal and trimmed along the axis of the pedicle with approximate dimensions of 30 x 30 x 80 (width x depth x length) mm. The samples were drilled, tapped, instrumented with conical 5.5 x 45mm pedicle screws to a minimal depth and frozen until the time of image data collection. PU samples were prepared by cutting through the thickness into a rectangular prism to approximate dimensions of 35 x 35 x 65 (width x depth x length) mm. A hole was drilled into each PU sample with a 3mm bit to depth equal to the pedicle screw insertion length. These samples were composed with densities of 0.16g/cc (10pcf) and 0.20g/cc (12.5pcf). These PU foam densities have been shown to be similar in apparent density and shear strengths of human trabecular bone (Chapman, 1996, and Thompson, 2003).

Table 1. Summary of Sample Labels and Source Type

Sample Name	Source Type
41258-l1-left	Human
41258-l1-right	Human
41270-l1-left	Human
41270-l1-right	Human
38424-l3	Human
38424-l4	Human
38424-l5	Human
Pig-l3	Porcine
Pig-l4	Porcine
Pig-l5	Porcine
10foam	PU foam
12.5foam	PU foam

Before image data acquisition the samples were thawed, trimmed flat at the mounted end, wrapped in gauze and the thumb portion of large latex gloves were stretched over them. This was done to decrease any risk of contamination to surrounding

areas during handling and to retain sample moisture content during testing. Although each tissue sample was tested for blood-borne pathogens, the utmost care was taken by assuming that each sample was contaminated. Finally, each sample was mounted in a 5mm deep platen using polymethylmethacrylate (PMMA) (**Figure 9**).

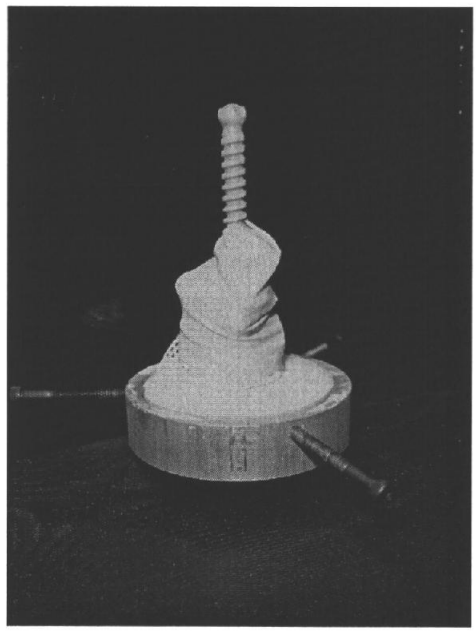

Figure 9. Pedicle Sample Prepared and Mounted

Pedicle screws were manufactured of either polyetheretherkeytone (PEEK) or carbon fiber (one sample). A preliminary study was done in order to assess the viability of each of the two materials for this study. Both materials performed in a similar manner with respect to the goals of the study. These materials were selected for the preliminary study for their radiolucent properties since a Computer Assisted Tomographic (CAT or CT) technique is utilized in this study. This minimized the microCT artifacts often associated with metallic implants during data acquisition utilizing CT imaging. X-ray artifacts occur in metallic samples due to their relatively high atomic numbers and density. As x-ray photons enter the boundaries of a metallic material, they are much more likely to collide with electrons and be either absorbed or scattered. When scattering occurs, x-ray photos are more likely to be deflected from their original paths and at varying degrees. This acts to blur the x-ray images and is called x-ray artifact.

It was assumed that the interaction between the PEEK and carbon fiber pedicle screws and the trabecular bone or PU foam of the samples would not differ from that of

metallic screws. Since PEEK, carbon fiber and titanium screws are stiffer and denser than trabecular bone and the study is focusing on how trabecular bone deforms around the pedicle screw, this is a reasonable assumption. However, there is a mechanical loading scenario during which this would not be a good assumption. If the trabecular bone is dense enough in certain regions, or if the screw interacts with cortical bone, then the screw will be put into bending during insertion. In this loading scenario each screw type behaves differently from one another due to the differences in elastic tensile moduli and ductility. The elastic tensile moduli for PEEK, carbon fiber and titanium are approximately 3.4GPa, 124-137GPa and 105-120GPa, respectively. Although carbon fiber is stiff as compared to titanium, it is brittle and can break into shards, which was the case for one of the early test samples. This sample was not used for data acquisition for this study. Titanium and carbon fiber pedicle screws will deform little under applied bending moments. These screws will stay relatively straight during the screw insertion path. PEEK screws under similar applied bending moments will deform to a greater degree. This translates to different screw paths and bone crushing profiles for the different screw types under bending. This type of loading was minimized for this study by ensuring straight tapped paths through the center of the samples.

Equipment and Image Data Collection

This study utilizes a custom functional microCT imaging system to collect experimental image data. This equipment includes an Instron mechanical tester, a Newport rotational stage, a Thomson image intensifier, a Retiga CCD Camera and a Fein

Focus x-ray source. **Table 2** summarizes the equipment included in the custom functional microCT imaging system.

Table 2. Summary of Equipment and Manufacturers for Functional Imaging System

Manufacturer	Model Number	Description
Instron Co.	Instron 4444	Mechanical Testing Apparatus
Newport, Inc.	RV120PP	Rotational Stages
Thomson Tubes Electroniques	TH9438HX	Image Intensifier
Qimaging, Burnaby	Retiga	1024 x 1280, 10-bit CCD Camera
Fein Focus, Inc.	FXE	160.20 μCT x-ray source

Figure 10 shows the functional imaging system as it lies within a lead chamber. The CCD camera resides behind the image intensifier as may be seen in the left image. The x-ray source and the mechanical tester with rotational stages are shown in the right image in Figure 10.

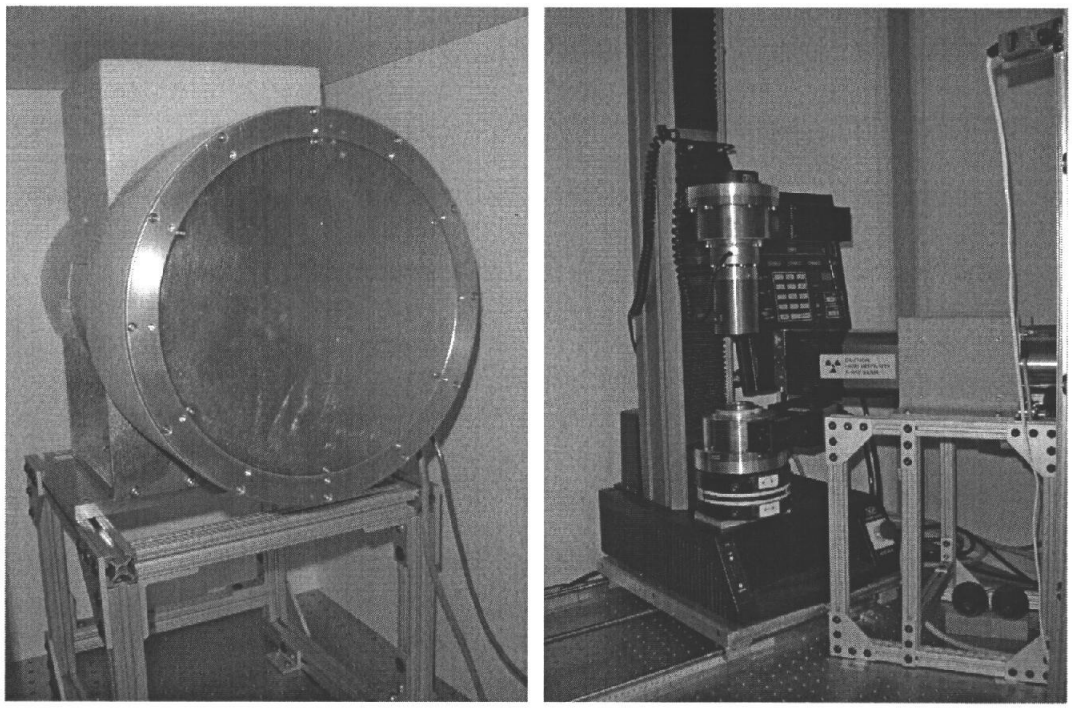

Figure 10. Functional CT imaging System including the x-ray source and mechanical tester with rotational stages (right) and image intensifier and CCD camera (left).

The functional imaging system allows the user to control the position of samples and the power of the x-ray source in order to produce high-resolution images of the sample. The rotational stages in the mechanical tester may be precisely controlled through 360 degrees of rotation. Samples in the system are subjected to x-rays, which produce an x-ray shadow that is intensified, converted to visible light and captured by the CCD camera as a high-resolution digital radiographic image. This is done for many angles and custom software is then used to correct the images for distortions caused by the image intensifier and to reconstruct these images (Feldkamp et al., 1984) into a digital image volume. Digital image volumes that coincide with unloaded and loaded states may be compared by utilizing additional custom software. The result is the direct measurement of deformations and the direct calculation of strains that occurred between the two states without any underlying assumptions of material properties.

Once mounted, image data sets were taken for each sample in an unloaded state. This image data is required for a baseline data set. A second image set was taken under identical conditions. These two image data sets are referred to as the repeat-unload image data sets. These image data sets are important in order to minimize and characterize the error associated with the process for each sample. Pedicle screws were then rotated until full screw insertion has occurred and an image data set was acquired. Then the pedicle screw was extracted to the initial position and a final image data set was acquired. These load steps were chosen in order to extract plastic, elastic and total full-field strain data as described in the Data Analysis section of this study.

Each image data set consisted of 500 radiographic images with a resolution of 504 x 636 that were collected through a full 360-degree rotation. This resulted in a total of

four (4) image data sets of 156.5 MB each for a total of 626 MB for each sample. There were twelve (12) samples for a total of 7.5 GB of raw data. The power level for the x-ray source was set to 50 KVp with a total exposure time of 200 ms per projection image. The power level for the PU foam samples was 41 KVp with an exposure time of 260 ms. Bright and dark field images were taken for each sample at the identical system settings. Bright and dark field images are used to set upper and lower grayscale values for each pixel location. These values are then used to scale the individual pixel grayscale values for each pixel in each digital image before image reconstruction.

Image Post Processing

The natural distortions caused by the x-ray source and the image intensifier, as discussed the *Equipment and Image Data Collection* section corrected using images of a metallic plate with a precisely machined grid of known geometry and the bright field and dark field images collected during data acquisition. After image correction, image volumes were reconstructed to 8-bit, 500 x 500 x 624 digital image volume composed of cubic voxels with a resolution of approximately 50 microns (Feldkamp et al., 1984).

Data Analysis

Reconstructed digital image volumes were reoriented for each sample by utilizing the similarities between human and porcine samples at the necked region of the trimmed pedicles. This reorientation was done for the sake consistency between samples. Software for the manipulation and visualization of digital image volumes included Scion

Image (Scion Corporation, Frederick, MD) and Image J (Wayne Rasband, National Institutes of Health, USA).

Three digital image volume states were used for image comparison with the goal of isolating plastic, elastic and total strains within the pedicles during pedicle screw insertion. These states were 1) before screw insertion (BI), at 2) full screw insertion (FI), and 3) after screw extraction (AE).

Digital Volume Correlation (DVC) was used to directly measure the elastic plastic and total strains for a distinct, three-dimensional region of interest within each sample. This region of interest was chosen for its proximity to the pedicle screw upon insertion and for its bone quality for each sample. Upon insertion and extraction, the pedicle screw entered and fully exited the selected regions of interest, respectively. Approximately 2000 points distributed within the regions were analyzed for displacements and strains by correlation of imaging volumes from the previously defined screw insertion and extraction states. **Figure 11** illustrates an example of a typical region

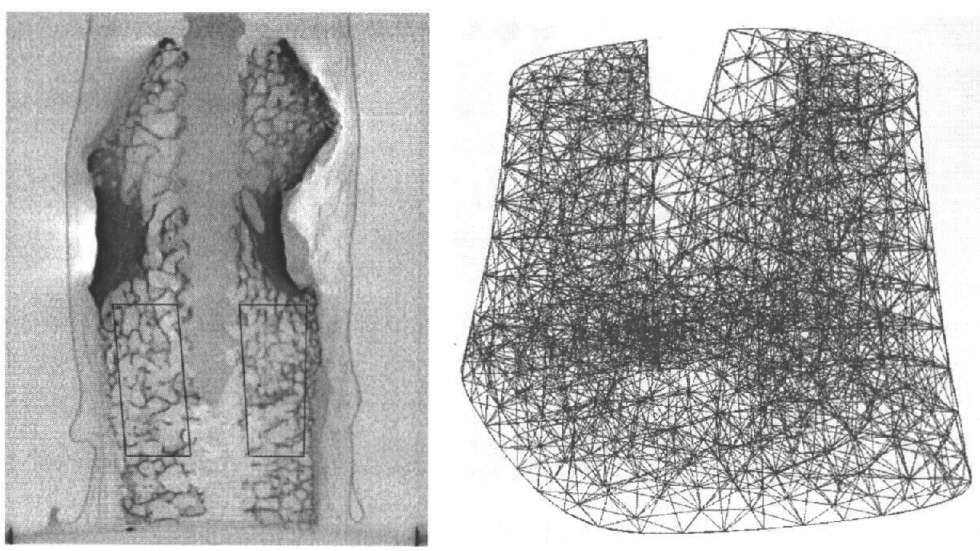

Figure 11. Example of a typical region of interest shown for sample: 41270-11-right. An outline of the region of interest for a vertically resliced cross-section of the sample (left) and modeled three-dimensional region of interest (right) are shown.

of interest. Image modeling and post processing of digital volume correlations were done using MSC Patran 2001 version r2a (MSC Software Corporation, Santa Ana, CA).

The region of interest for each sample was modeled and meshed with Patran with approximately 2000 nodes. These nodes are used as a basis for the measurement of displacements between digital image volumes. A nodal position file was exported from Patran for use in the Digital Volume Correlation procedure, which is discussed in the Digital Volume Correlation and Present Study section of this study. This procedure results in files containing the nodal displacements and nodal strains between selected digital image volumes for each region of interest.

Digital Volume Correlation was executed to isolate plastic, elastic and total strains during pedicle screw insertion and removal and Patran was used to post-process the data. Minimum principle and maximum shear strains were viewed and images were collected. Minimum principle strains were chosen to report since the insertion of pedicle screws into bone is compressive in nature. Maximum shear strains were chosen since an accepted mode of failure testing for pedicle screws is pullout testing. Pullout of pedicle screws occurs when a PU foam or trabecular bone fails in shear (Dawson, 2003; Blake, 1986). Report files containing data for plastic, elastic and total minimum principle and maximum shear strains were exported from Patran and were further processes using Microsoft Excel (Microsoft Corporation). Excel was used to produce various figures, which are shown in the results section.

Repeat unload digital image volumes were collected for the purposes of error minimization and quantification of system noise. This analysis is summarized in the results section.

Results

Plastic, elastic and total minimum principle strain results were generated and images taken for each region of interest. A typical example of these images is illustrated in **Figure 12** for sample 41270-l1-right with fixed scaling. It may be observed that the peak plastic strains (top) occur in a different region that the peak elastic strains (middle). This may be indicative of some local material properties within the sample such as low bone density or bone integrity in the plastic (crushing) zone. Regions of peak elastic strains (middle) are not well defined (dark) in the total strain plot (bottom). Remaining plastic, elastic and total minimum principle strain plots reside in Appendix A.

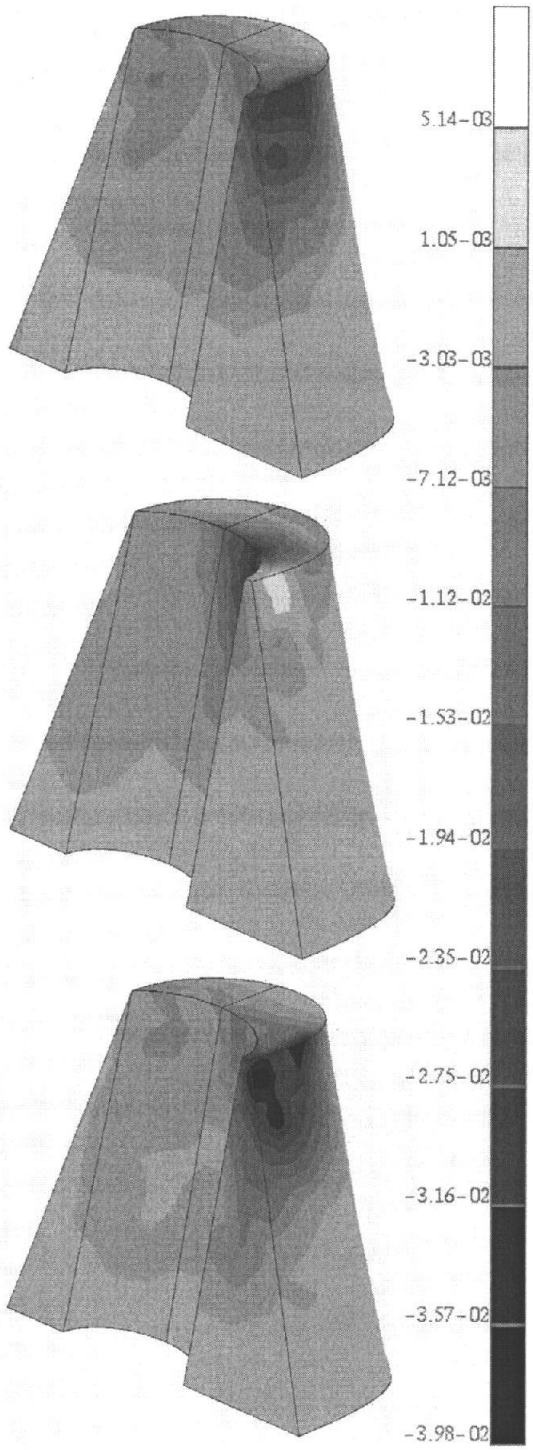

Figure 12. Typical plot of plastic (top), elastic (middle) and total (bottom) minimum principle strains for a sample region of interest. Sample 41270-l1-right is shown.

Plastic, elastic and total minimum principle strain results were generated and images taken for each region of interest. A typical example of these images is illustrated in **Figure 13** for sample pig-l4. It may be observed that the peak plastic strains (top) occur in a different region that the peak elastic strains (middle). This may be indicative of some local material properties within the sample. Peak plastic strain values do not dominate peak elastic strain values. This may be deduced by observing the total minimum principle strain plot and by understanding that the total minimum principle strains are a summation of plastic and elastic strains. Regions of peak elastic strains (middle) are well defined (dark) in the total strain plot (bottom). Remaining plastic, elastic and total minimum principle strain plots reside in Appendix A.

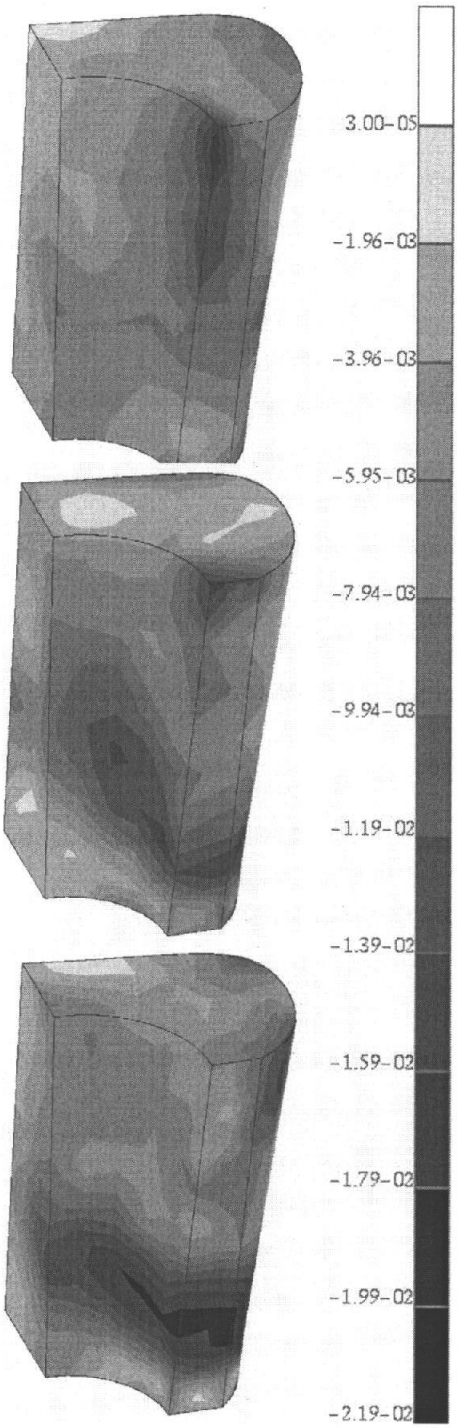

Figure 13. Typical plot of plastic (top), elastic (middle) and total (bottom) minimum principle strains for a sample region of interest. Sample pig-l4 is shown.

Plastic, elastic and total minimum principle strain results were generated and images taken for each region of interest. A typical example of these images is illustrated in **Figure 14** for sample 10foam. It may be observed that the peak elastic strains (middle) have greater magnitudes the peak plastic strains (top). Remaining plastic, elastic and total maximum shear strain plots reside in Appendix A.

Histograms of binned plastic, elastic and total strain values with fixed scaling were generated for minimum principle and maximum shear strains for each sample. **Figure 15** shows typical histograms for plastic, elastic and total minimum principle strain values for samples 41270-l1-right, pig-l4 and 10foam. It may be observed that sample pig-l4 has more uniformly distributed elastic and total strain values throughout the trabecular structure. Histograms were also plotted for maximum shear strains for each sample, which reside in Appendix A.

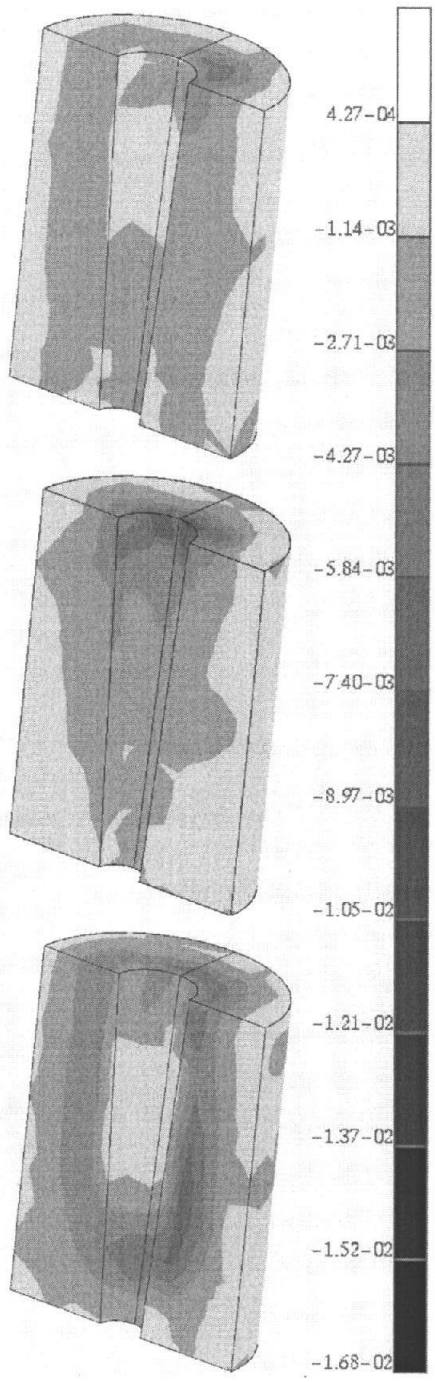

Figure 14. Typical plot of plastic (top), elastic (middle) and total (bottom) maximum shear strains for a sample region of interest. Sample 10foam is shown.

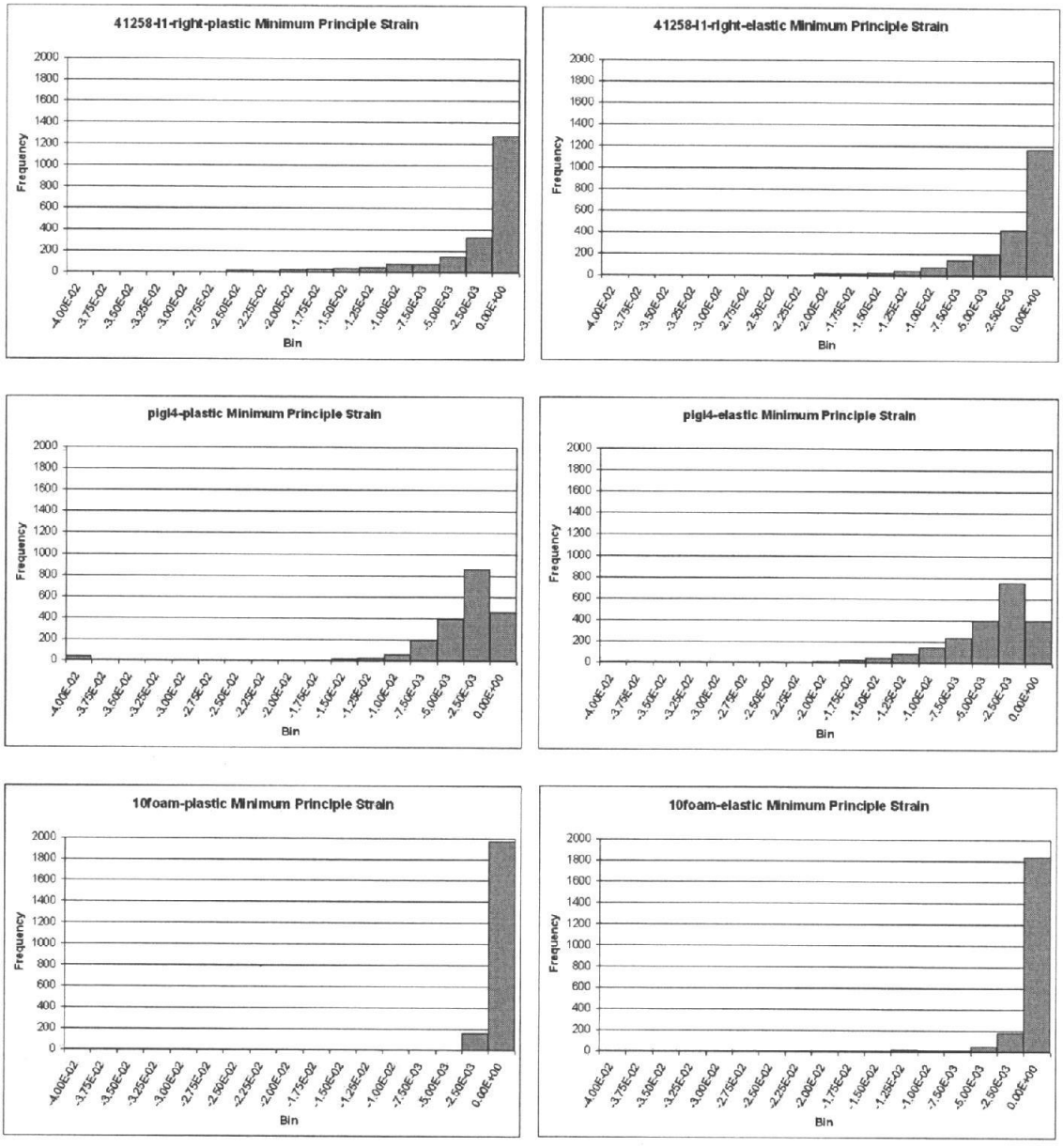

Figure 15. Typical histograms for plastic and elastic minimum principle strain values. Histograms for 41258-l1-right, pig-l4 and 10foam are shown.

Nonparametric statistical analyses were required to characterize the individual strain distributions since the data is not normally distributed. In this approach the 17th, 50th and 83rd percentile values, which correspond to one standard deviation from the mean on either side of normally distributed data, are extracted from the data for each result type. The assumption is then made that data is normally distributed across the sample set. **Figure 16** illustrates a typical nonparametric statistical comparison of each sample for plastic and elastic minimum principle strain values. The remaining nonparametric comparison results reside in Appendix A.

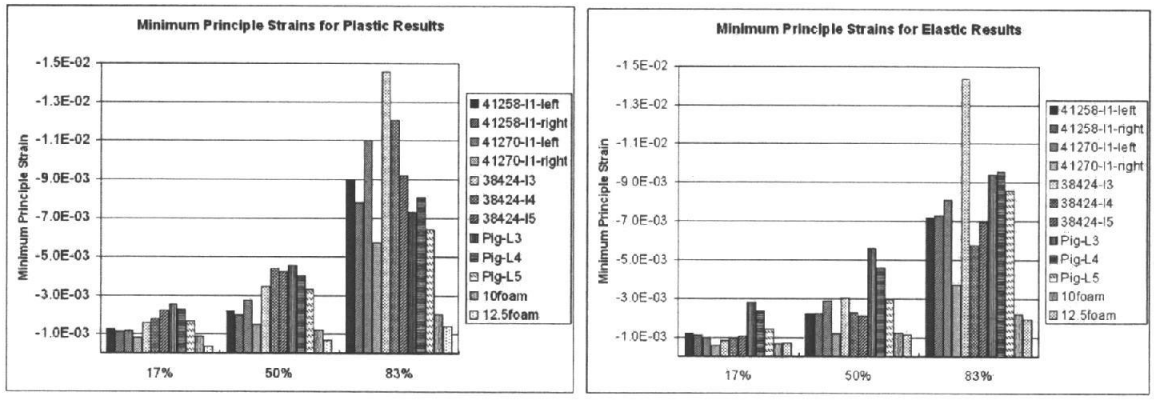

Figure 16. Typical nonparametric statistical comparison of each sample for plastic and elastic minimum principle strain values.

Plastic, elastic and total strain values were compared for minimum principle and maximum shear strains. ANOVA p-tests were used to determine whether the difference between human and porcine samples were significantly different with a criterion of $p<0.05$. **Figure 17** represents a comparison between human and porcine samples for plastic and elastic minimum principle strains using nonparametric statistical analysis and ANOVA p-test criterion. The strain values are also shown for PU-foam, but are not compared using the ANOVA p-test criterion. Only one of each type of PU foam was

tested since other studies have shown PU foams to be highly uniform and consistent properties (Chapman, 1996, Thompson, 2003) with little variability when compared to tissue samples (see previous studies section). It may be observed that the strain magnitudes and variations between percentile values are much lower than for human and porcine samples. The remaining results figures reside in Appendix A. **Table 3** summarizes the ANOVA p-value results for each of the results types and samples.

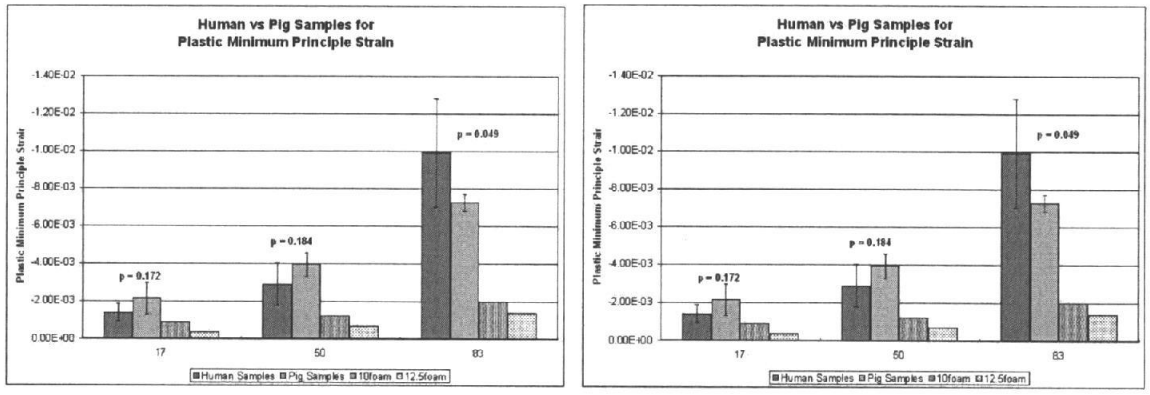

Figure 17. Typical nonparametric statistical comparison between human, porcine and PU-foam samples ($p<0.05$) for plastic and elastic minimum principle strain values.

Table 3. Summary of ANOVA p-test values upon comparison between human and porcine samples.

Strain Type	Min. Principle Strains			Max. Shear Strains		
	17%	50%	83%	17%	50%	83%
Plastic	0.172	0.184	0.049	0.284	0.385	0.395
Elastic	0.452	0.006	0.002	0.0007	0.041	0.686
Total	0.866	0.012	0.005	0.0007	0.004	0.501

It may be observed in Table 3 and Figure 17 that plastic strains are not different between samples, while elastic strains are different with the exception of the peak (17^{th} percentile minimum principle and 83^{rd} percentile maximum shear) values. The trend is for porcine samples to have similar plastic strains to human samples, while having larger elastic

strains. The trend for peak strains is for human samples to have higher plastic strains, while porcine samples have higher elastic strains.

Bone volume fraction within each region of interest for each sample was measured using Scion Image and a custom macro. The custom macro used grayscale thresholding to define BVF for each slice of the reconstructed image volume and averaged them to attain the total BVF for each region of interest. **Table 4** summarizes the bone volume fraction measurement for each sample and sample source type. This data was collected for the purpose of finding a correlation between bone volume fraction and plastic, elastic and total pedicle trabecular bone performance during pedicle screw insertion. Plastic, elastic and total strain values for the 17th, 50th and 83rd percentile were plotted against bone volume fraction values for minimum principle strains. A typical example of these figures for the 17th percentile plastic and elastic minimum principle strains is illustrated in **Figure 18**. It may be observed that for 17th percentile values of plastic and elastic minimum principle strain, the foam samples are not good models for pedicle trabecular bone strains for either human or porcine samples. The criteria for this observation is that for a foam sample to be a good model for this study, the density, and therefore the modulus, as well as the strain performance should be similar. Remaining figures for the 50th and 83rd percentile values exist in Appendix A.

Table 4. Bone Volume Fraction Summary for Each Sample

Sample	Bone Source	BVF (%)
41258-l1-left	Human	26.2
41258-l1-right	Human	24.3
41270-l1-left	Human	29.9
41270-l1-right	Human	24.5
38424-l3	Human	15.3
38424-l4	Human	19.7
38424-l5	Human	15.1
Pig-l3	Pig	46.6
Pig-l4	Pig	48.7
Pig-l5	Pig	43.2
10foam	PU-foam	21.4
12.5foam	PU-foam	31.4

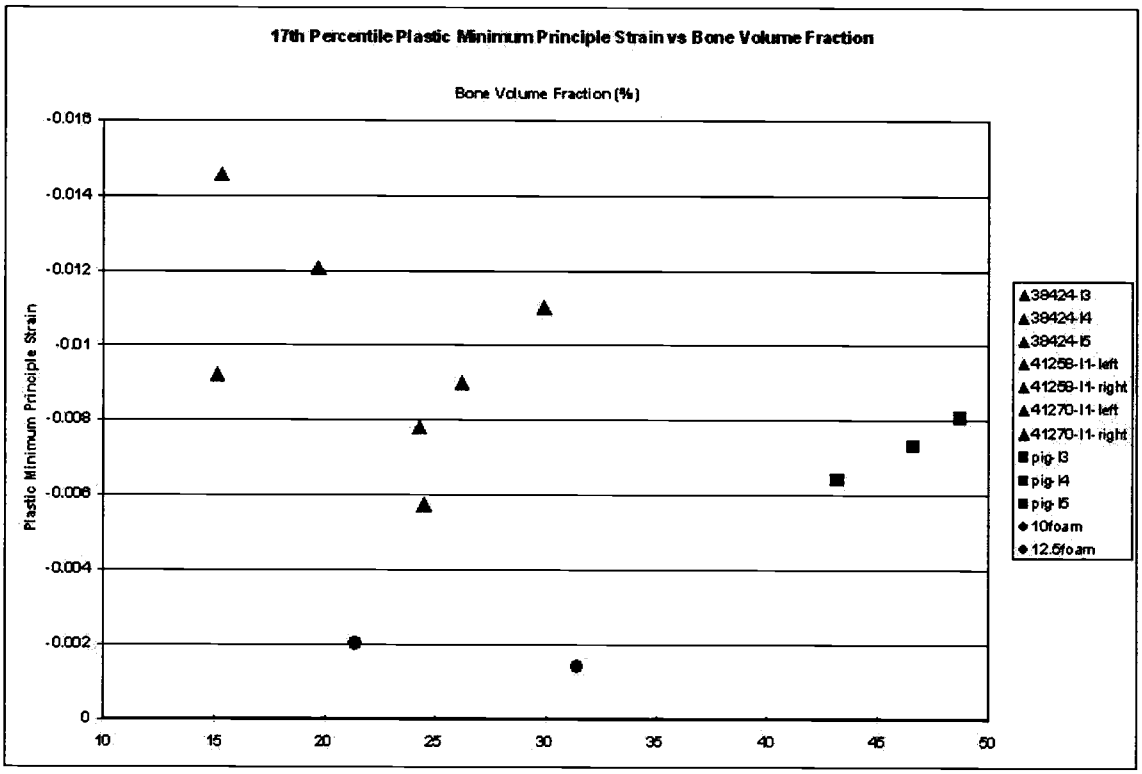

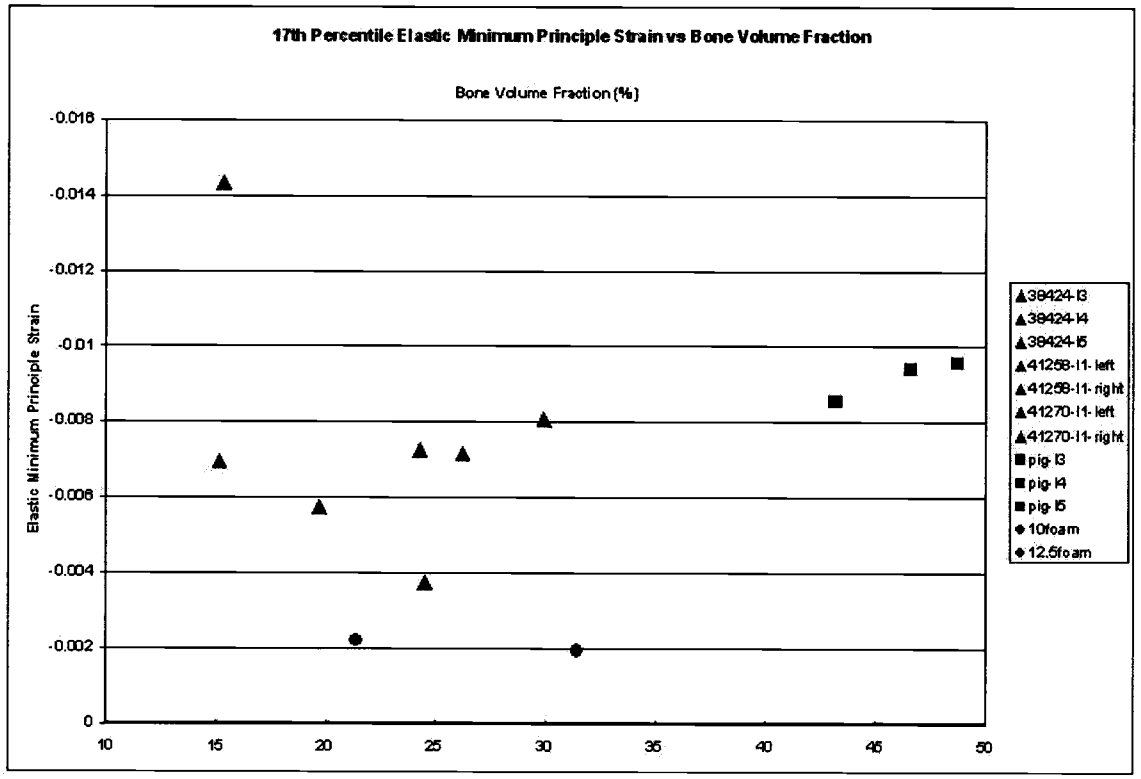

Figure 18. 17th percentile plastic and elastic minimum principle strain values versus bone volume fraction for each sample.

A performance criterion for whether a PU foam is an appropriate model for the study of pedicle screw purchase has been defined. For a PU foam to be an appropriate model for pedicle screw purchase in pedicle trabecular bone, the elastic and plastic strain results (minimum principle strains results for 17^{th}, 50^{th}, or 83^{rd} percentile values) must vary from the mean of the BVF group results by no more than the variability between BFV group samples from their mean. This statement is a requirement for the performance of PU foam to not be significantly different from bone performance. **Table 5** summarizes which foams are appropriate for modeling pedicle screw insertion for this study. It may be noted that only one result for 83^{rd} percentile plastic minimum principle strain value met the criterion, however this was very close, meaning that it would be an outlier in the data set if it were to be considered valid. The trends in the data support the lack of testing more PU foam samples.

Table 5. Summary of foams matching plastic and elastic minimum principle strain performance criterion for BVF groups. % variation of each foam from the mean for each group for each result.*

Foam Type	BVF Group	Ave. EMPS			Ave. PMPS		
		17	50	83	17	50	83
10foam	1	75.6(51.6)	50.7(20.3)	28.1(13.0)	83.2(22.4)	69.8(12.6)	50.9(18.0)
	2	66.5(29.4)	42.7(32.4)	29.9(28.9)	76.1(26.3)	41.8(24.5)	16.1(17.7)
	3	76.0(6.0)	72.3(30.2)	69.1(31.7)	72.4(11.4)	69.2(15.9)	57.9(20.9)
12.5foam	1	78.5(51.6)	53.7(20.3)	26.0(13.0)	88.3(22.4)	82.7(12.6)	80.1(18.0)
	2	70.4(29.4)	46.1(32.4)	29.7(28.9)	83.3(26.3)	66.8(24.5)	66.0(17.7)
	3	78.9(6.0)	73.9(30.2)	68.3(31.7)	80.8(11.4)	82.4(15.9)	83.0(20.9)

* ( ) indicates required % value of ± 1 STDEV from the mean for performance criteria

In order to explore the possibility of a correlation between bone volume fraction and strain performance during pedicle screw insertion, natural bone volume fraction groups were defined. The bone volume fraction group for each sample is summarized in **Table 6**.

Table 6. Bone volume fraction bin range assignment and definition for each sample.

Sample	Bone Volume Fraction (%)	Bone Volume Fraction Group
41258-l1-left	26.2	2
41258-l1-right	24.3	2
41270-l1-left	29.9	2
41270-l1-right	24.5	2
38424-l3	15.3	1
38424-l4	19.7	1
38424-l5	15.1	1
Pig-l3	46.6	3
Pig-l4	48.7	3
Pig-l5	43.2	3

The bone volume fraction bin designations in Table 5 were used to plot 17th, 50th and 83rd percentile values of plastic, elastic and total strain for minimum principle and maximum shear strains versus bone volume fraction bins. **Figure 19** shows 17th, 50th, and 83rd percentile plastic and elastic minimum principle strain values versus bone volume fraction groups. The remaining figures reside in Appendix A.

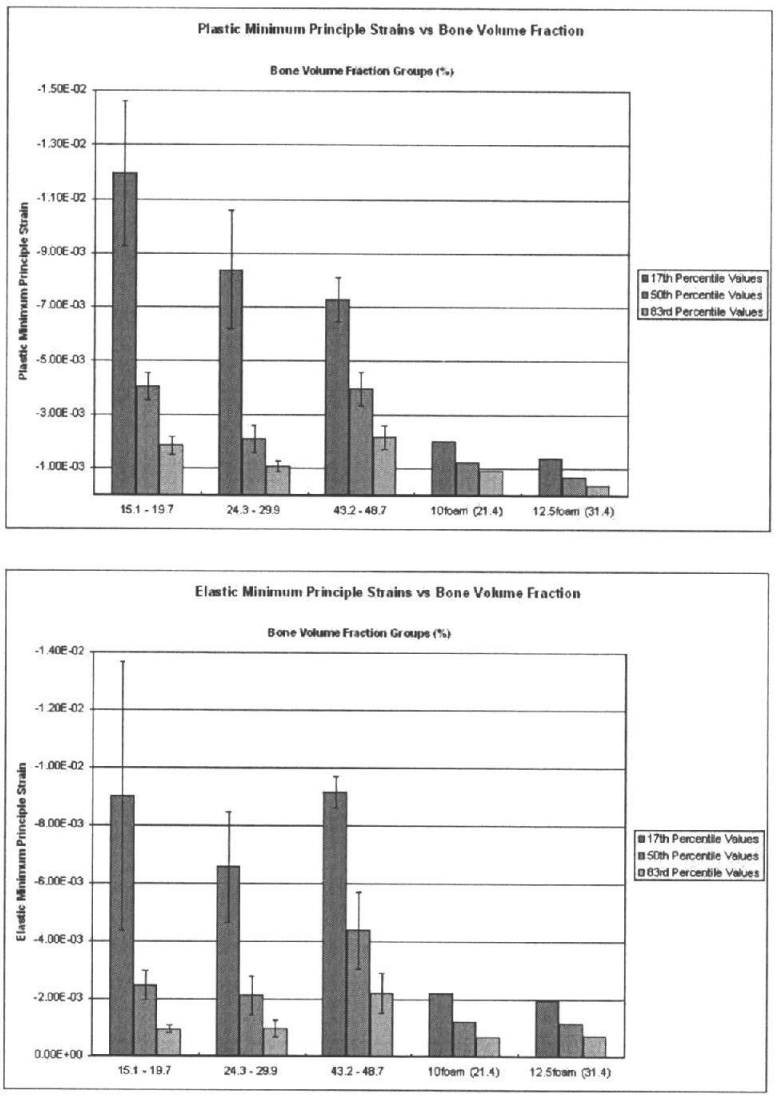

Figure 19. 17th, 50th and 83rd percentile plastic (top) and elastic (bottom) minimum principle strain values versus bone volume fraction groups.

It is clear that the lowest bone volume fraction group had greater mean 17th percentile plastic minimum principle strains than the denser groups. There is no significant difference between the mean 17th percentile values of elastic minimum principle strain; however, their deviations from the means are different. As the bones become more dense the plastic and elastic deviation from the mean become much less (**Figure 20**). This suggests that low bone volume fraction (osteoporotic) samples are non-

uniformly elastic and not stiff, while greater bone volume fraction samples are uniformly elastic and stiff throughout the trabecular structure. **Table 7** summarized the ANOVA p-test values for significant difference ($p<0.05$) between bone volume fraction groups. A Complete table including maximum shear results resides in Appendix A.

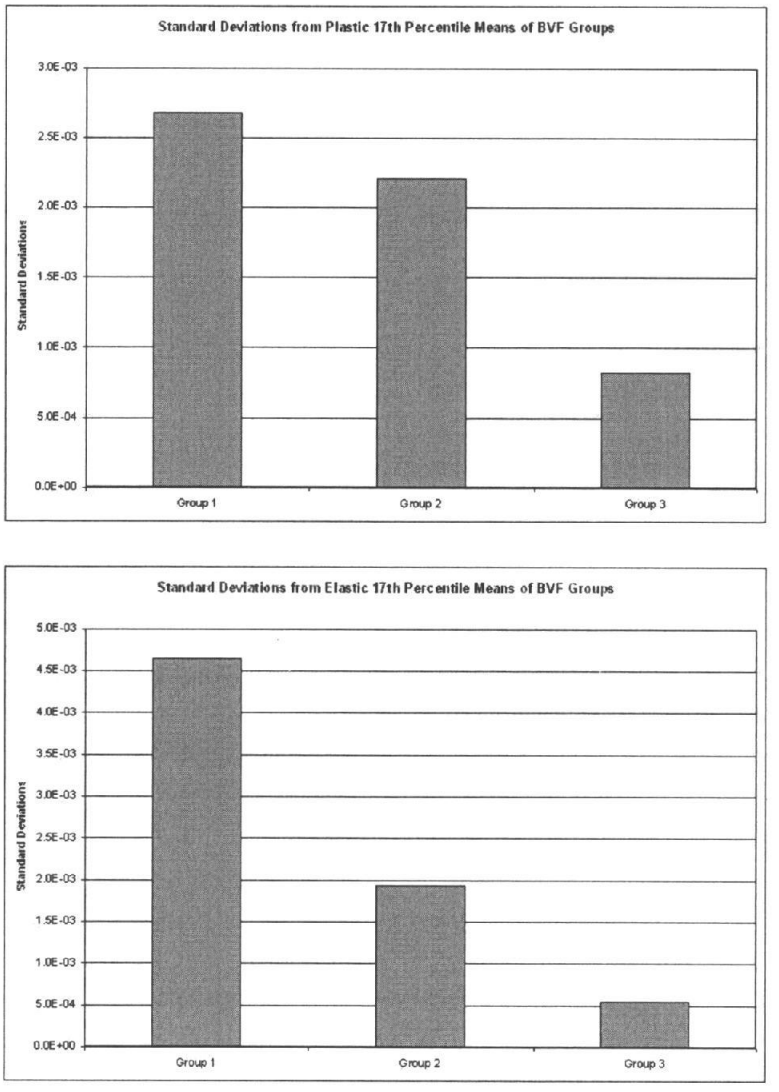

Figure 20. Standard deviations from the 17th percentile plastic and elastic minimum principle strain values for bone volume fraction groups.

Table 7. Summary of ANOVA p-test values ($p<0.05$) in comparisons between groups for 17th, 50th and 83rd percentile values of plastic elastic and total minimum principle strain (MPS).

BVF Group * Compared	Percentile Value	Elastic MPS	Plastic MPS	Total MPS
1 - 2	17%	0.374	0.110	0.209
	50%	0.498	0.004	0.047
	83%	0.894	0.011	0.064
2 - 3	17%	0.076	0.451	0.369
	50%	0.031	0.007	0.005
	83%	0.022	0.007	0.005
1 - 3	17%	0.957	0.045	0.409
	50%	0.079	0.887	0.024
	83%	0.037	0.393	0.054

* Bone Volume Fraction Groups (%):
Group 1: 15.1 - 19.7; Group 2: 24.3 - 29.9; Group 3: 43.2 - 48.7.

Error Analysis

The validity of experimental data requires some knowledge of error inherent to the data acquisition system. Error analysis for the system used in this study was accomplished by the comparison on two distinct unloaded or repeat-unloaded image volumes. Theoretically, the comparison of the unloaded and repeat-unloaded image volumes should result in null strain tensors. Therefore, by comparison of these two image volumes total system error may be assessed. Sources of error within the system may be mechanical or analytical in nature.

Repeat unloaded images were taken for each sample and post-processed in Patran. The results were used to refine the parameters used for the Digital Volume Correlation until the error was minimized for each sample. Error results were then analyzed for three typical sample types. One error analysis was completed for a typical sample from each of the bone volume fraction subgroups. This not only allowed errors to be compared

between human and porcine samples, but between the three bone volume fraction subgroups as well.

Total system error results were generated for minimum principle and maximum shear strains for each of the three samples. These errors ranged from between a minimum and maximum of 0.03% to 0.9%, respectively, for minimum principle strain. These errors ranged from between a minimum and maximum of 0.01% to 0.99%, respectively, for maximum principle strain. Extreme values are not necessarily good indicators of sample behavior. Nonparametric analysis similar to that done for other results for this study was applied to the error analysis as well. The minimum and maximum minimum principle and maximum shear strain values of the 17^{th}, 50^{th} and 83^{rd} percentile values are summarized in **Table 8**. These strains are deemed acceptable when considering that maximum measured strains are on the order of 7%. This equates to approximately 3% error at maximum strain reading.

Table 8. Summary of errors for minimum principle and maximum shear strains for the average 17^{th}, 50^{th} and 83^{rd} percentile values.

Average Minimum Principle Strain Error (%)			Average Maximum Shear Strain Error (%)		
17^{th}	50^{th}	83^{rd}	17^{th}	50^{th}	83^{rd}
0.22	0.11	0.06	0.08	0.13	0.21

Discussion

Plastic, elastic and total pedicle trabecular bone full-field strains have been characterized for regions immediately surrounding pedicle screws during insertion into human, porcine and PU-foam samples. A functional microCT 3-D imaging technique has been utilized to accomplish this. Pedicle trabecular bone strains were measured by comparisons between varying loading states for each sample. Digital image volumes were created for before insertion (BI), full insertion (FI), and after extraction (AE) states of pedicle screw insertion. Total strains, which include both plastic and elastic strains, are introduced into the samples during pedicle screw insertion. Total strain results were generated upon comparison of BI and FI image volume states. Plastic strains were isolated by the notion that no new plastic strains were introduced during pedicle screw extraction. Comparison between BI and AE loading states produced solely plastic strains. Elastic strains were revealed during the extraction of the pedicle screw. As the screw is extracted all elastic energy is restored to its equilibrium state. Elastic strains results were generated with comparisons between FI and AE loading states. Plastic, elastic and total strain behavior of human, porcine and polyurethane (PU) foam samples were compared. Bone volume fraction (BVF) groups were defined and used as a means of comparison as well.

We hypothesized that these different types of trabecular bone strains contribute to pedicle screw purchase in different ways. Plastic strains, or crushing of trabecular bone, contribute to screw purchase by mechanical interlocking between screw thread geometry. Elastic strains contribute to screw purchase by exerting normal forces to the screw geometry. Normal patient motion causes implant loading, which is distributed along

implant-bone interfaces. Elastic strains also act as a sort of shock absorber for the forces involved in normal in vivo loading. Characterization of elastic and plastic strains in human, porcine and synthetic trabecular bone analogs may create a greater understanding of how these strain components contribute to pedicle screw purchase and give insight into the validity of using PU foams as models for trabecular bone tissue.

The experimental technique utilized for this study directly measures sample strains without any underlying assumptions of pedicle trabecular bone material properties. The variability between samples, uncertainty about material properties and the highly nonlinear material behavior of trabecular bone during plastic deformation make the use of analytical models unreliable for this type of study.

Characterization of bony deformations in pedicles during pedicle screw insertion required various comparisons. Plastic, elastic and total minimum principle and maximum shear strain results were generated for each sample. Minimum principle strains results were chosen to present since the loading and crushing of bone during pedicle screw insertion is compressive in nature. Maximum shear strain results were generated since previous research has shown that trabecular bone fails in shear during pedicle screw pullout (Chapman, 1996, and Thompson, 2003).

Pullout testing in tissue and PU foam has been established as a means of comparing different pedicle screw instrumentation designs. Dawson et al. (2003) discussed the clinical relevance of such testing and how the in vivo environment rarely causes pedicle screws to fail in the pullout mode. The group concluded that pullout testing should not be used as an indicator of clinical performance. We hypothesized that plastic and elastic strains in any synthetic bone analog should behave in a similar manner

to that of trabecular bone in order to be considered as valid in vivo models. We have shown that synthetic bone analogs have dissimilar strain performance and therefore should not be considered as accurate models for trabecular bone. Others have also suggested that PU foams should not be used to model yield and ultimate properties of trabecular bone without further testing (Thompson, 2003).

Plastic, elastic and total strain measurements during pedicle screw insertion were much lower in magnitude for PU-foams as is illustrated in **Figure 17.** This may be explained on a mechanistic basis. Trabecular bone tissue is much different that PU-foam. Trabecular bone tissue is highly variable in its strut-like structures creating an open cellular solid network. PU-foams are a closed cellular solid with material stiffness much greater than that of trabecular bone (see previous studies section). The differences in strain behavior may be attributed to the micro-interaction between these very dissimilar structures.

Future Research

Continued research may focus on the differences in pedicle trabecular bone performance while using varying pedicle screws designs. These screw designs may include tapered and cylindrical geometries. Since bovine and porcine bone specimens as animal models are often utilized in the assessment of new spinal instrumentation, understanding the differences in bone performance between human and animal bones may improve instrumentation designs. Future research may focus on the differences between human and animal models with the purpose of ascertaining the most efficient way to use animal models for research into better human spinal instrumentation. More

realistic loading with instrumented spine segments and cyclic loading could help in understanding how pedicle screws fail in vivo. Synthetic bone analogs have real benefits is orthopedic research, but researchers must not be too hasty in using them. PU foams may be studied for performance criteria in contrast to nonrealistic loading scenarios such as pullout testing. The experimental technique used for this study could be used to develop new PU-foams that more closely exhibit the behavior of trabecular bone.

Limitations of Study

The experimental technique utilized for this study is unique and valuable, yet its limitations must be fully disclosed. The sample sizes that may be processed in the system are limited to approximately 80 x 80 x 200 (width x depth x height) mm. This limits many application of the technique. The technique only works for samples with distinct internal patterns or geometry of varying density. X-ray artifact must also be considered when utilizing this technique and minimized for maximum resolution and useful image data. This study was limited in scope to loads occurring during pedicle screw insertion.

Conclusion

MicroCT imaging and Digital Volume Correlation have been utilized to characterize the plastic, elastic and total pedicle trabecular bone strains during pedicle screw insertion. Human, porcine and PU-foam samples have been compared with the intent of finding tends or similarities in material behavior. Bone volume fraction groups were also created and compared. The validity of using PU foams as synthetic analogs for trabecular bone with pedicle screw research has been investigated.

Comparison between human and porcine samples showed that there are differences between many of their strain magnitudes and strain distributions as summarized in Table 3. The main points are summarized below:

- Peak values of plastic and elastic strains were *not different* between human and porcine samples.
- Mean and lower magnitudes of plastic strains were *not different* between human and porcine samples
- Mean and lower magnitudes of elastic strains were *different* between human and porcine samples, with porcine elastic strains being greater.
- Peak plastic strains were considerably lower for porcine samples than for the least dense (osteoporotic) human samples

Elastic and plastic strain behavior is similar between human and porcine samples during the application of relatively high strains. Elastic behavior of porcine trabecular bone is greater than human trabecular bone for relatively lower loading. This suggests that during normal loading conditions such as daily activities, that porcine trabecular bone may not be a good model for human trabecular bone. This is important since the elastic properties are what give trabecular bone the ability to adjust to in vivo loading during healing before trabecular bone damage occurs. This may be important to fusion studies done on live animals under restricted activity schedules as models for human bone tissue. Osteoporotic trabecular bone crushes much more easily that porcine bone, which is to be expected.

Bone volume fraction (BVF) groups were defined and data was compared between groups. It was shown that:

- Peak plastic strains are greatest in samples with the least BVF.
- Elastic strains are *not different* between human and porcine samples, however the magnitudes of the standard deviations from their means are greater as BVF decreases.

This suggests that low bone volume fraction (osteoporotic) samples are non-uniformly elastic and plastic and not stiff, while samples with greater bone volume fraction are uniformly elastic and plastic and stiff throughout the trabecular structure.

Comparisons between trabecular bone tissue and PU foam samples show that their behavior is different. It has been shown that the PU foams are valid models for pedicle screw pullout when comparing pedicle screw holding strengths (Chapman, 1996). Dawson et al. (2003) discussed the clinical relevance pullout testing of pedicle screws in PU foams and suggested that they should not be used as such. Thompson et al. (2003) suggested that PU foams should not be used to model the yield and ultimate properties of trabecular bone without further testing. We have found that PU foams are not relevant as models for pedicle screws in trabecular bone, since their plastic and elastic strain behaviors are not within any reasonable measure close to that of human or porcine trabecular bone.

Previous attempts to verify the validity of PU foams as trabecular bone models have focused on measurements of continuous material properties such as the modulus of elasticity, density, compressive maximum stress, shear modulus and the maximum shear stress. These properties are useful, but focus mainly on the failure properties of the implant in trabecular bone. We suggest that these become secondary to the specification of PU foams as models for trabecular bone by elastic and plastic strain performance below failure level loading. If the plastic and elastic strain behavior of PU foams are matched to that of trabecular bone, then inexpensive testing may be done to better understand the affects of implants on trabecular bone surrounding spinal instrumentation

during in vivo loading. Pedicle screws rarely fail in the in vivo environment by pullout, but as a consequence of screw loosening during normal in vivo loading.

Pedicle screw designs that maximize screw purchase by utilizing the elastic or plastic interaction with trabecular bone may improve the performance of pedicle screw instrumentation. Understanding the bony deformations around the screws is critical to this process. Due to the highly nonlinear nature of the trabecular bone deformations and the uncertainty of local material properties, it is unlikely that analytical approaches would yield relevant information.

Bibliography

1. Bay, BK; Smith, TS; Tyhrie, DP; Saad, M. *Digital Volume Correlation: Three-dimensional Strain Mapping Using X-ray Tomography.* Experimental Mechanics, 1999, 39:217-226.
2. Blake, Alexander; *What Every Engineer Should Know About Threaded Fasteners: Material and Design.* Lawrence Livermore National Laboratory; Marcel Dekker, Inc.; copyright 1986.
3. Bruck, HA; McNeil, SR; Sutton, MA; Peters, WH, III. *Digital Image Correlation Using Newton-Raphson Method of Partial Differential Correction.* Experimental Mechanics, 1989, 29: 261-267.
4. Oktenoglu, B. Tunc, MD; Ferrara LA, MS; Andalkar N, BA; Fahir Ozer A, MD; Sarioglu AC, MD; Benzel EC, MD. *Effects of Hole Preparation on Screw Pullout Resistance and Insertional Torque: A Biomechanical Study.* Journal of Neurosurgery, 2001, 94:91-96.
5. Chapman, JR; Harrington, RM; Lee, KM; Anderson, PA; Tencer, AF; Kowalski, D. *Factors Affecting the Pullout Strength of Cancellous Bone Screws.* Journal of Biomechanical Engineering, 1996, 118:391-398.
6. Currey, JD. *Mechanical Properties of Vertebrate Hard Tissues.* Proceedings of the Institution of Mechanical Engineers, Part H: Journal of Engineering in Medicine, 1998, 212:399-411.
7. Dawson, JM; Boschert, P; Macenski, MM; Rand, N. *Clinical Relevance of Pull-out Strength Testing of Pedicle Screws. Spinal Implants: Are We Evaluating Them Appropriately, ASTM STP 1431.* Melkerson, MN; Griffith, SL; Dirkpatrick, S Eds.; ASTM International, West Conshohocken, PA, 2003.
8. Dickman, CA; Fessler, RG; MacMillan, M; Haid, RW. *Transpedicular Screw-Rod Fixation of the Lumbar Spine: Operative Technique and Outcome in 104 Cases.* Journal of Neurosurgery, 1992, 77: 860-870.
9. Feldkamp, LA; Davis, LC; Dress, JW. *Practical Cone-beam Algorithm.* Journal of the Optical Society of America A: Optics and Image Science. 1984, 1, no. 6: 612-619.
10. Fenech, CM; Keaveny, TM. *A Cellular Solid Criterion for Predicting the Axial-Shear Failure Properties of Bovine Trabecular Bone.* Transaction of the ASME, 1999, 121:414-422.
11. Geers, MGD; DeBorst, R; Bredelmans, WAM. *Computing Strain Fields from Discrete Displacement Fields in 2-D Solids.* International Journal of Solids and Structures, 1996, 33: 4293-4307.
12. Gibson, LJ. *The Mechanical Behavior of Cancellous Bone.* Journal of Biomechanics, 1985, 18, no. 5:317-328.
13. Gibson, L and Ashby, M. *Cellular Solids: Structures & Properties*, Cambridge University Press, New York, 2nd ed., 1997, pp. 316-331.
14. Gill, PE; Murray, W; Wright, MH. *Practical Optimization*, Academic Press, London, 1981: 133-140.

15. Glaser, J; Stanley, M; Sayre, H; Woody, J; Found, E; Spratt, K. *A 10-Year Follow-up Evaluation of Lumbar Spine Fusion With Pedicle Screw Fixation.* Spine, 2003, 28 no. 13: 1390-1395.
16. Halvorson, TL; Kelley, LA; Thomas, KA; Whitecloud, TS; Cook, SD. *Effects of Bone Mineral Density on Pedicle Screw Fixation.* Spine, 1994, 19 no. 21: 2415-2420.
17. Isador H. Lieberman, BSc, MD, FRCS(C), * Rabi Khazim, MD, FRCS(C), and Terence Woodside, BScEng. *Anterior Vertebral Body Screw Pullout Testing.* SPINE, 1998, 23:908-910.
18. Knauss, P. *Materialkennwerte und Fesitgkeitsverhalten des Spongiosen Knochengewebes am Coxalen Human-Femur.* Biomedizinische Technik, 26:200-210.
19. Kowalski, JM; Ludwig, SC; Hutton, WC; Heller, JG. *Cervical Spine Pedicle Screws: A Biomechanical Comparison of Two Insertion Techniques.* Spine, 2000, 25 no. 22: 2865-2867.
20. Kwok, AWL; Finkelstein, JA; Woodside, T; Hearn, TC; Hu, RW. *Insertional Torque and Pull-out Strengths of Conical and Cylindrical Pedicle Screws in Cadaveric Bone.* Spine, 1996, 21 no. 21:2429-2434.
21. Lancaster, P and Salkauskas, K. *Curve and Surface Fitting-An Introduction.* Academic Press, London, 1986: 190.
22. Lindahl, O. *Mechanical Properties of Dried Defatted Spongy Bone.* Acta Orthopaedica Scandinavica, 1976, 47, no. 1:11-19.
23. Mcafee, PC; Weiland, DJ; Carlow, JJ. *Survivorship Analysis of Pedicle Spinal Instrumentation. Spine*, 1991, 16 no. 8 supplement: S422-427.
24. Manohar M. Panjabi, PhD, Eon K. Shin, BA, Neal C. Chen, BS, and Jaw-Lin Wang, PhD. *Internal Morphology of Human Cervical Pedicles.* SPINE, 2000, 25:1197-1205.
25. McKinley, TO; McLain, RF; Yerby, SA; Sharkey, NA; Sarigul-Klijn, N; Smith, TS. *Characteristics of Pedicle Screw Loading.* Spine, 1999, 24 no. 1: 18-25.
26. McKinley, TO; McLain, RF; Yerby, SA; Sarigul-Klijn, N; Smith, TS. *The Effect of Pedicle Morphometry on Pedicle Screw Loading.* Spine, 1997, 22 no. 3: 246-252.
27. Moran, JM; Berg, WS; Berry, JL; Geiger, JM; Steffee, AD. *Transpedicular Screw Fixation.* Journal of Orthopaedic Research, 1989, 7 no. 1: 107-114.
28. Myers, BS; Belmont, PJ; Richardson, WJ; Yu, JR; Harper, KD; Nightingale, RW. *The Role of Imaging and In Situ Biomechanical Testing in Assessing Pedicle Screw Pull-out Strength.* Spine, 1996, 21 no. 17: 1962-1968.
29. Rohl, L; Larsen, E; Linde, F; Odgaard, A; Jorgensen, J. *Tensile and Compressive Properties of Cancellous Bone.* Journal of Biomechanics, 1991, 24, no. 12:1143-1149.
30. Rohlmann, A; Zilch, H; Bergmann, G; Kolbel, R; *Material Properties of Femoral Cancellous Bone in Axial Loading. Part I: Time Independent Properties.* Archives of Orthopaedic Trauma Surgery, 97, no. 2, 1980: 95-102.
31. Rohlmann, A; Graichen, F; Bergmann, G. *Influence of Load Carrying on Loads in Internal Spinal Fixators.* Journal of Biomechanics, 2000, 33:1099-1104.

32. Smith, TS; Bay, BK. *Experimental Measurement of Strains Using Digital Volume Correlation.* ASTM Special Technical Publication, 2001, n 1402: 117-126.
33. Smith, TS; Bay, BK; Rashid, MM. *Digital volume correlation including rotational degrees of freedom during minimization.* Experimental Mechanics, 2002, 42 no. 3: 272-278.
34. Sutton, MA; Wolters, WJ; Peters, WH; Ranson, WF; McNeil, SR. *Determination of Displacements Using an Improved Digital Correlation Method.* Image and Vision Computing, 1983, 1: 133-139.
35. Szivek, JA; Thompson, JD; Benjamin, JB. *Characterization of Three Formulations of a Synthetic Foam as Models for a Range of Human Cancellous Bone Types.* Journal of Applied Biomaterials, 1995, 6:125-128.
36. Tait S. Smith, Scott A. Yerby, Robert F. McLain, and Todd O. McKinley. *A Device for the Measurement of Pedicle Screw Moment by Means of Internal Strain Gages.* Journal of Biomechanical Engineering, 1996, 118:423-425.
37. Tan, JS; Kwon, BK; Samarasekera, D; Dvorak, MF; Fisher, CG; Oxland, TR. *Vertebral Bone Density - A Critical Element in the Performance of Spinal Implants.* ASTM Technical Publication, 2002, no. 1431: 217-230.
38. Thompson, MS; McCarthy, ID; Lidgren, L; Ryd, L. *Compressive and Shear Properties of Commercially Available Polyurethane Foams.* Transactions of the ASME, 2003, 125:732-734.
39. Weinstein, JN; Rydevik, BL; Rauschning, W. *Anatomic and Technical Considerations of Pedicle Screw Fixation.* Clinical Orthopaedics and Related Research, 1992, 284: 34-46.
40. Yerby, SA; Ehteshami, JR; McLain, RF. *Loading of Pedicle Screws within the Vertebra.* Journal of Biomechanics, 1997, 30 no. 9: 951-954.
41. Yerby, SA; Toh, E; McLain, RF. *Revision of Failed Pedicle Screws Using Hydroxyapatite Cement: A Biomechanical Analysis.* Spine, 1998, 23 no. 15: 1657-1661.
42. Zdeblick, TA; Kunz, DN; Cooke, ME; McCabe, R. *Pedicle Screw Pullout Strength: Correlation with Insertionl Torque.* Spine, 1993, 18 no. 12: 1673-1676.

Appendix A

Additional Results

PLASTIC STRAINS

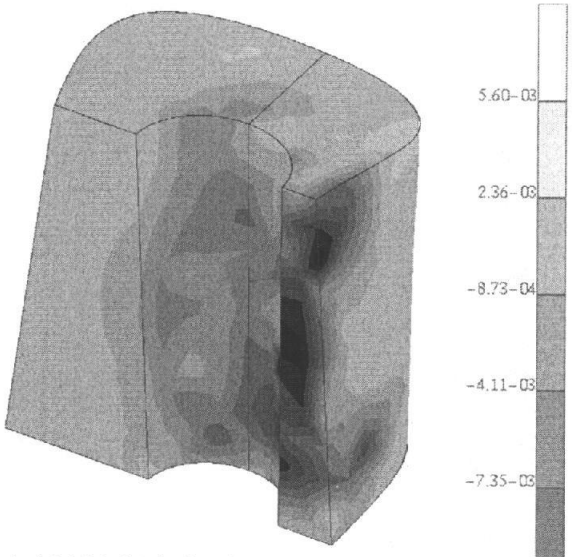

a) 41258-l1-left-plastic-minprin

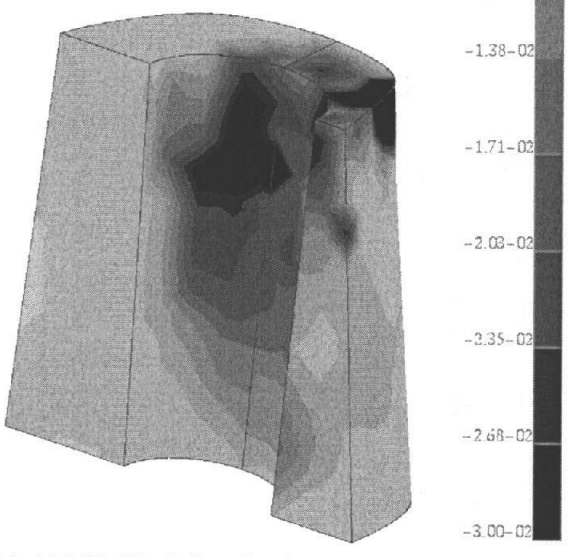

b) 41258-l1-right-plastic-minprin

Figure 21. Minimum principal strains within the regions of interest: Before insertion correlated with after extraction.

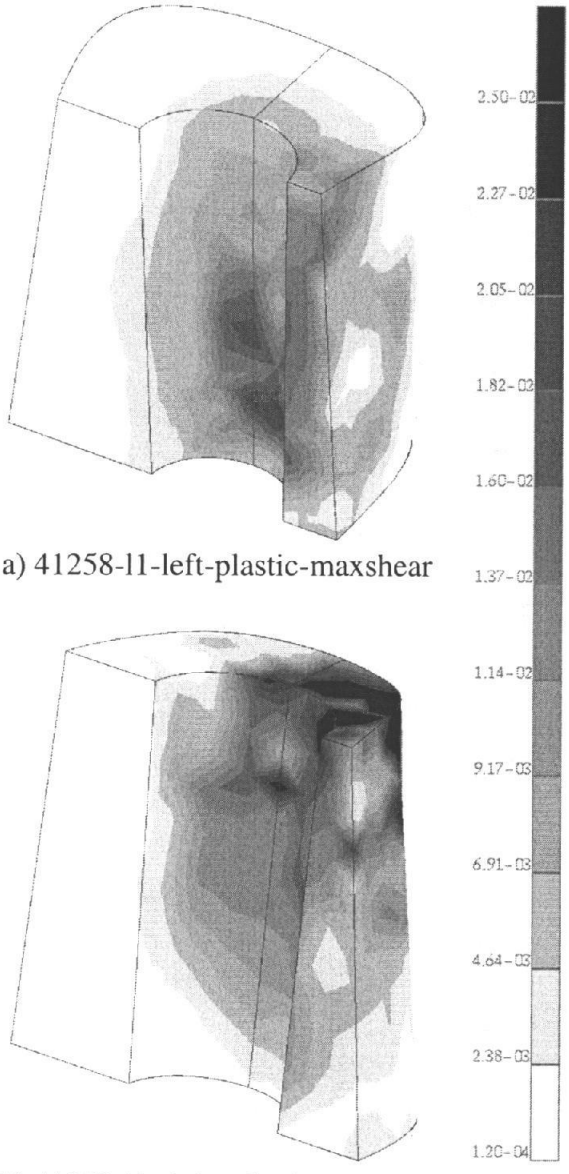

a) 41258-l1-left-plastic-maxshear

b) 41258-l1-right-plastic-maxshear

Figure 22. Maximum shear strains within the regions of interest: Before insertion correlated with after extraction.

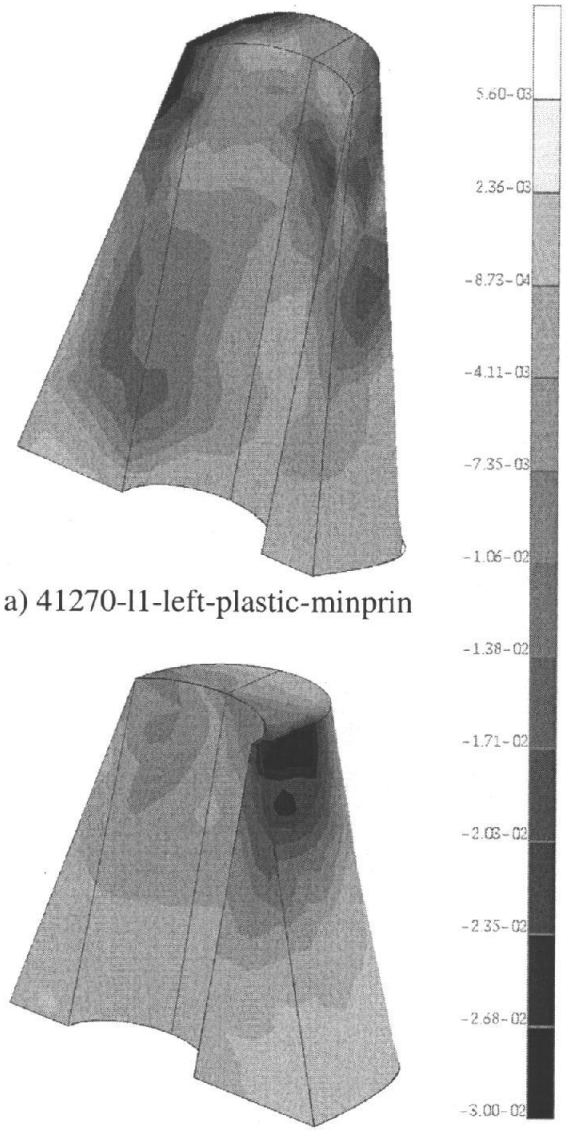

a) 41270-l1-left-plastic-minprin

b) 41270-l1-right-plastic-minprin

Figure 23. Maximum shear strains within the regions of interest: Before insertion correlated with after extraction.

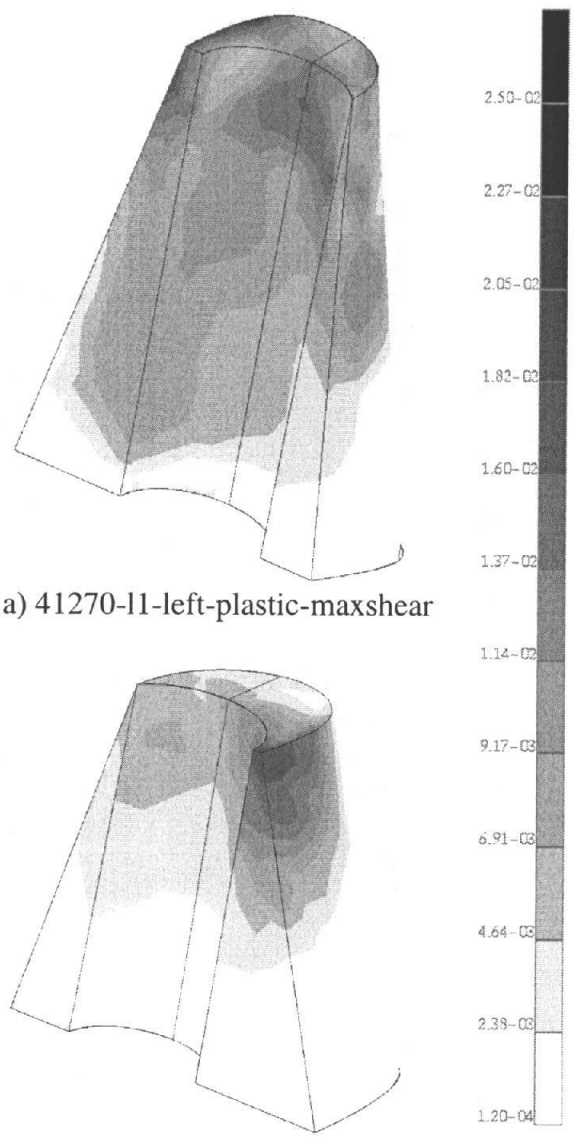

a) 41270-l1-left-plastic-maxshear

b) 41270-l1-right-plastic-maxshear

Figure 24. Maximum shear strains within the regions of interest: Before insertion correlated with after extraction.

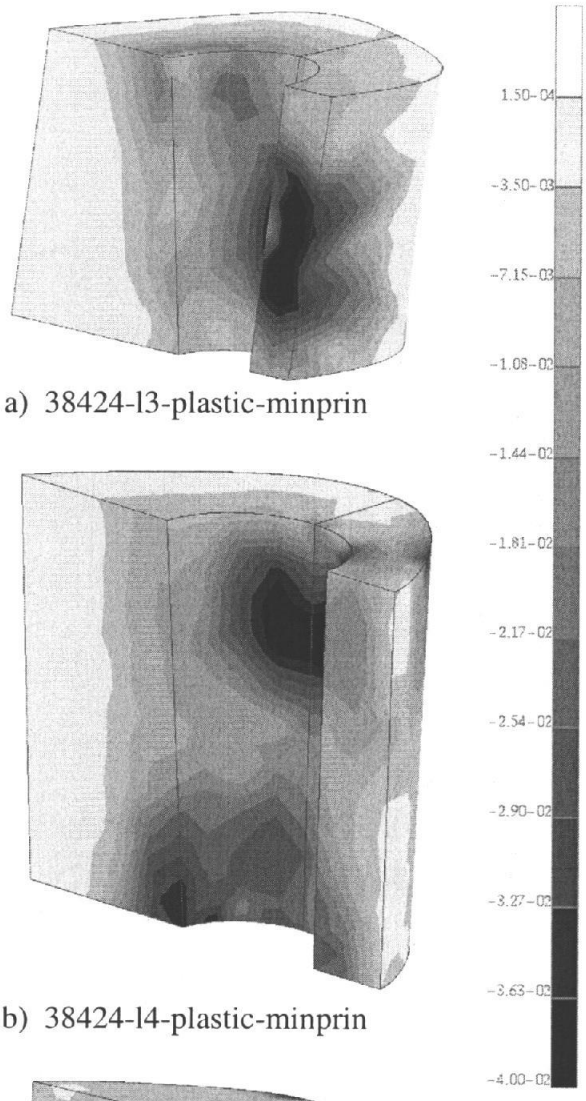

a) 38424-l3-plastic-minprin

b) 38424-l4-plastic-minprin

c) 38424-l5-plastic-minprin

Figure 25. Minimum principle strains within the regions of interest: Before insertion correlated with after extraction.

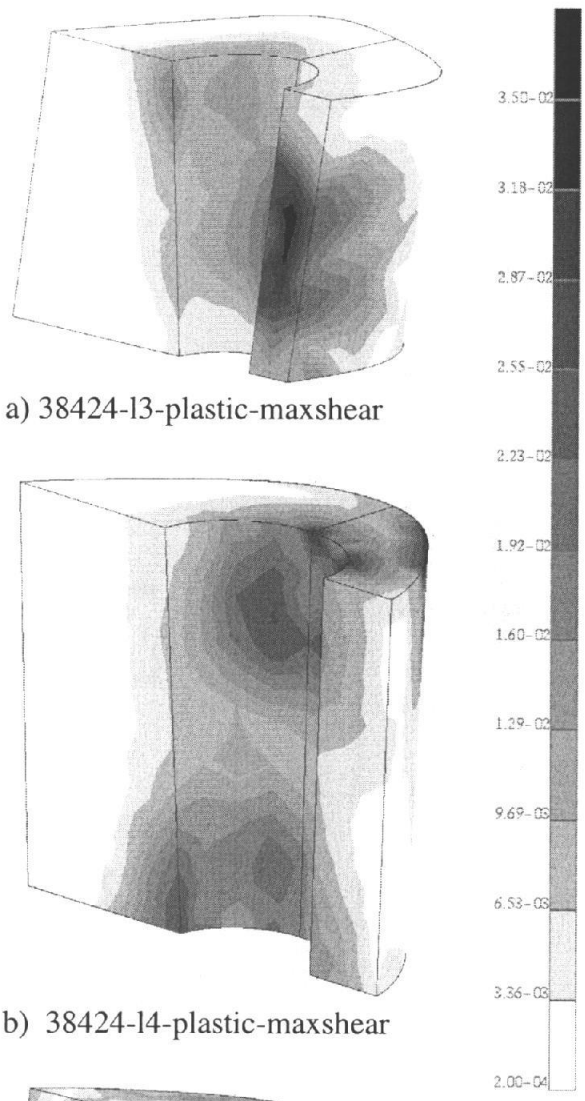

a) 38424-l3-plastic-maxshear

b) 38424-l4-plastic-maxshear

c) 38424-l5-plastic-maxshear

Figure 26. Maximum shear strains within the regions of interest: Before insertion correlated with after extraction.

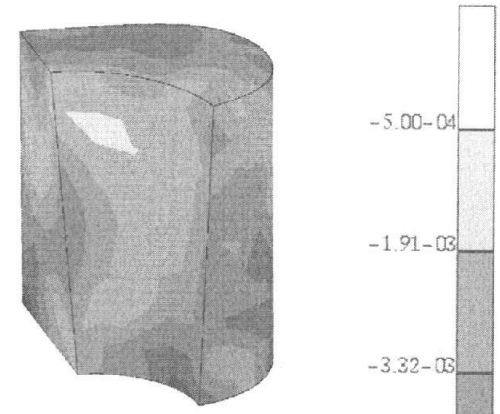

a) pigl3-plastic-minprin

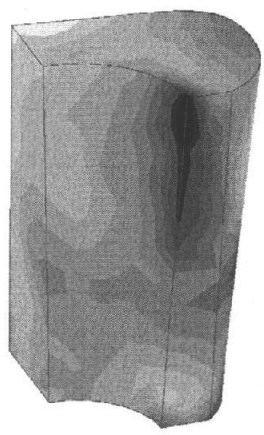

b) pigl4-plastic-minprin

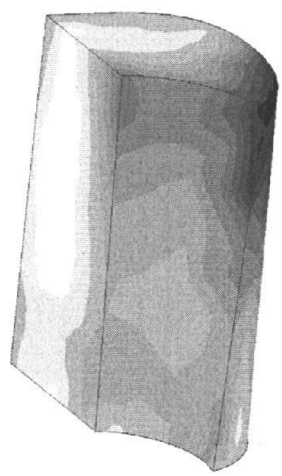

c) pigl5-plastic-minprin

Figure 27. Minimum principle strains within the regions of interest: Before insertion correlated with after extraction.

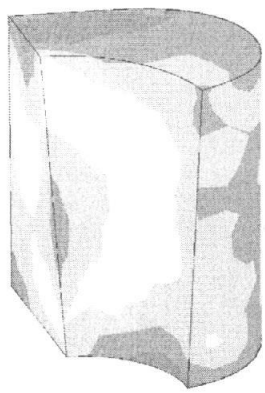

a) pigl3-plastic-maxshear

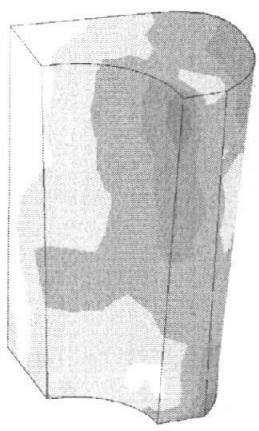

b) pigl4-plastic-maxshear

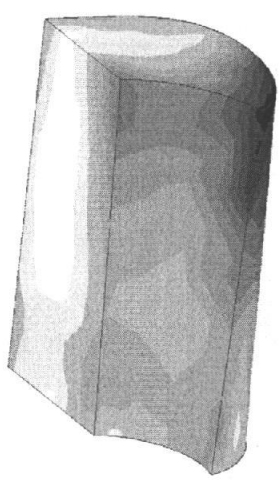

c) pigl5-plastic-maxshear

Figure 28. Maximum shear strains within the regions of interest: Before insertion correlated with after extraction.

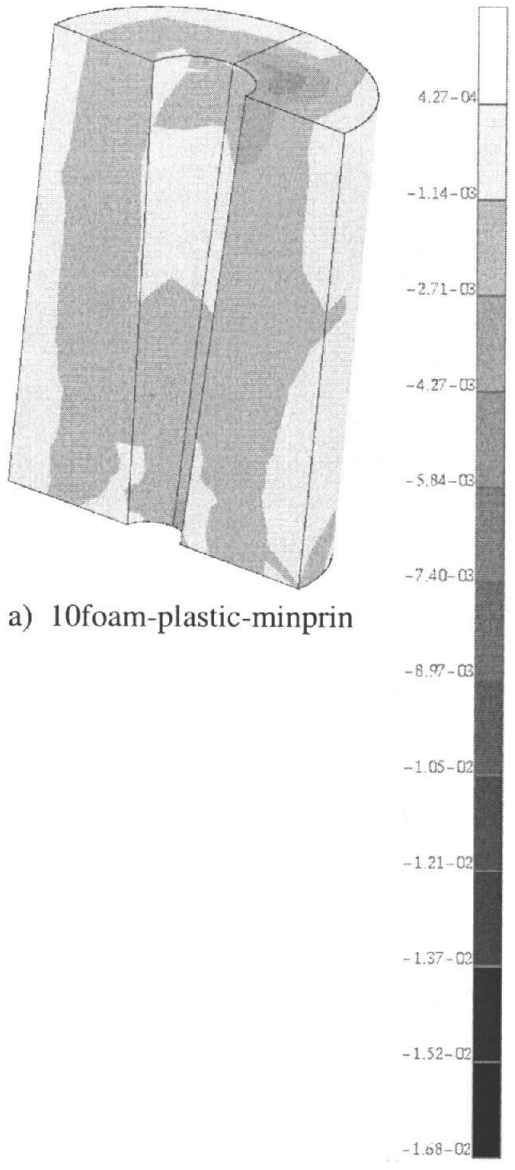

a) 10foam-plastic-minprin

Figure 29. Minimum principle strains within the regions of interest: Before insertion correlated with after extraction.

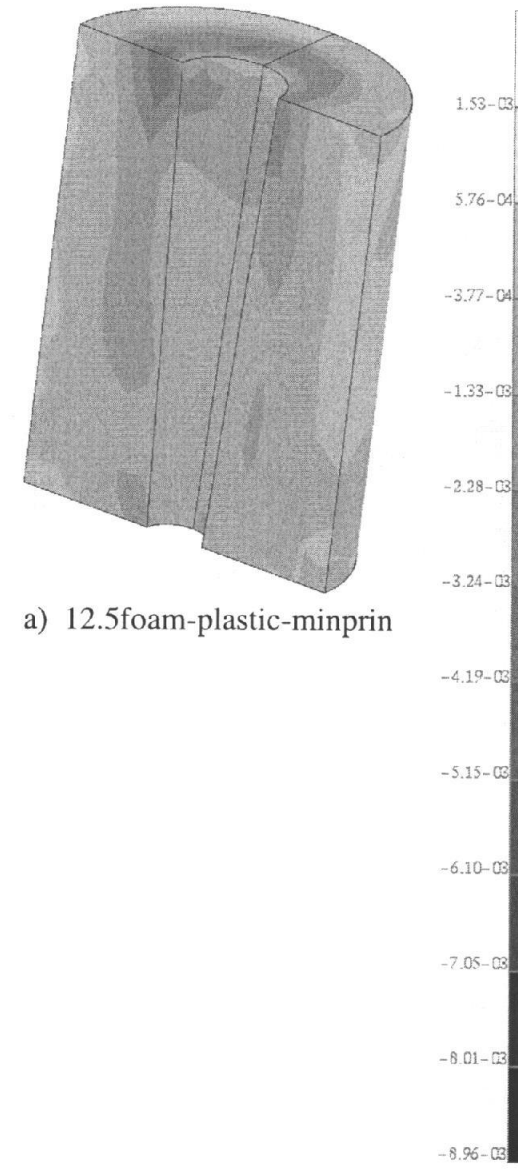

a) 12.5foam-plastic-minprin

Figure 30. Minimum principle strains within the regions of interest: Before insertion correlated with after extraction.

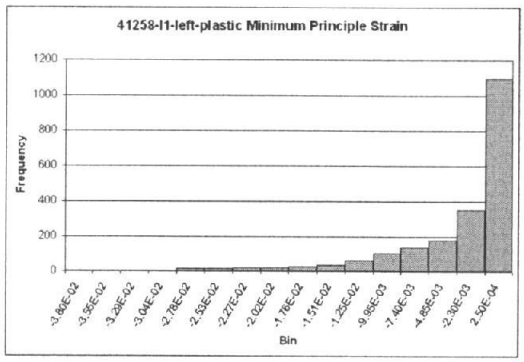

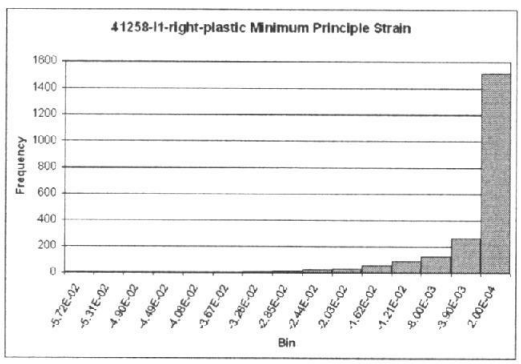

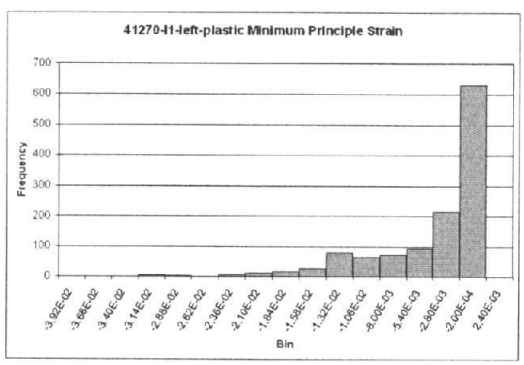

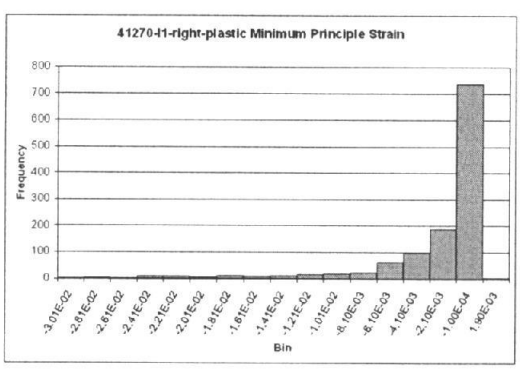

Figure31. Histograms of plastic minimum principle strains for each sample.

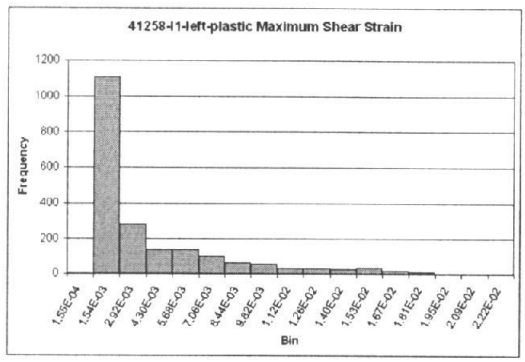

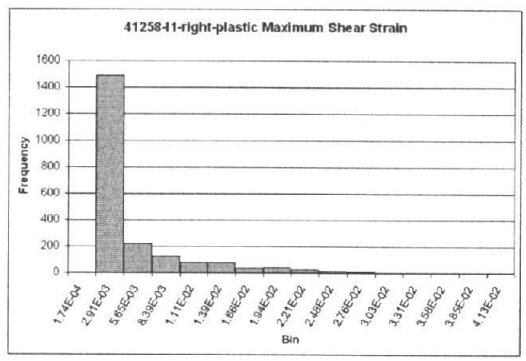

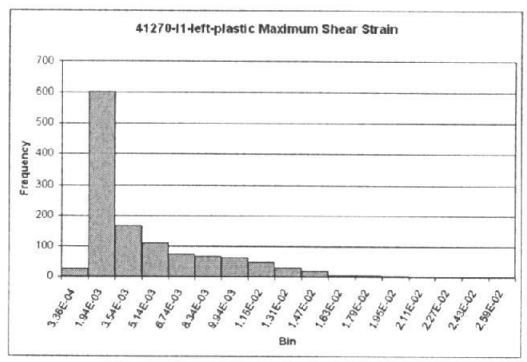

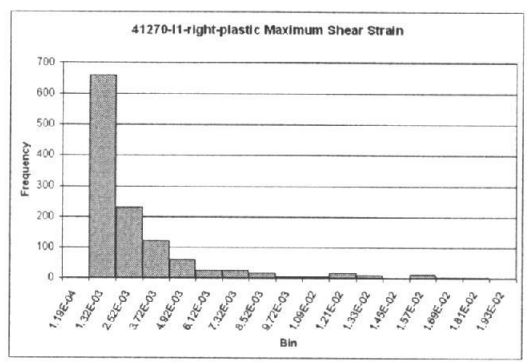

Figure 32. Histograms of plastic maximum shear strains for each sample.

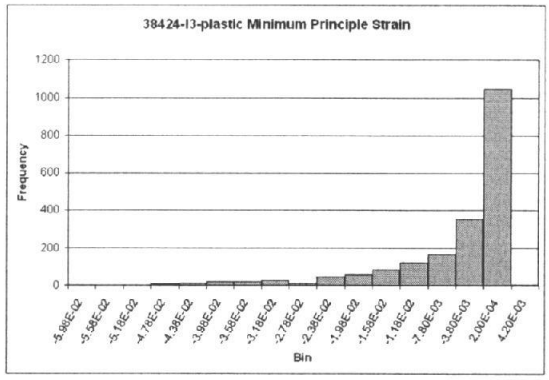

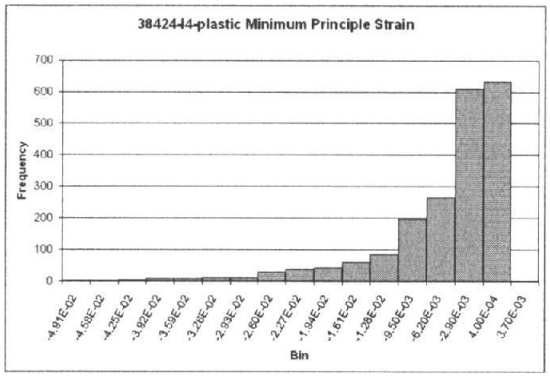

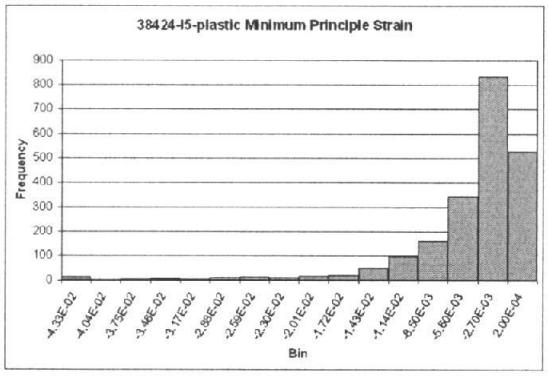

Figure 33. Histograms of plastic minimum principle strains for each sample.

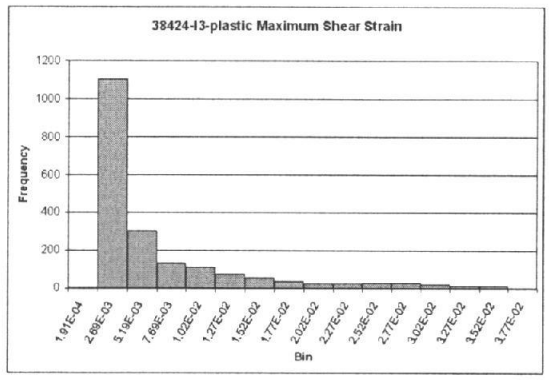

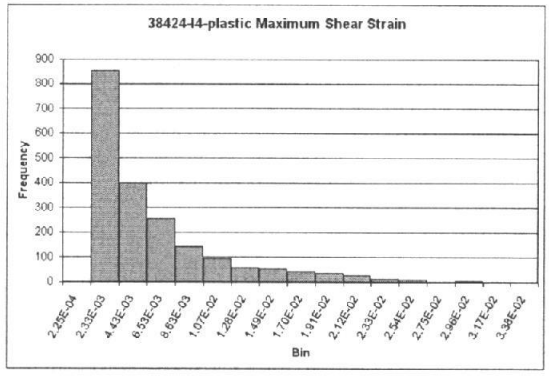

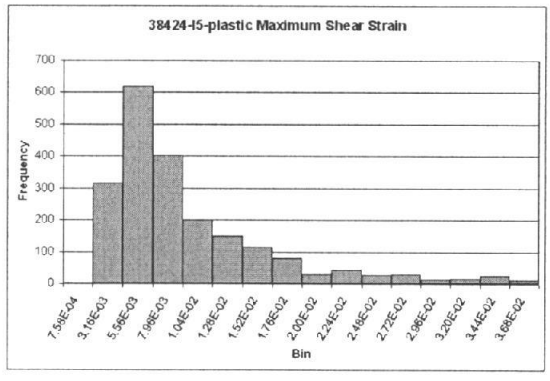

Figure 34. Histograms of plastic maximum shear strains for each sample.

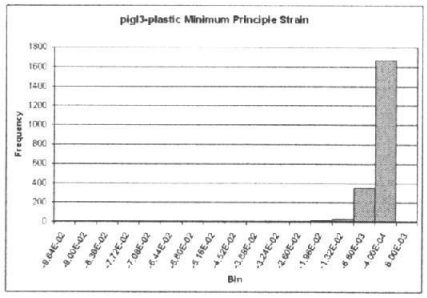

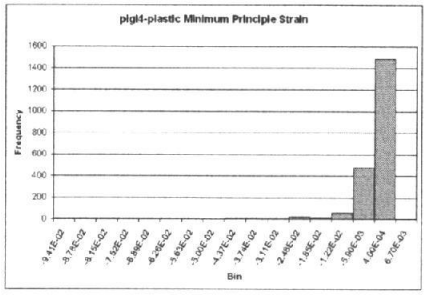

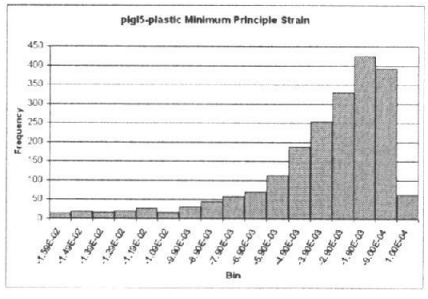

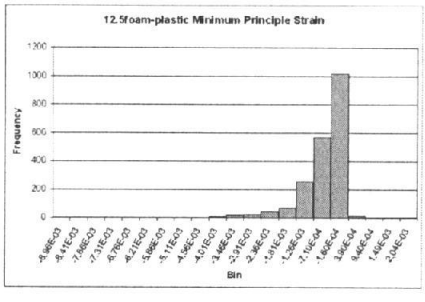

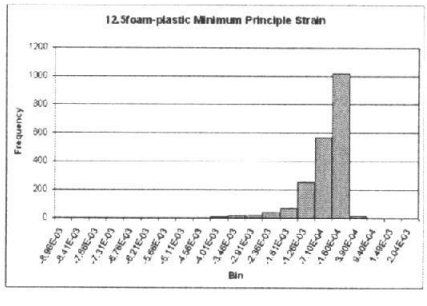

Figure 35. Histograms of plastic minimum principle strains for each sample.

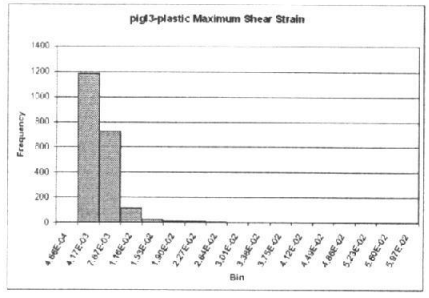

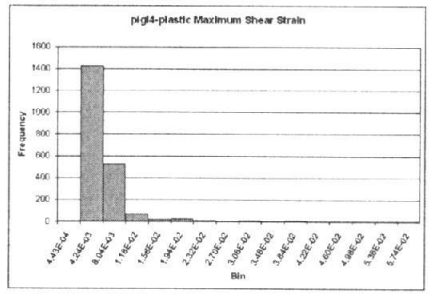

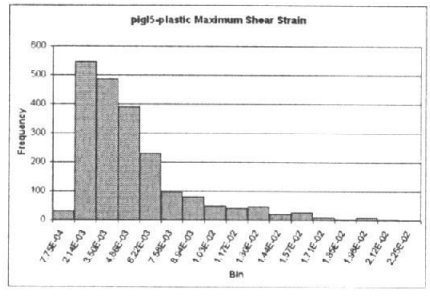

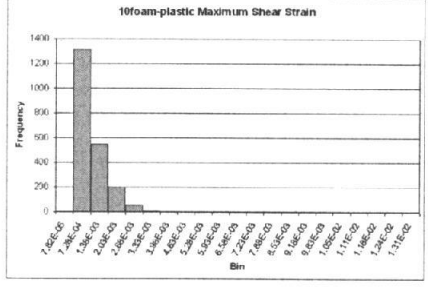

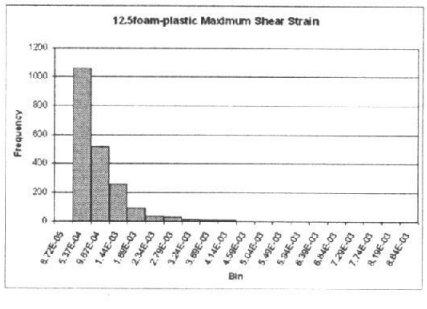

Figure 36. Histograms of plastic maximum shear strains for each sample.

ELASTIC STRAINS

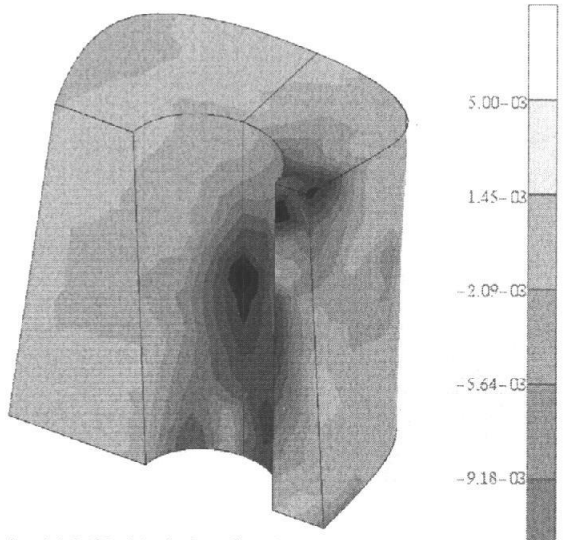

a) 41258-l1-left-elastic-minprin

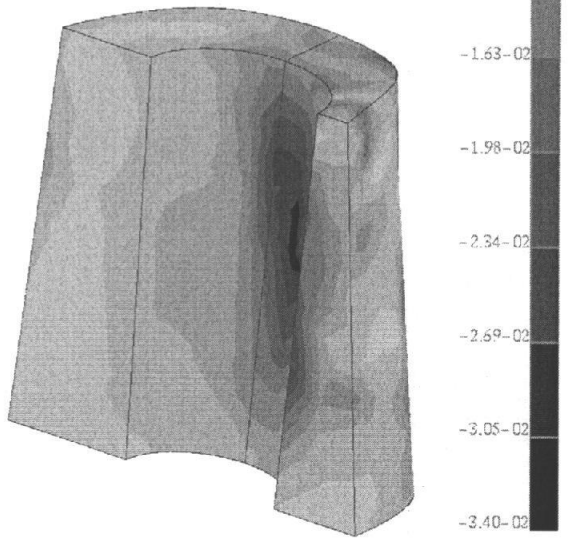

b) 41258-l1-right-elastic-minprin

Figure 37. Minimum principle strains within the regions of interest: Full insertion correlated with after extraction.

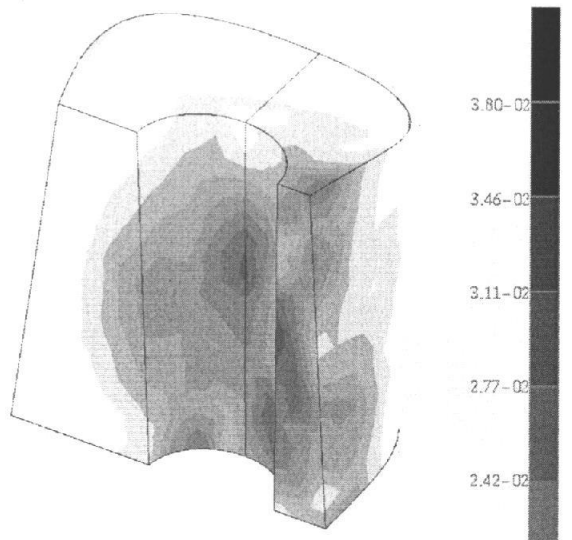

a) 41258-l1-left-elastic-maxsh.

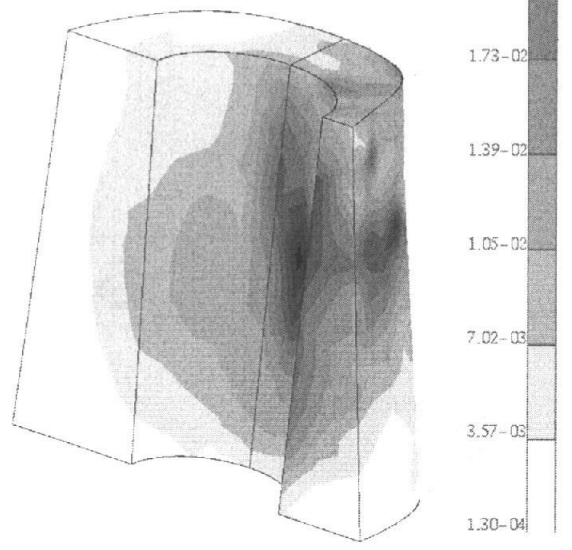

b) 41258-l1-right-elastic-maxshear

Figure 38. Maximum shear strains within the regions of interest: Full insertion correlated with after extraction.

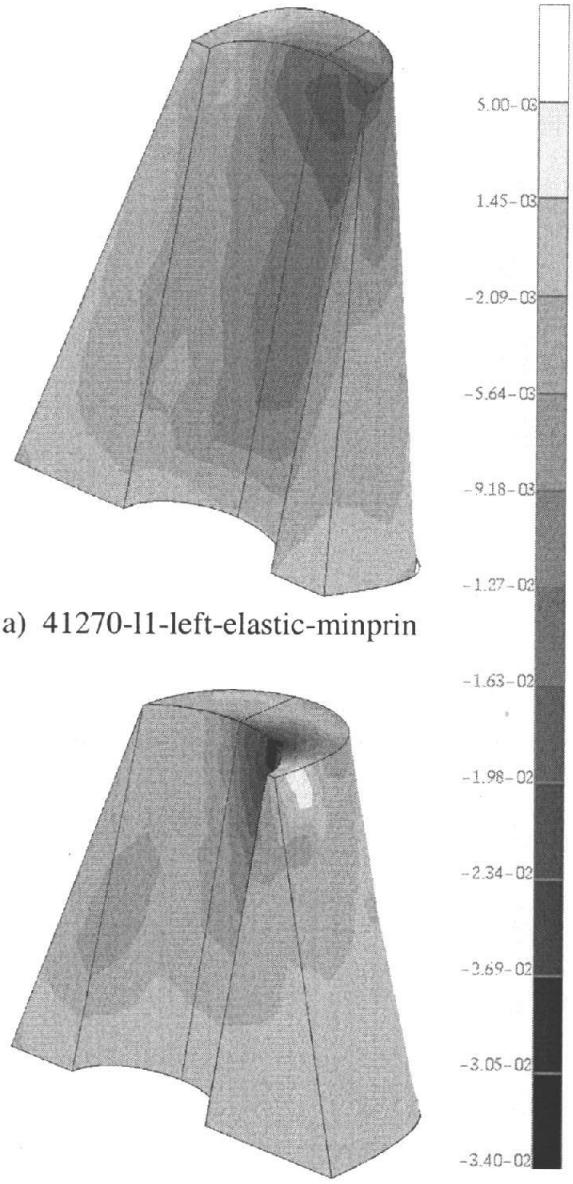

a) 41270-l1-left-elastic-minprin

b) 41270-l1-right-elastic-minprin

Figure 39. Minimum principle strains within the regions of interest: Full insertion correlated with after extraction.

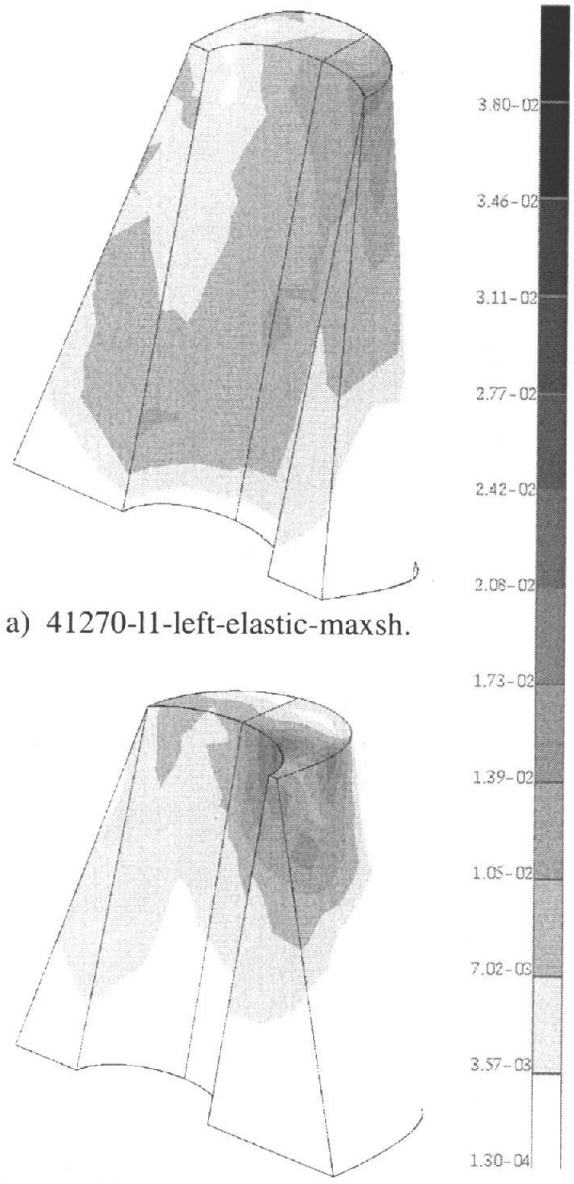

a) 41270-l1-left-elastic-maxsh.

b) 41270-l1-right-elastic-maxshear

Figure 40. Maximum shear strains within the regions of interest: Full insertion correlated with after extraction.

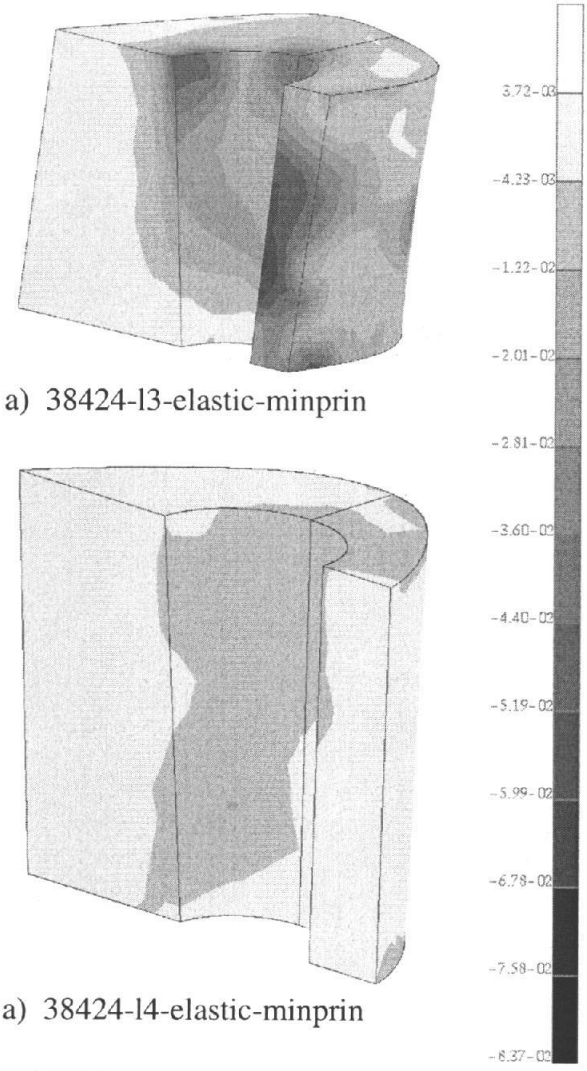

a) 38424-l3-elastic-minprin

a) 38424-l4-elastic-minprin

a) 38424-l5-elastic-minprin

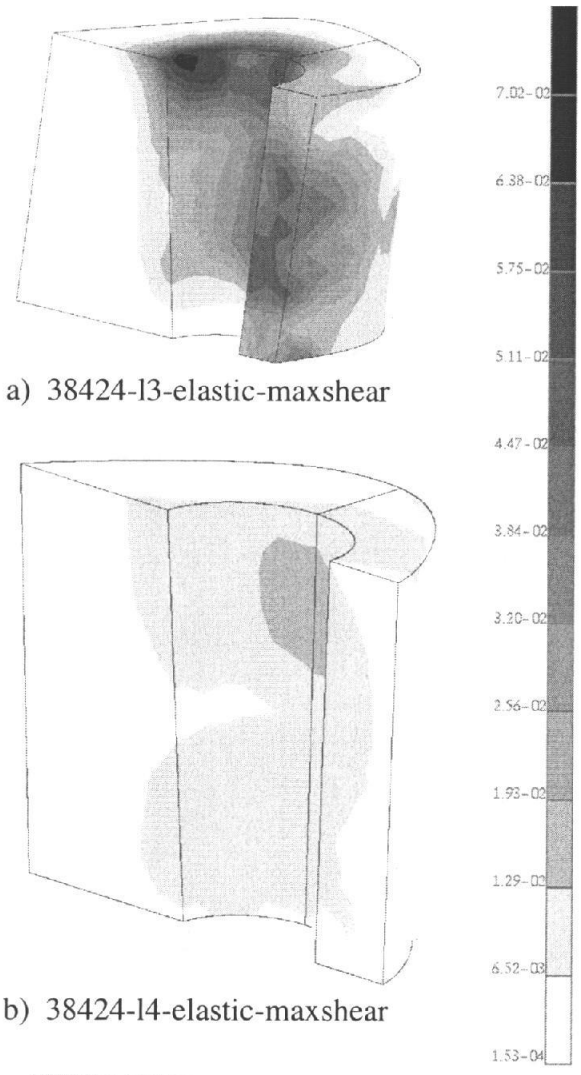

a) 38424-l3-elastic-maxshear

b) 38424-l4-elastic-maxshear

c) 38424-l5-elastic-maxshear

Figure 41. Minimum principle strains within the regions of interest: Full insertion correlated with after extraction.

Figure 42. Maximum shear strains within the regions of interest: Full insertion correlated with after extraction.

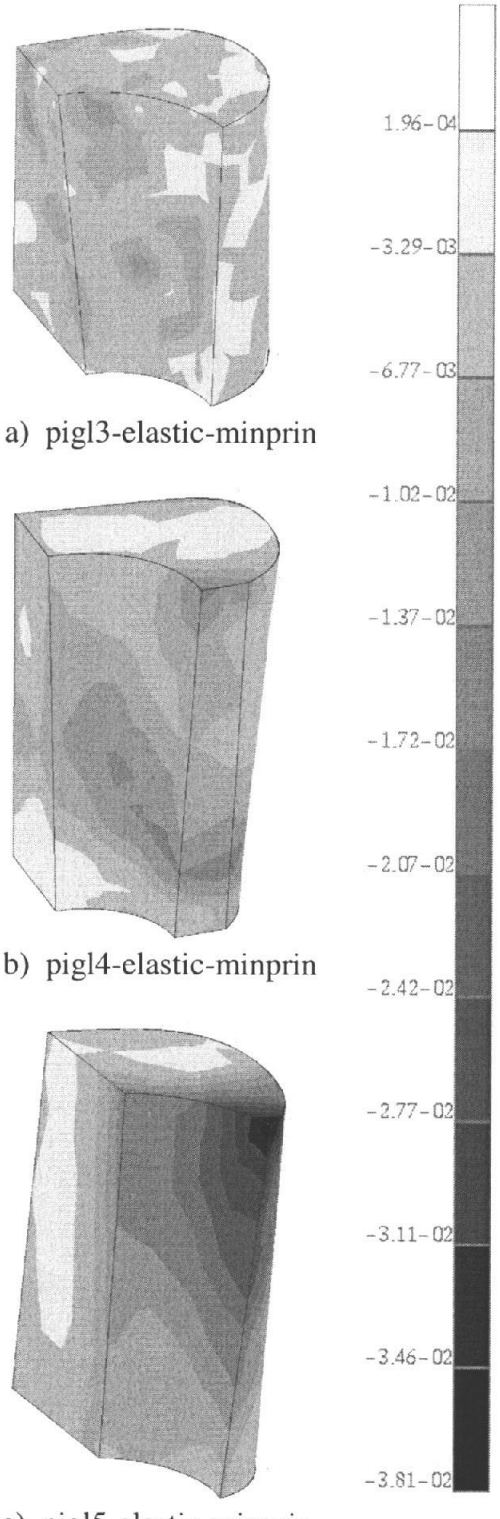

a) pigl3-elastic-minprin

b) pigl4-elastic-minprin

c) pigl5-elastic-minprin

Figure 43. Minimum principle strains within the regions of interest: Full insertion correlated with after extraction.

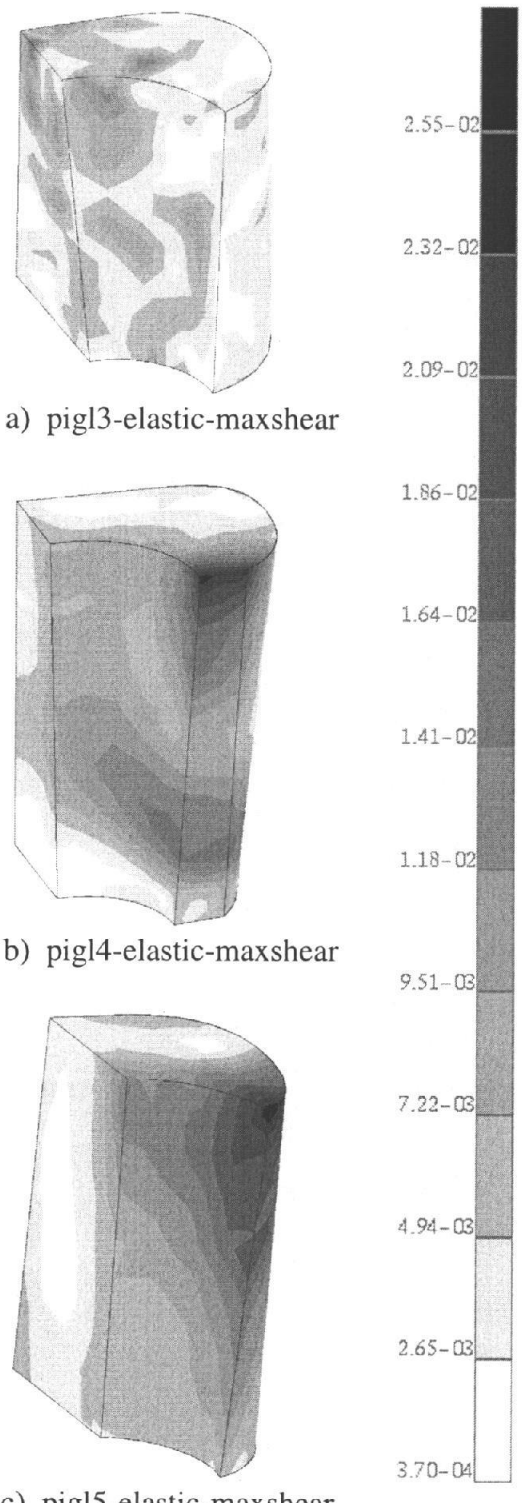

a) pigl3-elastic-maxshear

b) pigl4-elastic-maxshear

c) pigl5-elastic-maxshear

Figure 44. Maximum shear strains within the regions of interest: Full insertion correlated with after extraction.

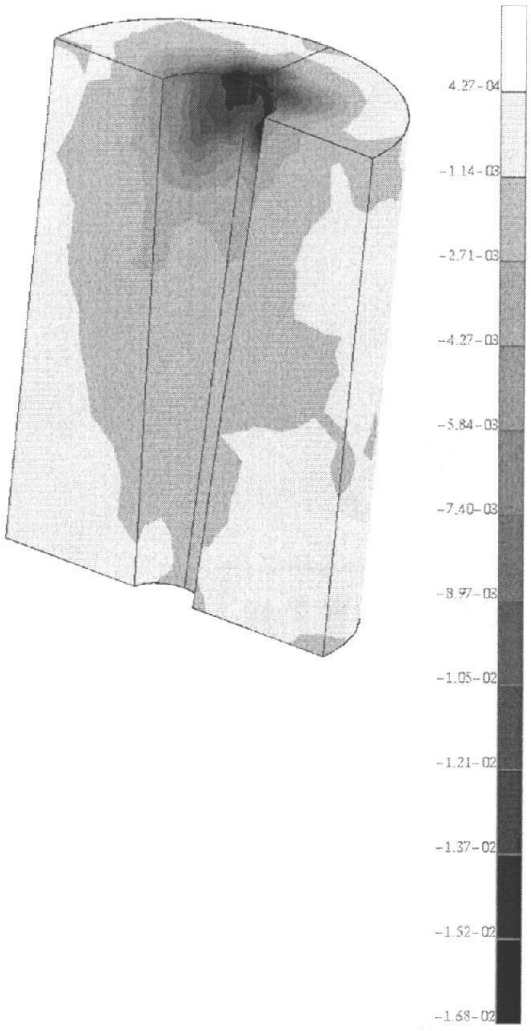

Figure 45. Minimum principle strains within the regions of interest: Full insertion correlated with after extraction.

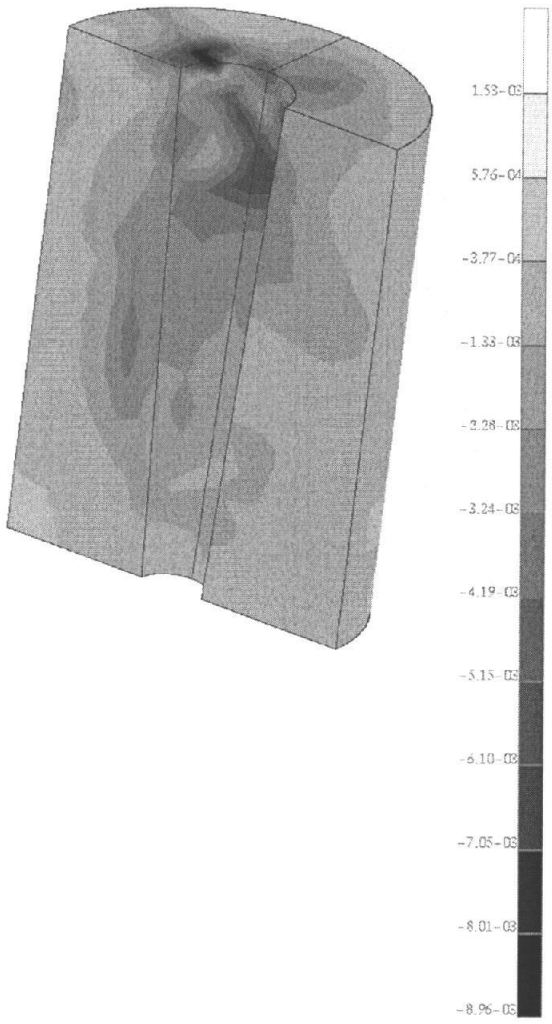

Figure 46. Minimum principle strains within the regions of interest: Full insertion correlated with after extraction.

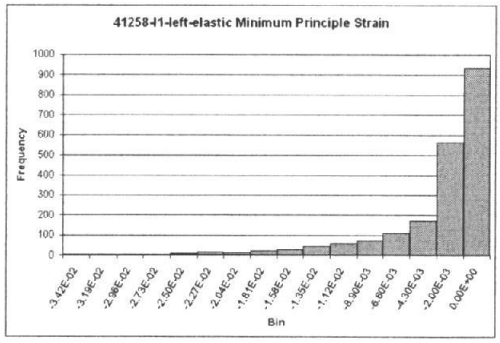

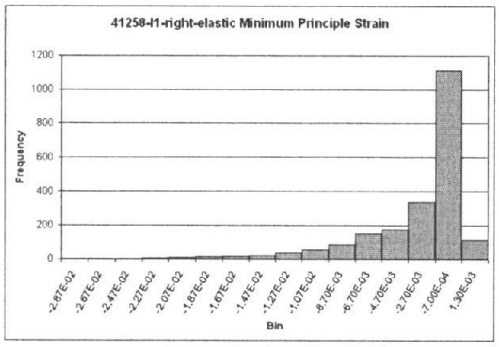

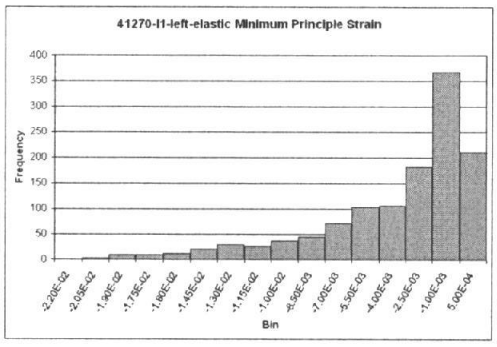

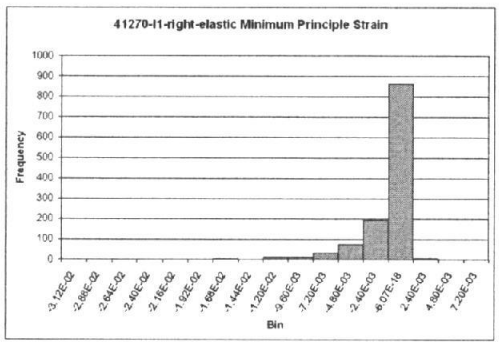

Figure 47. Histograms of elastic minimum principle strains for each sample.

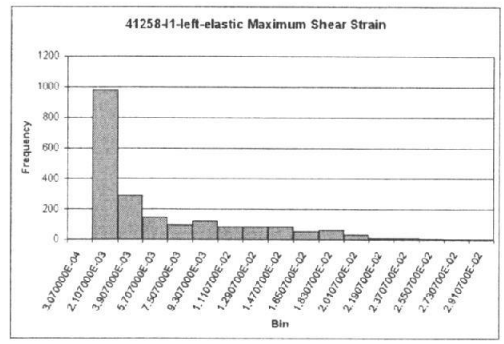

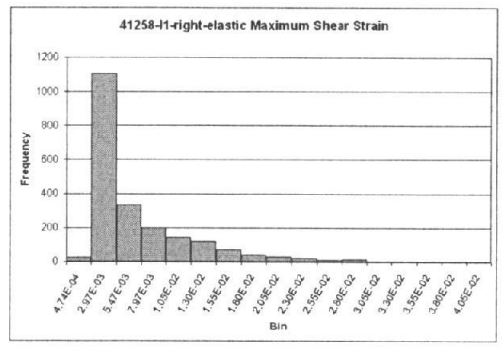

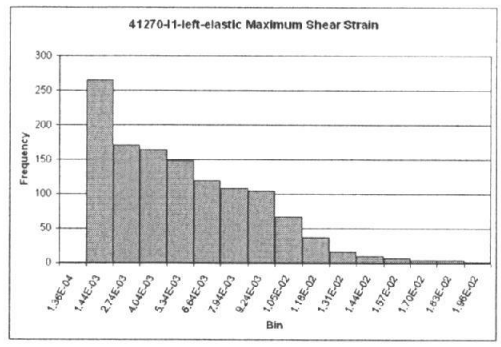

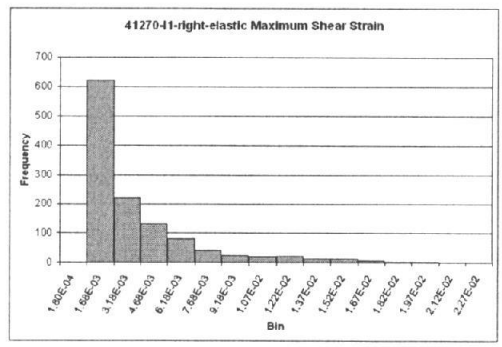

Figure 48. Histograms of elastic maximum shear strains for each sample.

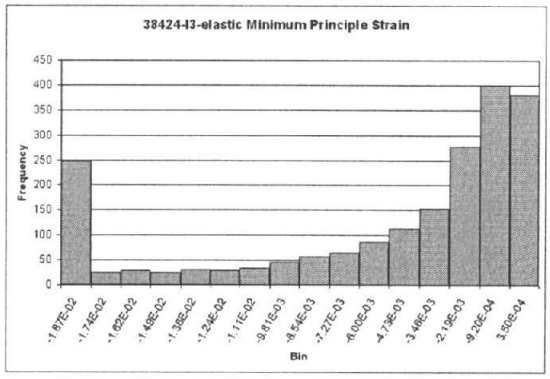

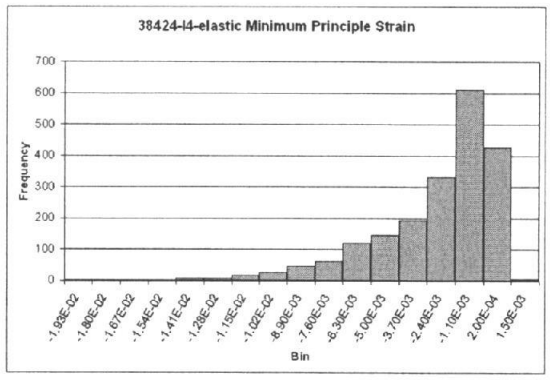

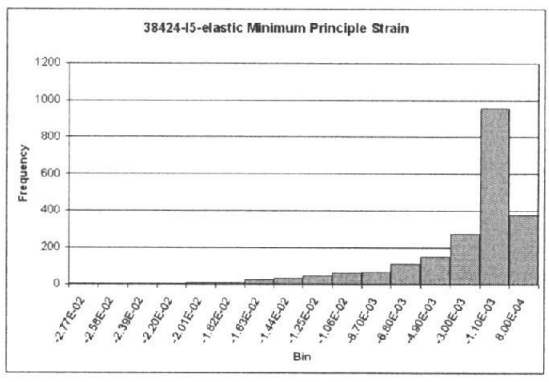

Figure 49. Histograms of elastic minimum principle strains for each sample.

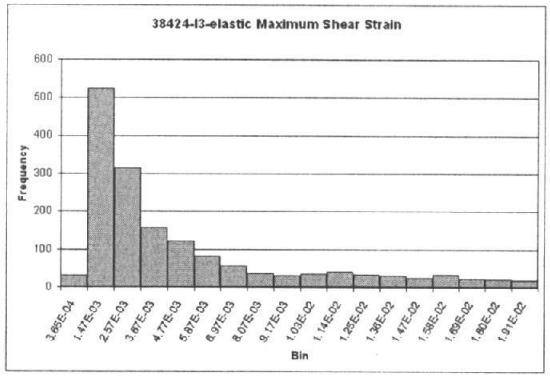

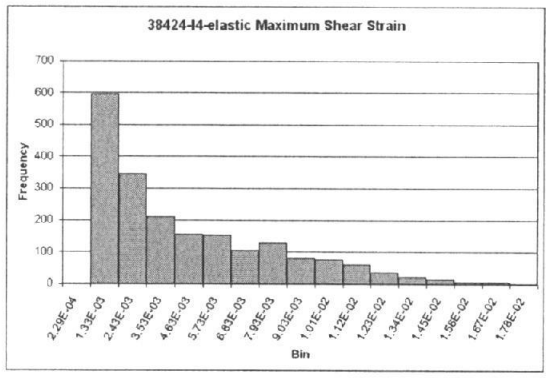

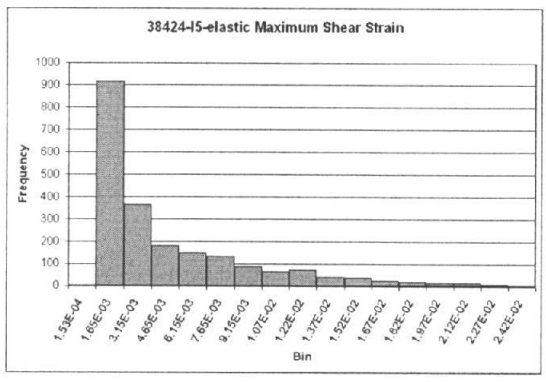

Figure 50. Histograms of elastic maximum shear strains for each sample.

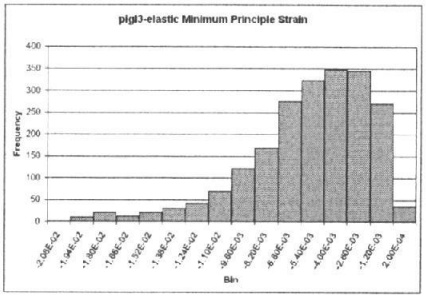

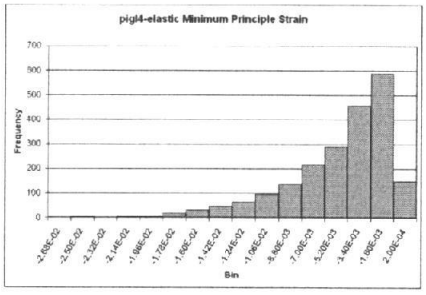

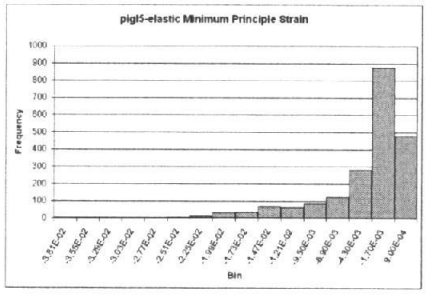

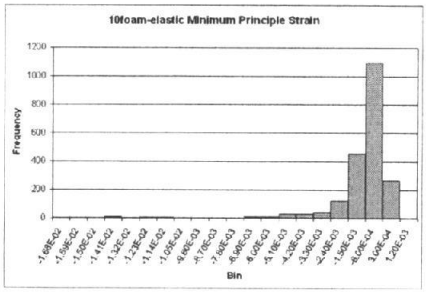

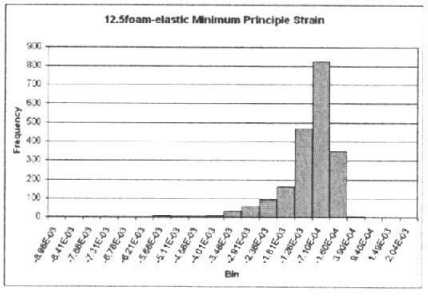

Figure 51. Histograms of elastic minimum principle strains for each sample.

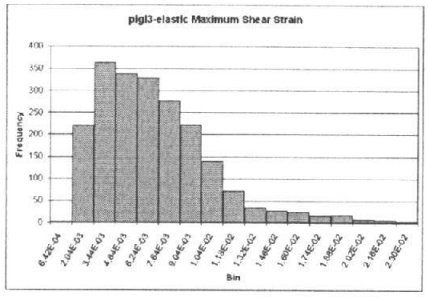

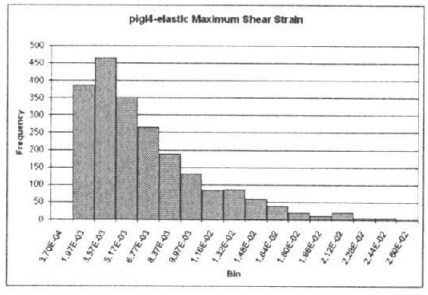

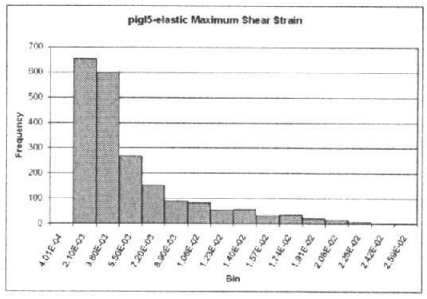

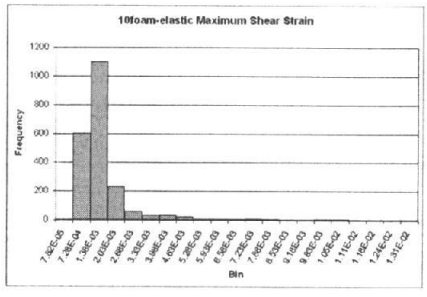

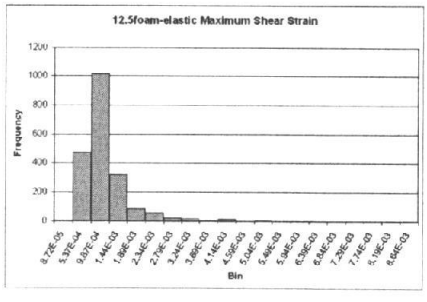

Figure 52. Histograms of elastic maximum shear strains for each sample.

TOTAL STRAINS

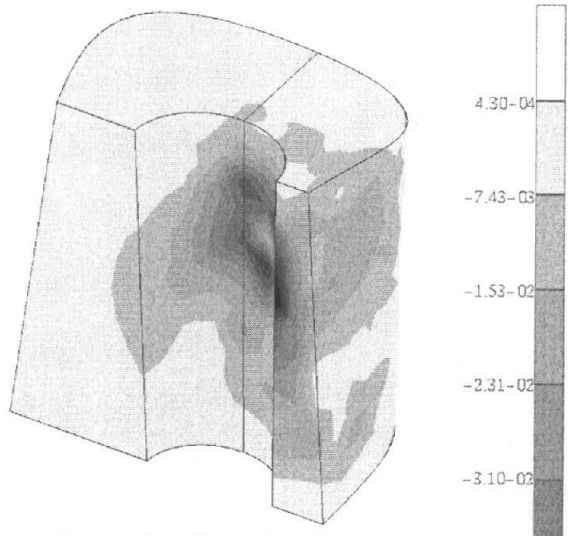

a) 41258-l1-left-total-minprin

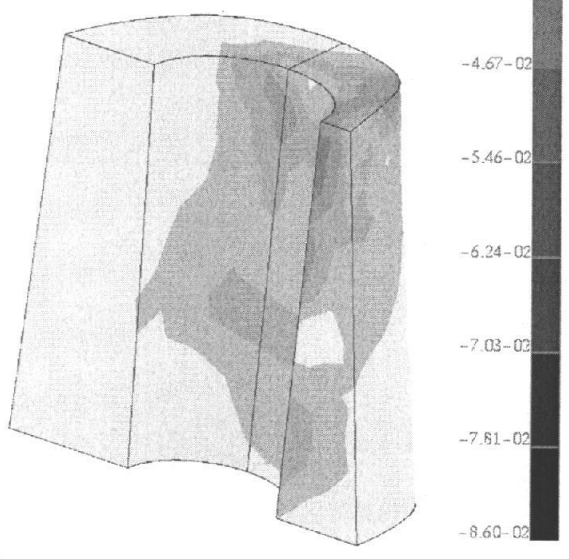

b) 41258-l1-right-total-minprin

Figure 53. Minimum principle strains within the regions of interest: Before insertion correlated with full insertion.

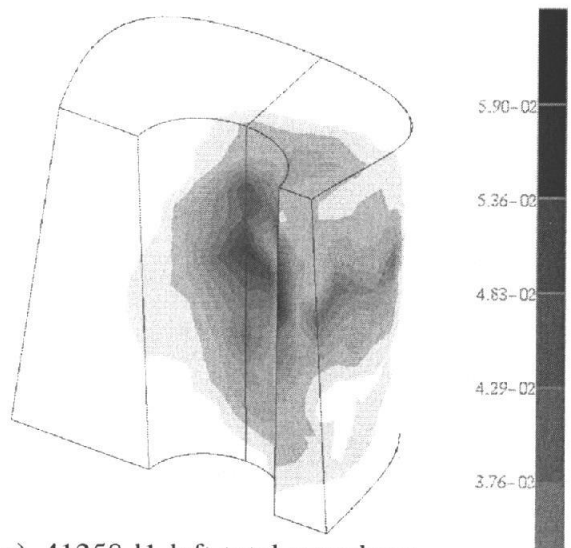

a) 41258-l1-left-total-maxshear

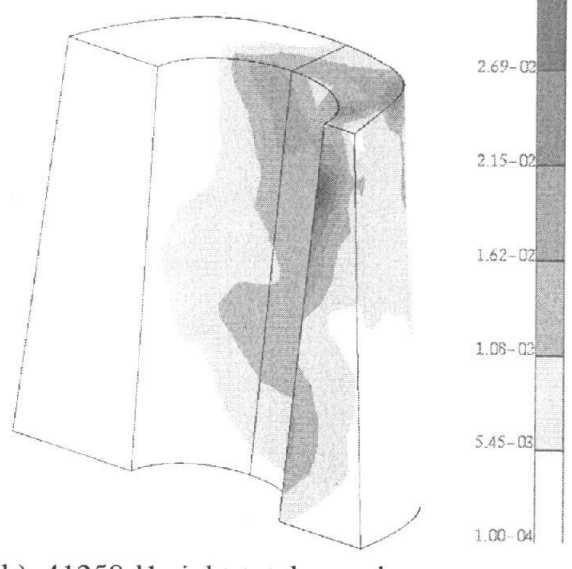

b) 41258-l1-right-total-maxshear

Figure 54. Maximum shear strains within the regions of interest: Before insertion correlated with full insertion.

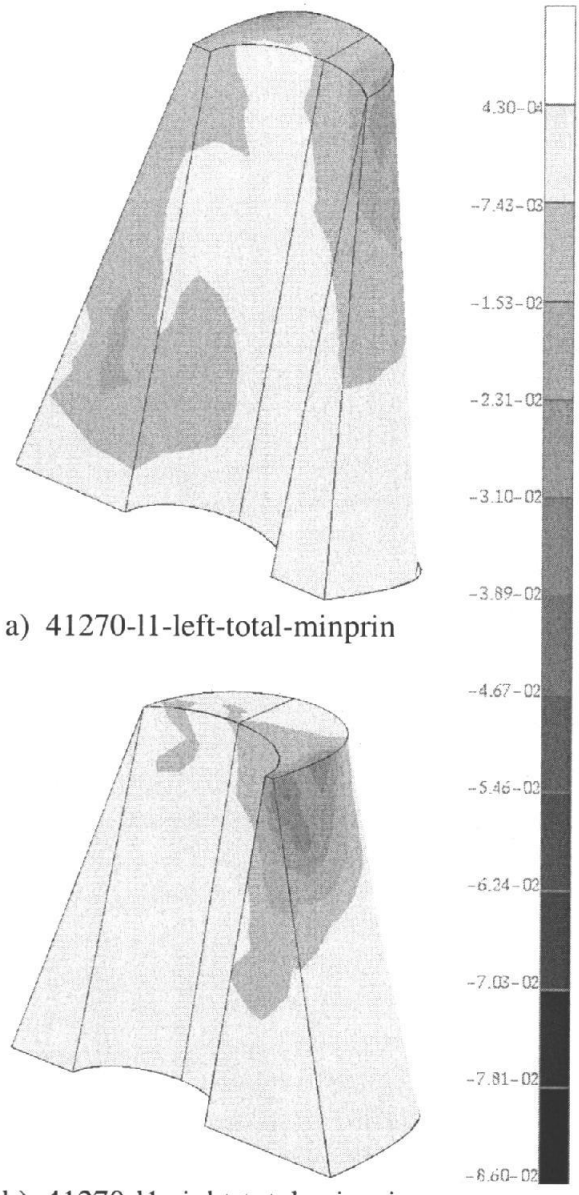

a) 41270-l1-left-total-minprin

b) 41270-l1-right-total-minprin

Figure 55. Minimum principle strains within the regions of interest: Before insertion correlated with full insertion.

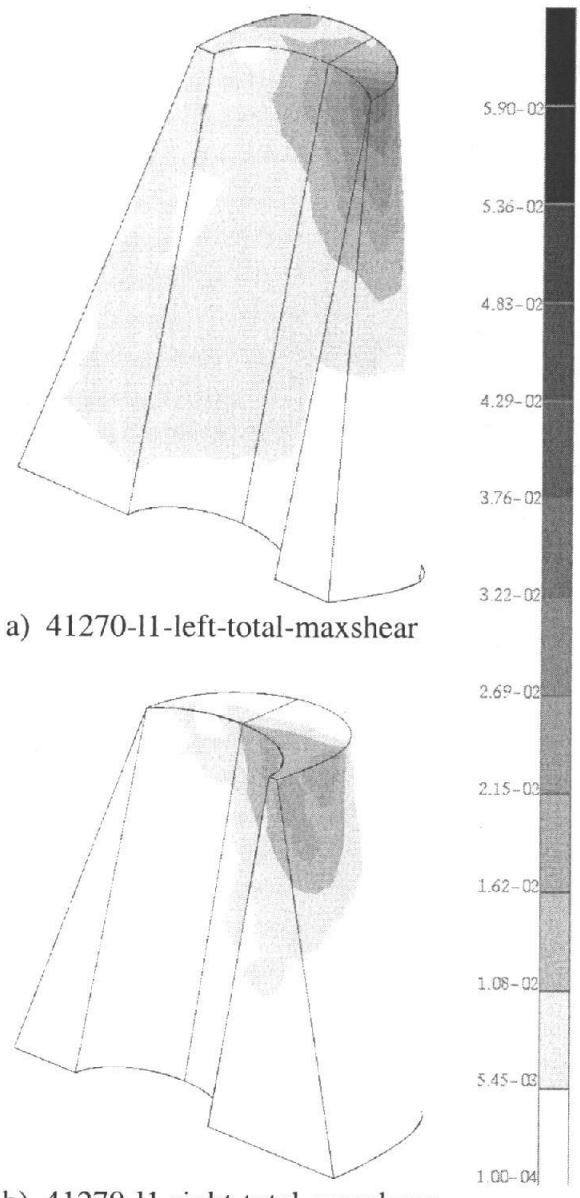

a) 41270-l1-left-total-maxshear

b) 41270-l1-right-total-maxshear

Figure 56. Maximum shear strains within the regions of interest: Before insertion correlated with full insertion.

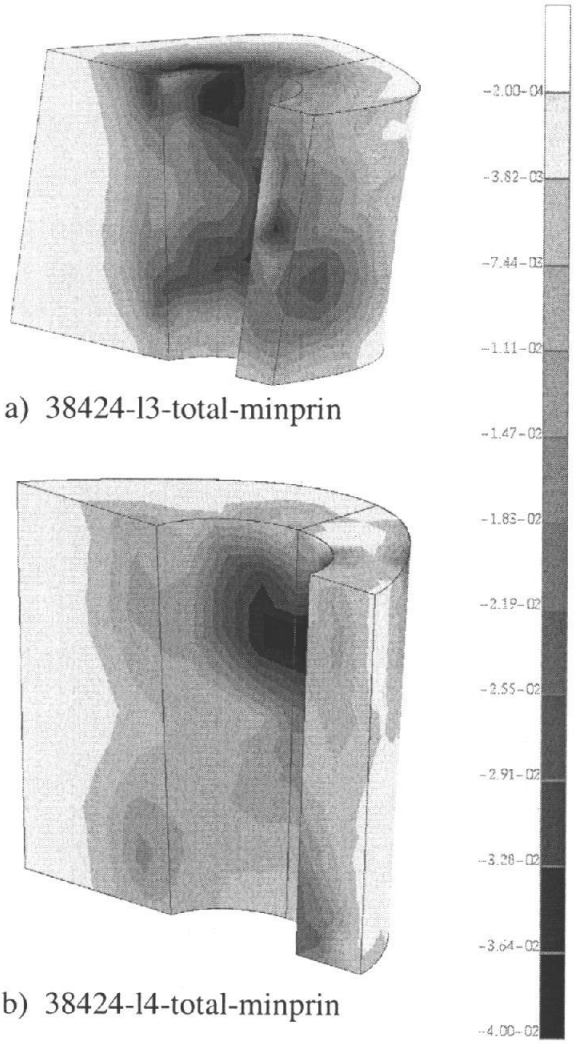

a) 38424-l3-total-minprin

b) 38424-l4-total-minprin

c) 38424-l5-total-minprin

Figure 57. Minimum principle strains within the regions of interest: Before insertion correlated with full insertion.

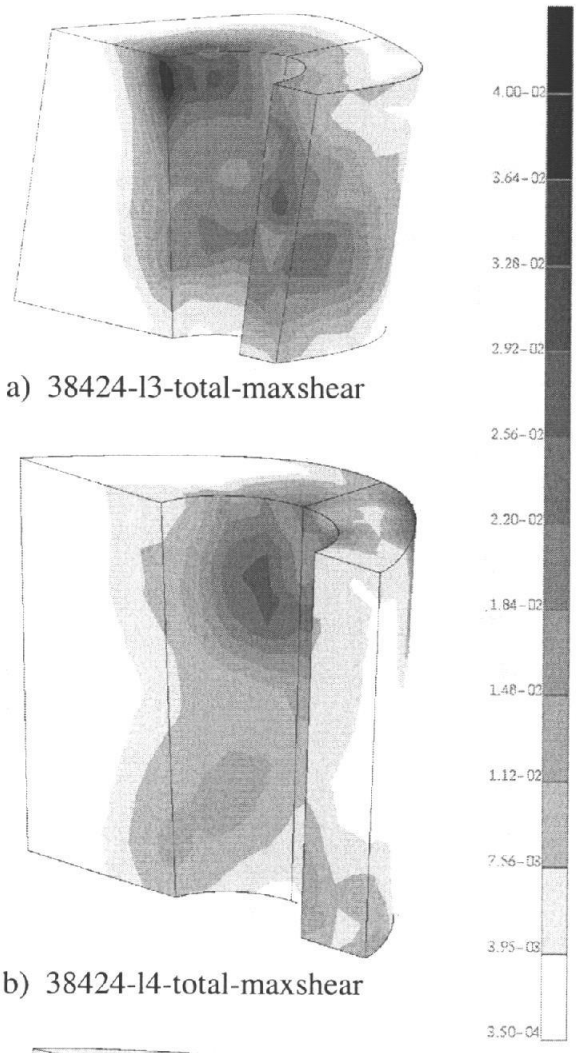

a) 38424-l3-total-maxshear

b) 38424-l4-total-maxshear

c) 38424-l5-total-maxshear

Figure 58. Maximum shear strains within the regions of interest: Before insertion correlated with full insertion.

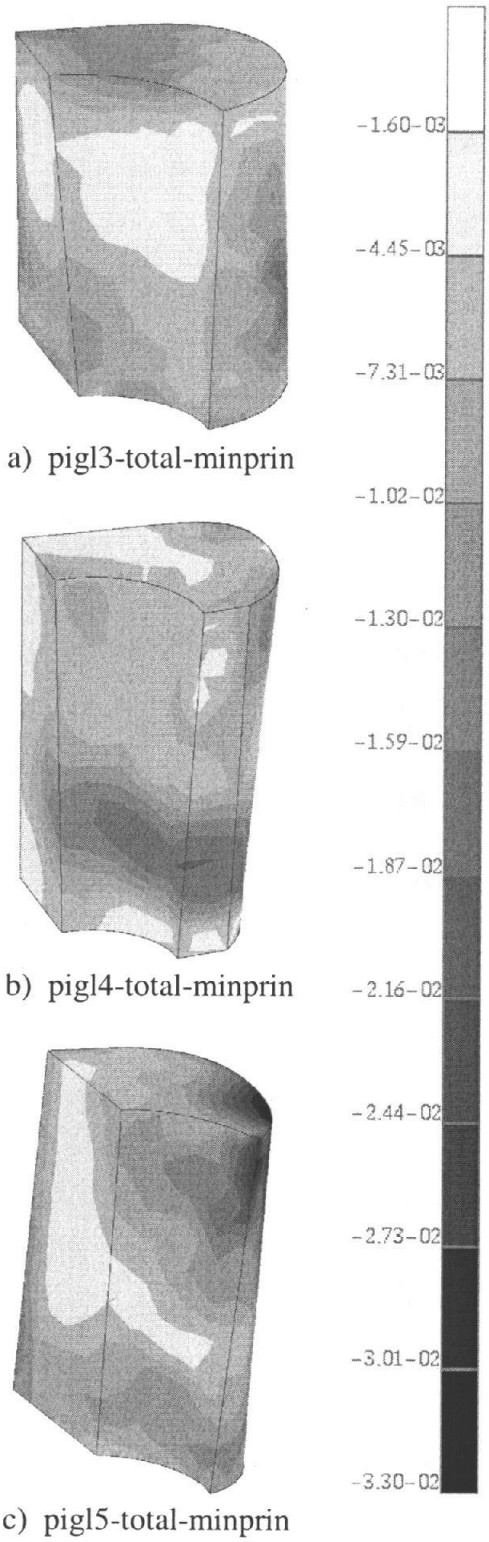

a) pigl3-total-minprin

b) pigl4-total-minprin

c) pigl5-total-minprin

Figure 59. Minimum principle strains within the regions of interest: Before insertion correlated with full insertion.

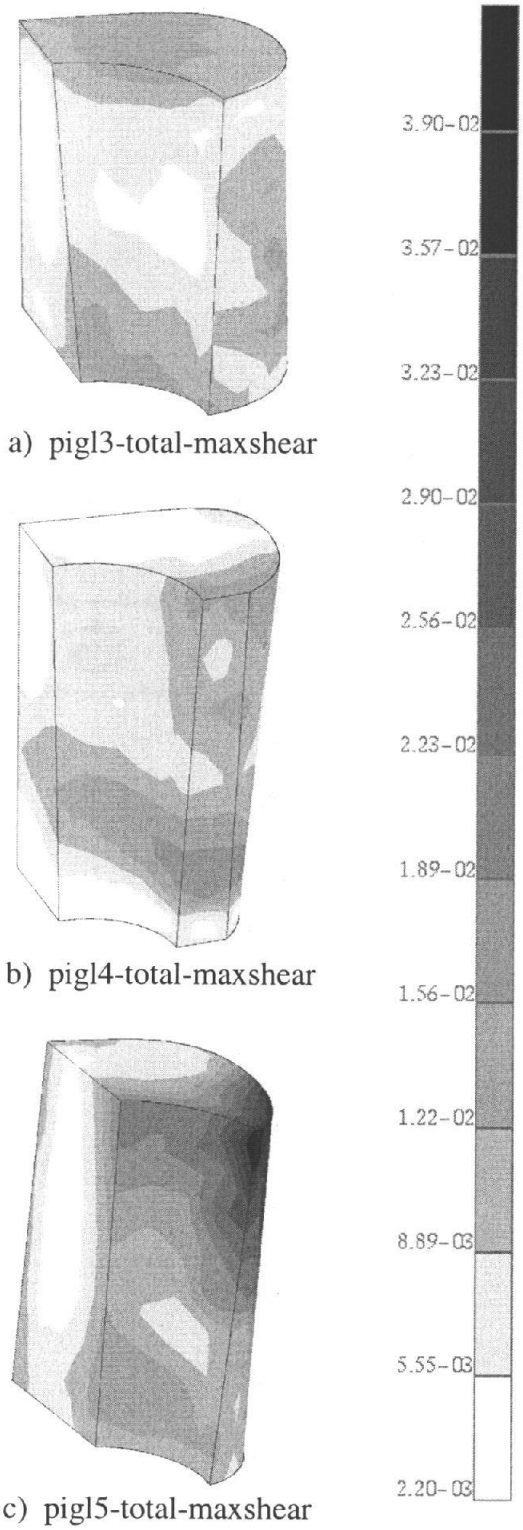

a) pigl3-total-maxshear

b) pigl4-total-maxshear

c) pigl5-total-maxshear

Figure 60. Maximum shear strains within the regions of interest: Before insertion correlated with full insertion.

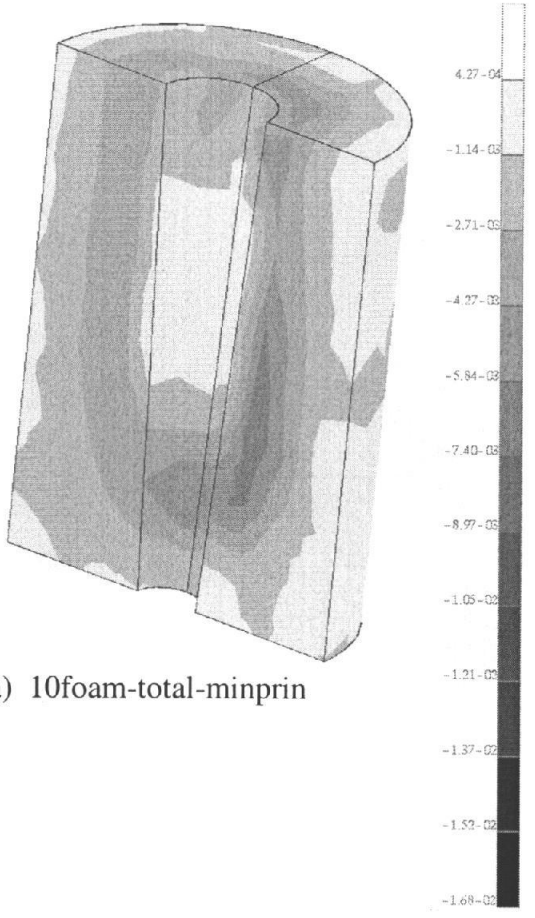

a) 10foam-total-minprin

Figure 61. Minimum principle strains within the regions of interest: Before insertion correlated with full insertion.

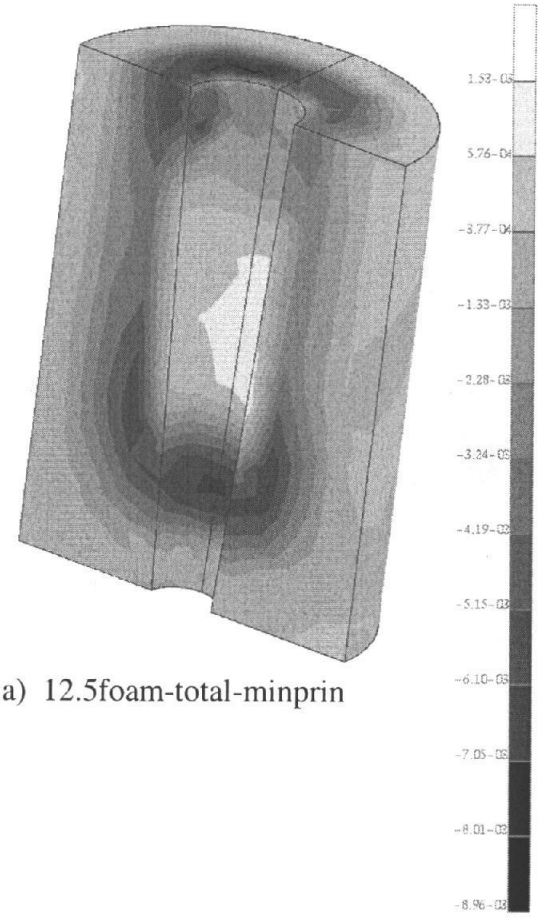

a) 12.5foam-total-minprin

Figure 62. Minimum principle strains within the regions of interest: Before insertion correlated with full insertion.

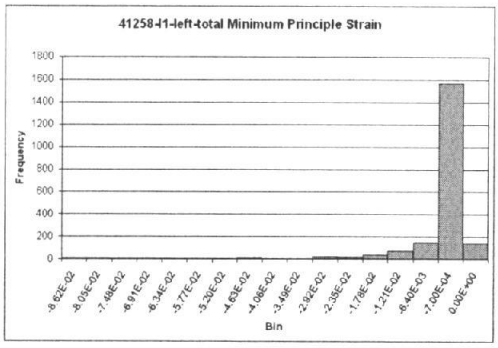

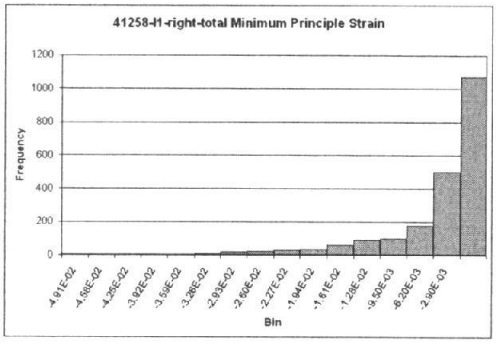

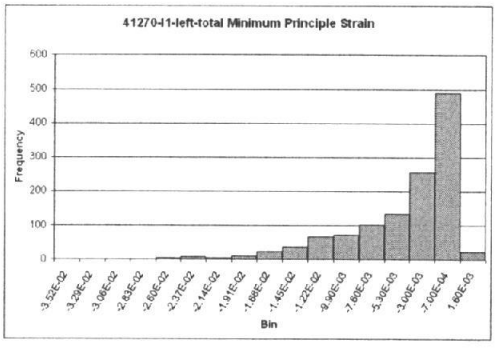

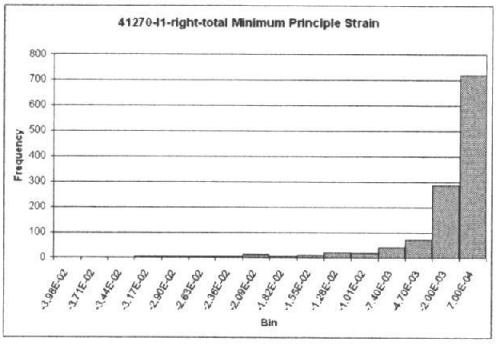

Figure 63. Histograms of total minimum principle strains for each sample.

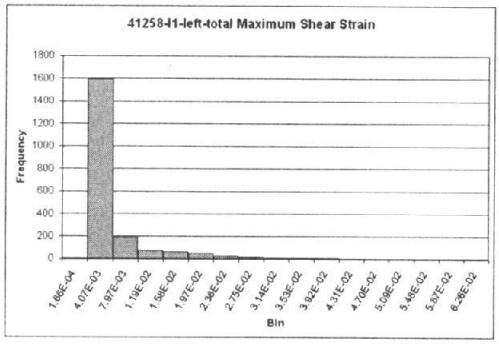

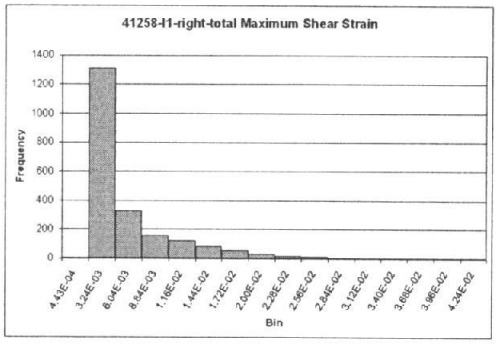

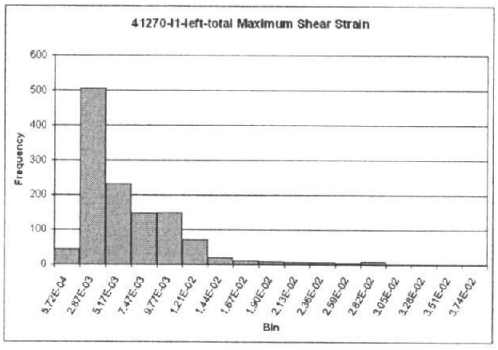

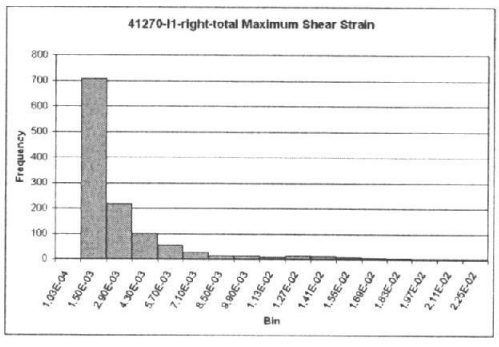

Figure 64. Histograms of total maximum shear strains for each sample.

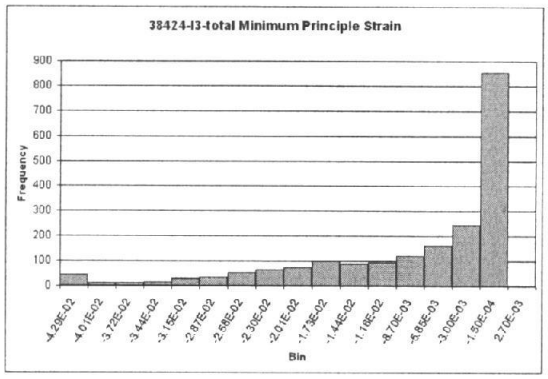

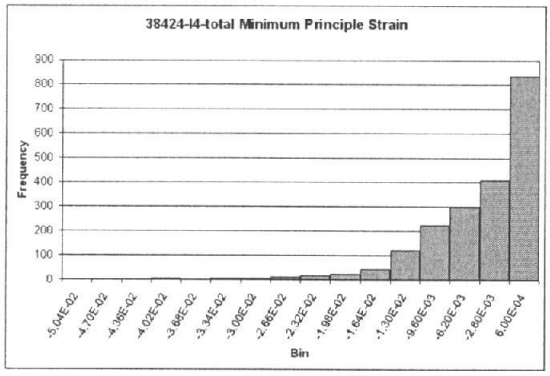

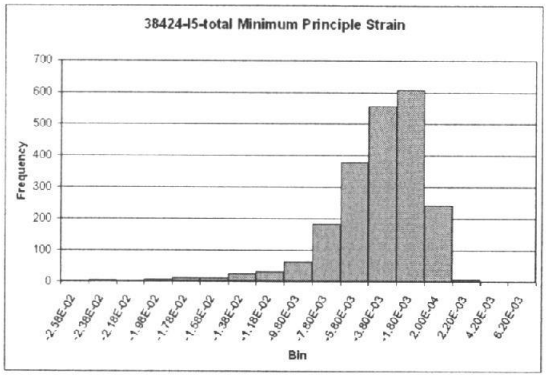

Figure 65. Histograms of total minimum principle strains for each sample.

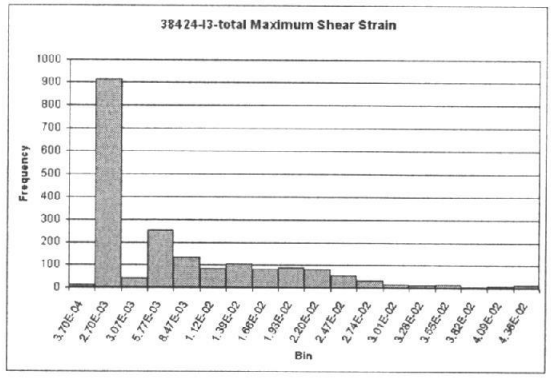

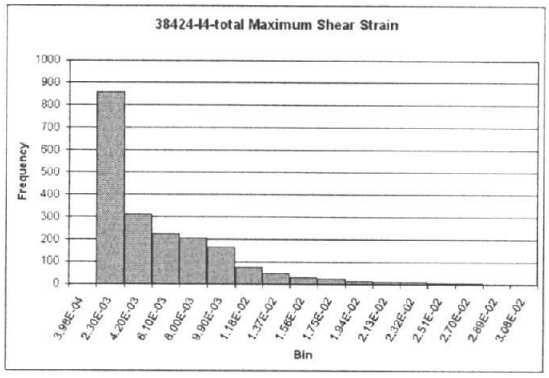

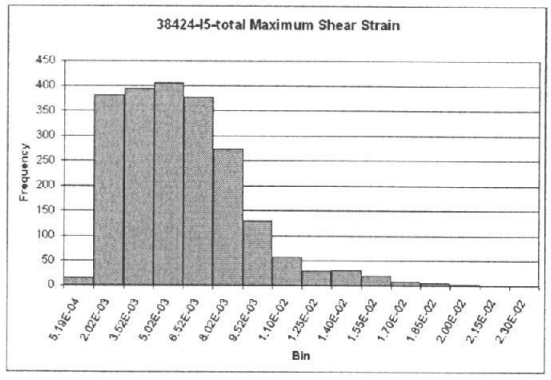

Figure 66. Histograms of total maximum shear strains for each sample.

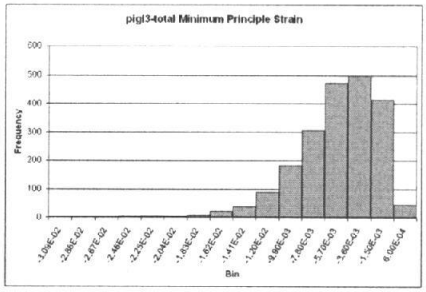

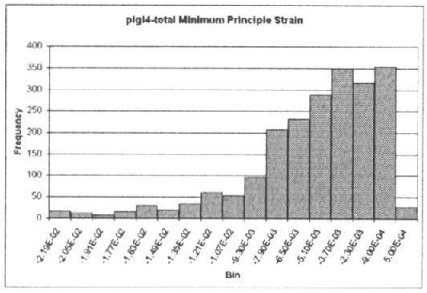

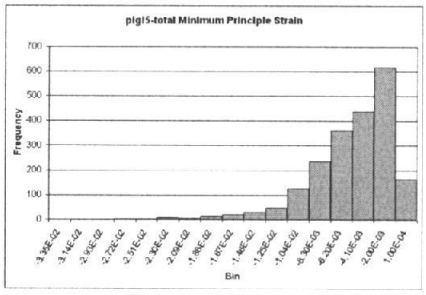

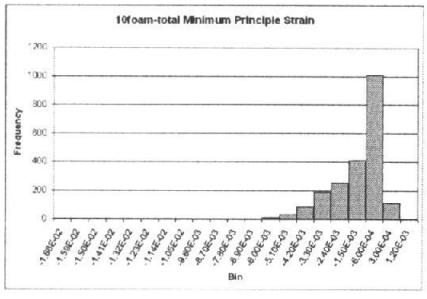

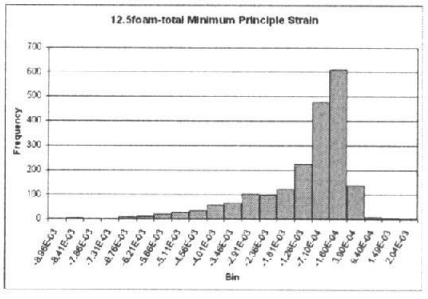

Figure 67. Histograms of total minimum principle strains for each sample.

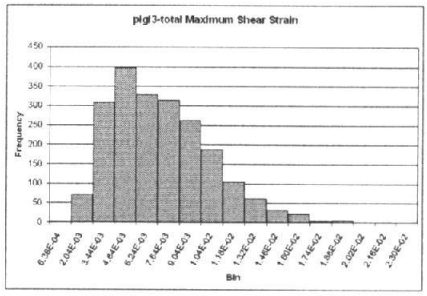

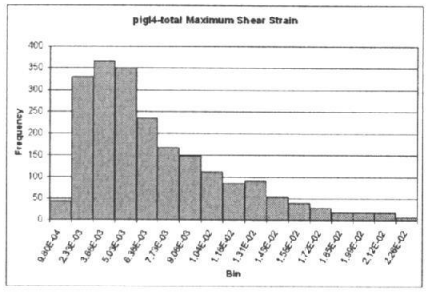

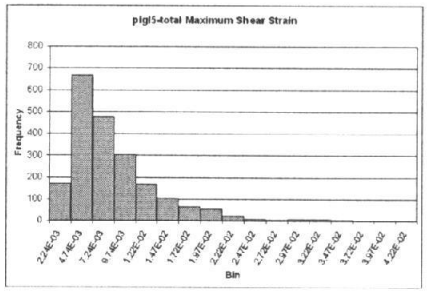

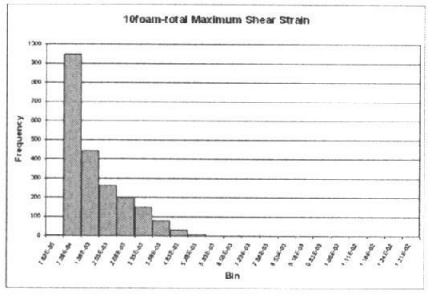

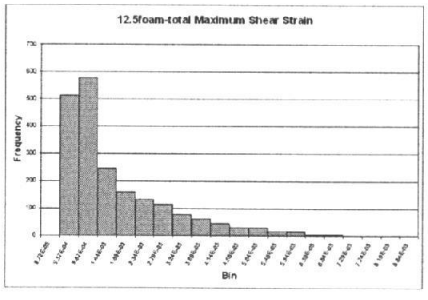

Figure 68. Histograms of total maximum shear strains for each sample.

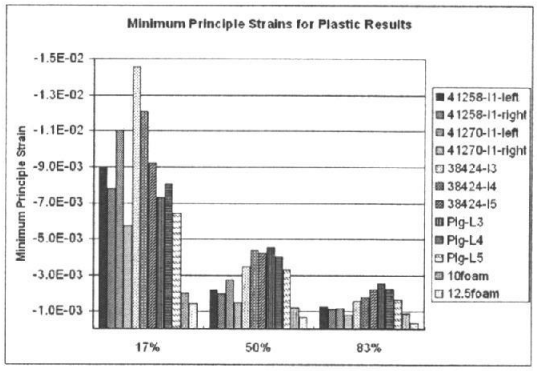

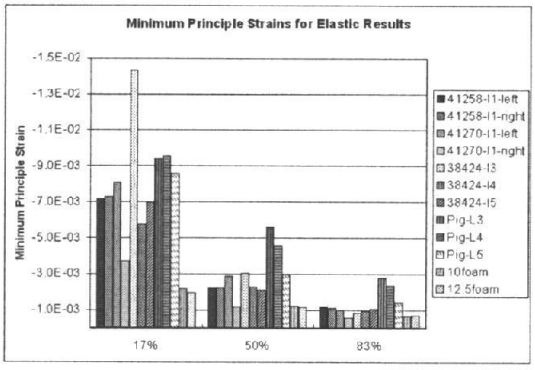

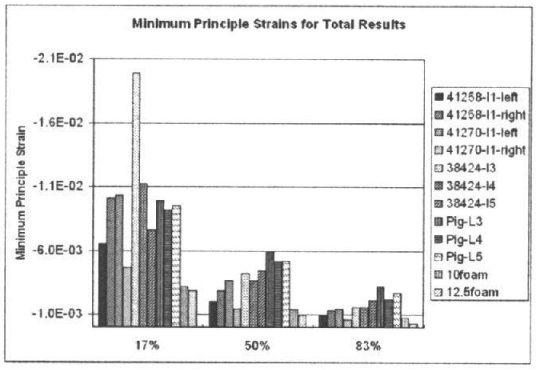

Figure 69. Non-parametric analysis of plastic, elastic and total minimum principle strain results for each sample.

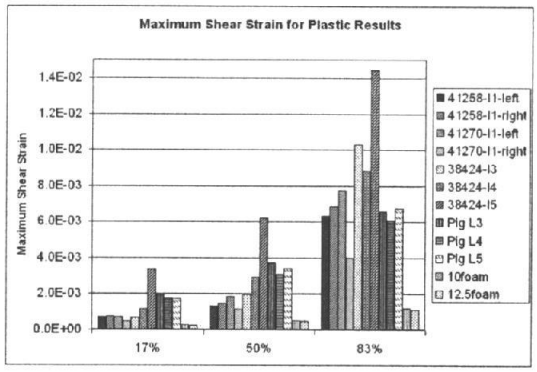

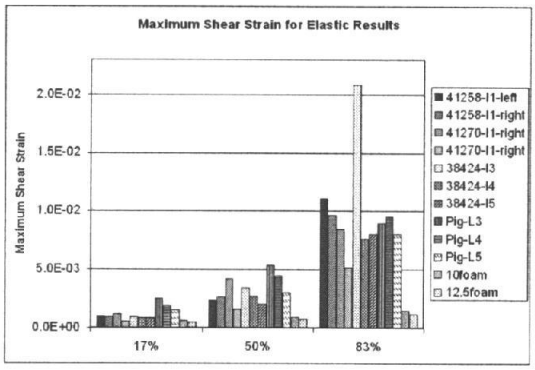

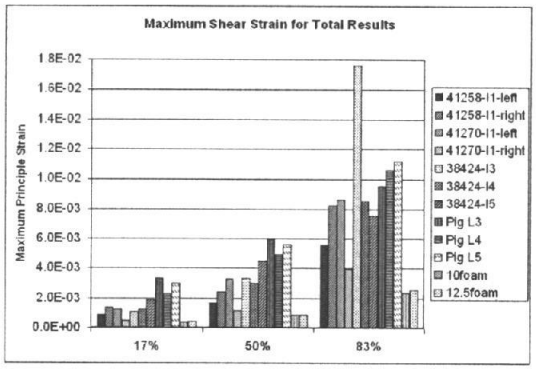

Figure 70. Non-parametric analysis of plastic, elastic and total maximum shear strain results for each sample.

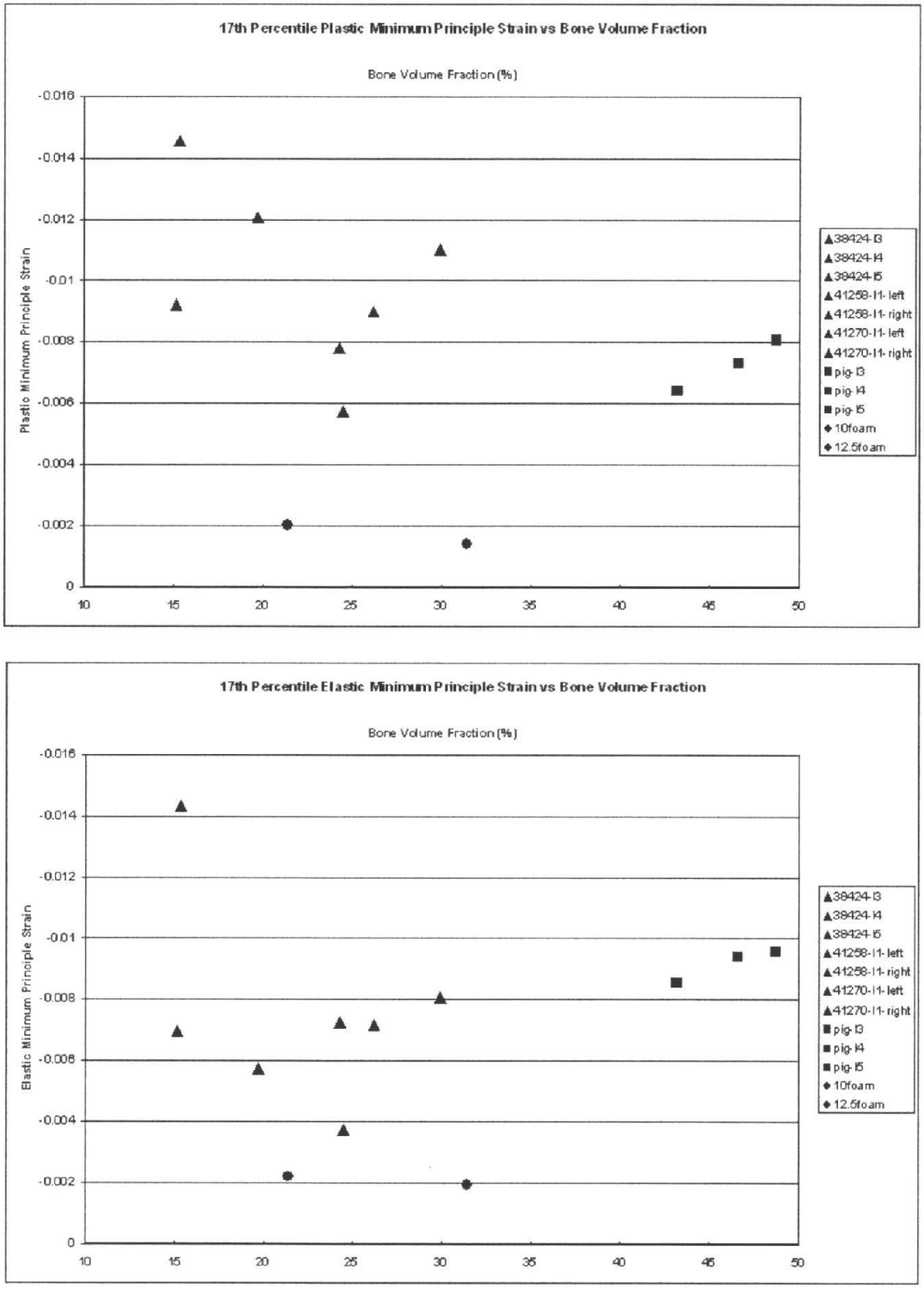

Figure 71. Comparison of bone volume fraction versus 17th percentile plastic and elastic minimum principle strains for each sample.

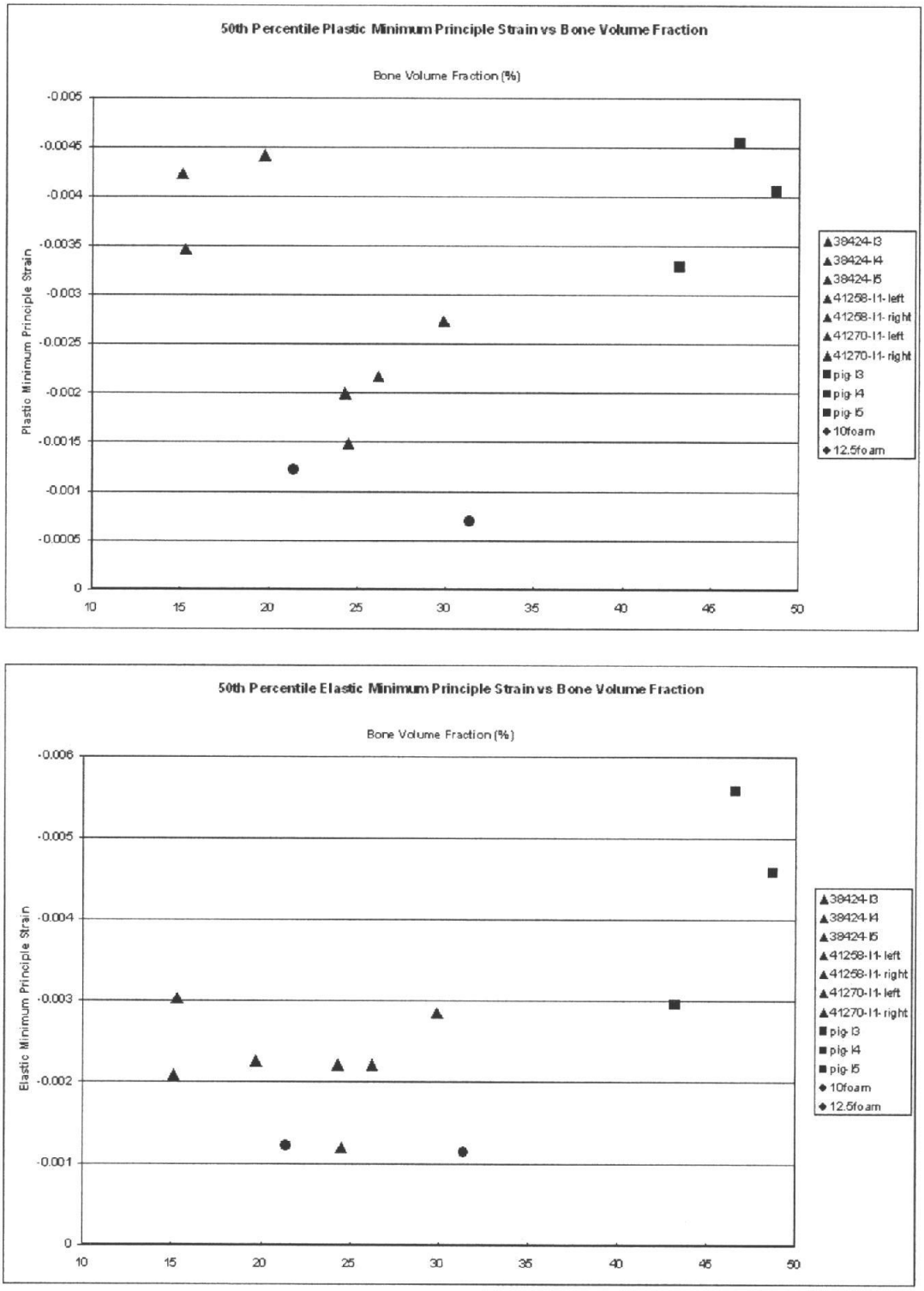

Figure 72. Comparison of bone volume fraction versus 50th percentile plastic and elastic minimum principle strains for each sample.

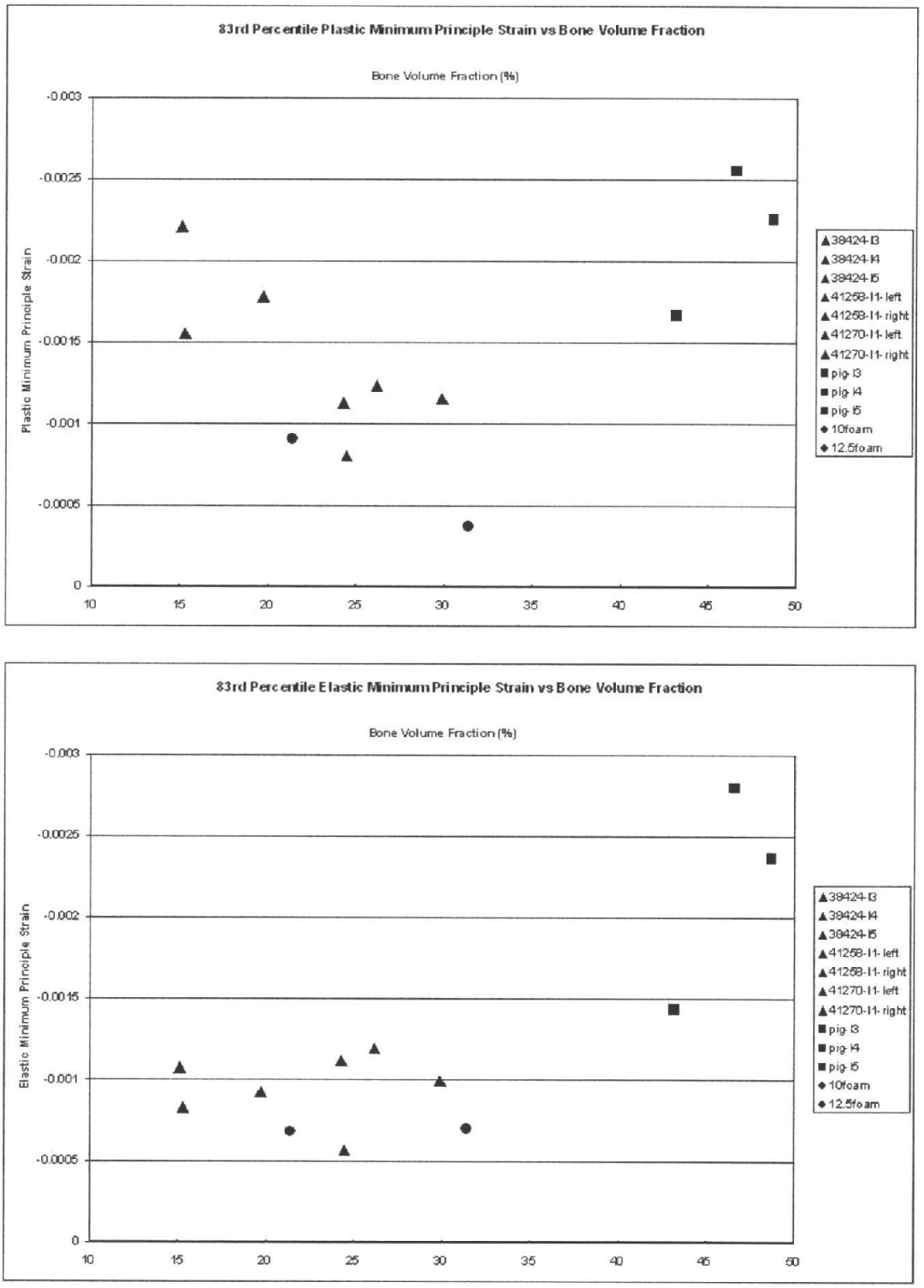

Figure 73. Comparison of bone volume fraction versus 83rd percentile plastic and elastic minimum principle strains for each sample.

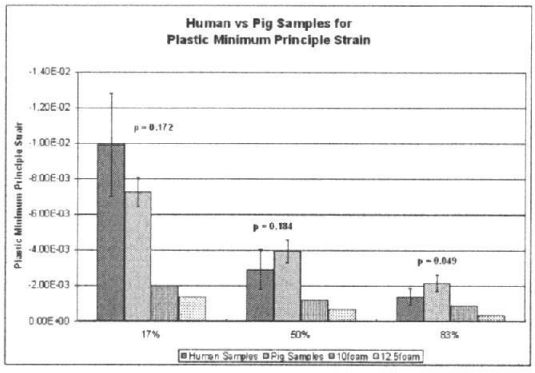

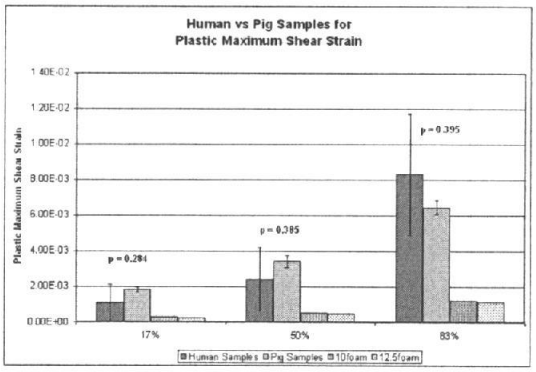

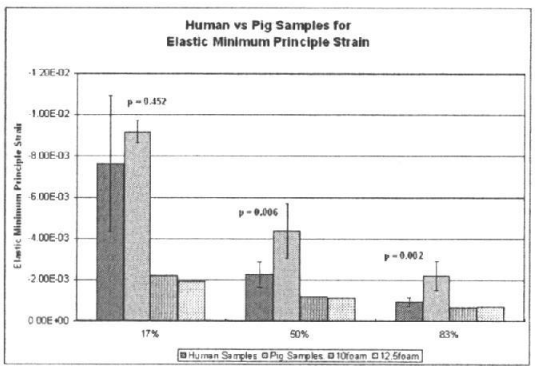

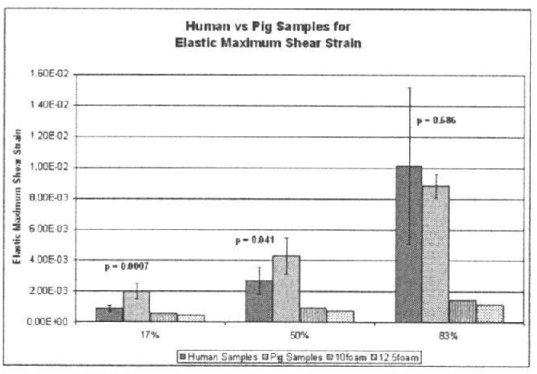

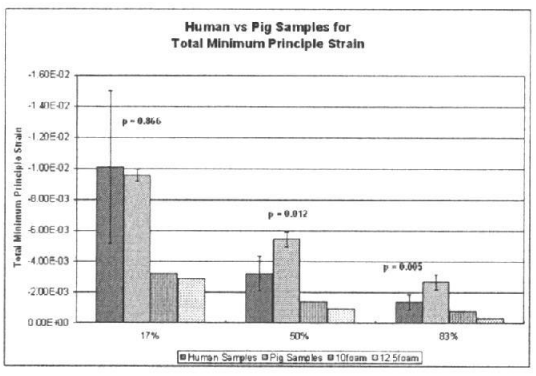

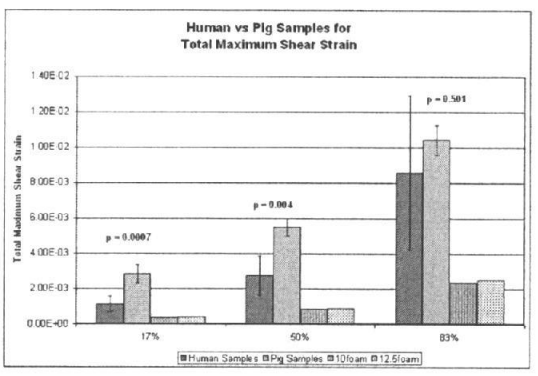

Figure 74. Nonparametric statistical comparison of minimum principle strains for human vs porcine and PU-foam samples using ANOVA p-values ($p<0.05$).

Figure 75. Nonparametric statistical comparison of maximum shear strains for human vs porcine and PU-foam samples using ANOVA p-values ($p<0.05$).

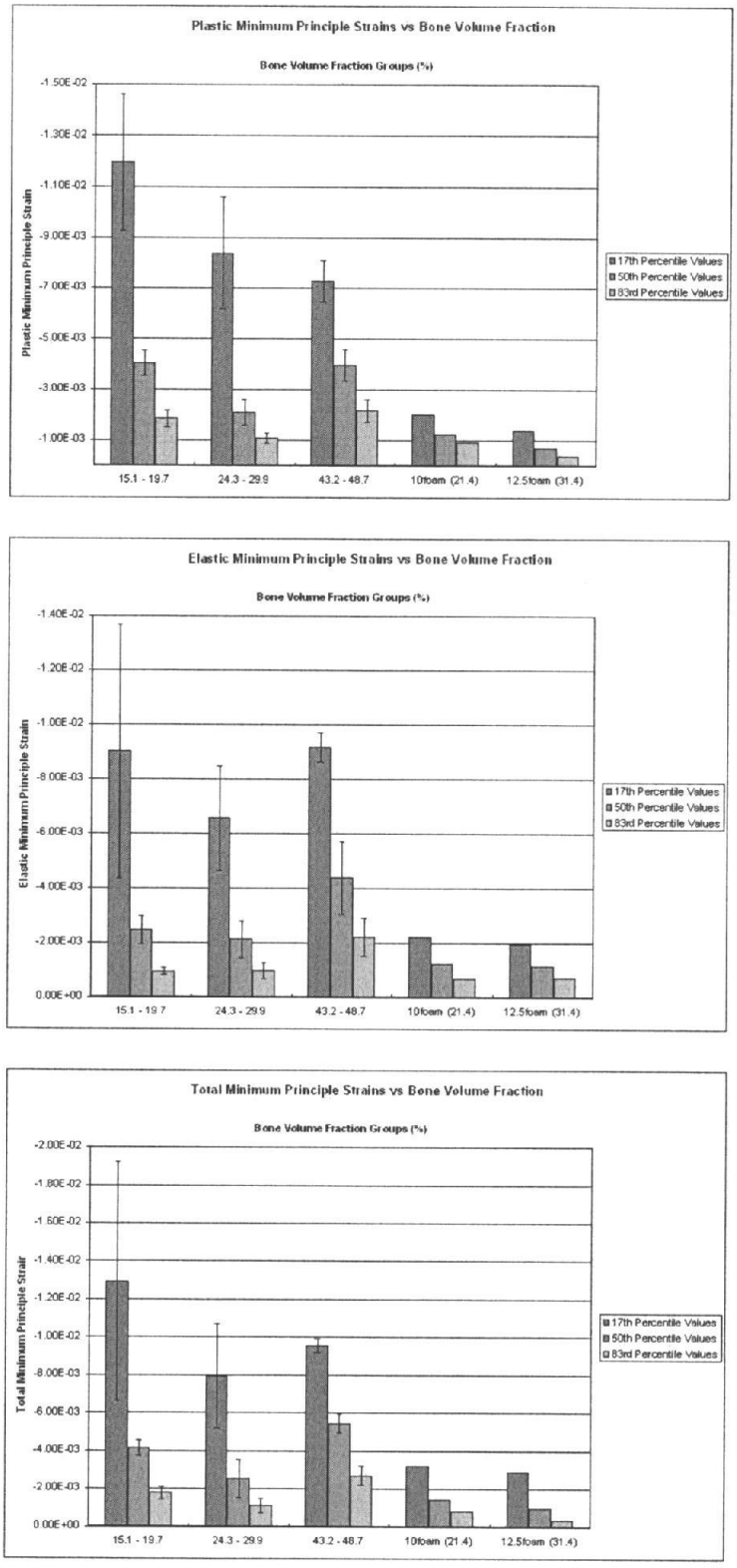

Figure 76. Comparison of grouped bone volume fractions versus plastic, elastic or total minimum principle strains for the 17th, 50th and 83rd percentile values.

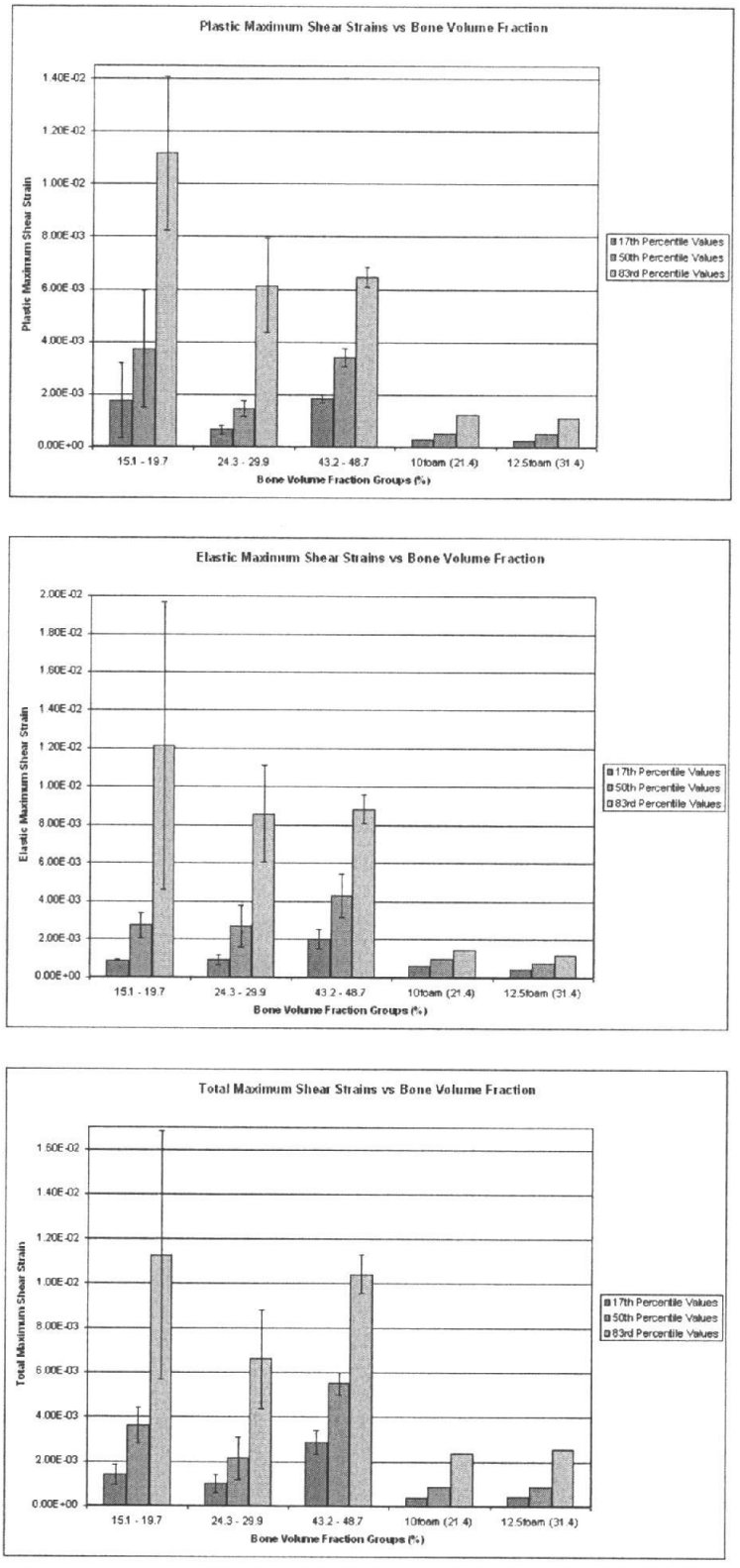

Figure 77. Comparison of grouped bone volume fractions versus plastic, elastic or total maximum shear strains for the 17^{th}, 50^{th} and 83^{rd} percentile values.

Table 9. Summary of ANOVA p-test values ($p<0.05$) in comparisons between groups for 17th, 50th and 83rd percentile values of plastic, elastic and total minimum principle strain (MPS).

BVF Group *	Percentile Value Compared	Elastic MPS	Plastic MPS	Total MPS	Elastic MSS	Plastic MSS	Total MSS
1 - 2	17%	0.374	0.110	0.209	0.844	0.175	0.247
	50%	0.498	0.004	0.047	0.963	0.093	0.078
	83%	0.894	0.011	0.064	0.406	0.035	0.181
2 - 3	17%	0.076	0.451	0.369	0.013	0.0002	0.003
	50%	0.031	0.007	0.005	0.119	0.0004	0.003
	83%	0.022	0.007	0.005	0.875	0.777	0.038
1 - 3	17%	0.957	0.045	0.409	0.019	0.9330	0.021
	50%	0.079	0.887	0.024	0.111	0.8230	0.025
	83%	0.037	0.393	0.054	0.490	0.050	0.815

* Bone Volume Fraction Groups (%):
Group 1: 15.1 - 19.7; Group 2: 24.3 - 29.9; Group 3: 43.2 - 48.7.